Electrical and Mathematical Models of PV Cells

Strategies and Critical Assessment

Marco Semeraro

Thesis to obtain the Master of Science Degree in

Energy Engineering and Management

Supervisor: Prof. Luís Filipe Moreira Mendes

Examination Committee

Chairperson: Prof. Jorge de Saldanha Gonçalves Matos

Supervisor: Prof. Luís Filipe Moreira Mendes

Member of the Committee: Prof. José Manuel Dias Ferreira de Jesus

July 2020

Abstract

Modelling of a device is essential to analyse, optimize and predict its performance with respect to the physics at the basis of its functioning. In a world struggling with energy-related issues, effective modelling of Photovoltaic (PV) systems can be a key factor for today's society betterment and progress. The main concerns with PV modelling are on the one hand, the number of degrees of freedom of the (most accurate) mathematical models with respect to the number of available data (information available on the device datasheet) and, on the other hand, their dependency on widely varying operating conditions. In this study, a framework for PV modelling is built with the aim to provide a tool for a reasoned selection of the modelling strategies, based on their physical implications. The diode-based models are analysed and the conventional techniques to extract their model parameters and account for their dependency on irradiance and temperature are presented along with their issues. The Complete Single-Diode Model featuring 5 model parameters proves to represent the best trade-off between simplicity and accuracy. For this reason, it is further analysed by comparing two different irradiance-temperature approaches, i.e. the Adaptive-Parameter Modelling (APM) and the Constant-Parameter Modelling (CPM). The parameter extraction based on the Newton-Raphson method proves to be a key step for the accuracy of both the models: when properly designed, it allows both the models to show excellent fit with the experimental data, whereas APM proves to perform slightly better than CPM at the expenses of the computing time.

Keywords:

PV Modelling

Parameter Extraction

Five-Parameter Model

Single-Diode Equivalent Circuit

I-V Curve

Resumo

A modelação de um dispositivo com base nos processos físicos envolvidos no seu funcionamento é essencial para a análise, otimização e previsão do seu desempenho. As principais questões associadas à modelação de sistemas PV são, por um lado, o número de graus de liberdade dos modelos matemáticos face ao número de dados disponíveis (informação disponível na ficha de dados do dispositivo) e, por outro lado, a sua dependência de condições de funcionamento muito variáveis. Neste trabalho é apresentado um enquadramento para a modelação de sistemas PV com o objetivo de fornecer uma ferramenta para uma seleção fundamentada das estratégias de modelação, baseada na física do funcionamento das células PV. São analisados os modelos baseados em díodos e são apresentadas as técnicas convencionais para extrair os seus parâmetros e para descrever a sua dependência da irradiância e temperatura, assim como as questões mais relevantes. O Modelo completo de um díodo com 5 parâmetros provou representar o melhor compromisso entre simplicidade e precisão. Assim, este modelo é analisado mais em detalhe, comparando-se duas abordagens diferentes à questão da variabilidade da irradiância e temperatura: a Modelação Adaptativa-Paramétrica (APM) e a Modelação a Parâmetros-Constantes (CPM). A extração de parâmetros com base no método *Newton-Raphson* revelou-se um aspeto fundamental para a precisão de ambas as abordagens. Quando os parâmetros são corretamente extraídos ambos os modelos mostram uma excelente reprodução dos dados experimentais, apresentando o método APM um desempenho ligeiramente superior que o CPM, ainda que a expensas de tempo de computação.

Palavras-chave:

Modelação PV

Extração de parâmetros

Modelo de cinco parâmetros

Circuito equivalente de um díodo

Curva I-V

Table of Contents

List of Figures

List of Tables

Abbreviations and Symbols

Symbol	***Description***	***Unit***
a	Diode ideality factor	
APM	Adaptive Parameter Modeling	
CPM	Constant Parameter Modeling	
CSDM	Complete Single-Diode Model	
DDM	Double-Diode Model	
DHI	Diffuse Horizontal Irradiance	Wm^{-2}
DNI	Direct Normal Irradiance	Wm^{-2}
E_g	Bandgap energy	eV
I	PV Output current	A
I_{SC}	Short-circuit current	A
k_B	Boltzmann constant	JK^{-1}
KCL	Kirchhoff's Law of Currents	
KVL	Kirchhoff's Law of Voltages	
MDDM	Modified Double-Diode Model	
MPP	Maximum power point	
NOCT	Nominal Operating Cell Temperature	
NR	Newton-Raphson (numerical method)	
q	Electron charge	C
R_p	Parallel (or shunt) resistance	Ω
R_s	Series resistance	Ω
SSDM	Simplified Single-Diode Model	
STC	Standard Test Conditions	
T_c	PV Cell Temperature	K (°C)
TDM	Three-Diode Model	
TRP	Three Remarkable Points	
V	PV Output voltage	V
V_{OC}	Open-circuit voltage	V
V_{th}	Thermal voltage	V

To those whose main professional goal
is to make this World a better place,
while feeding their curiosity.

1 Introduction

1.1 The Role of Photovoltaic Technology in Today's Society

It is hard to argue that one of the main purposes of scientific research is the betterment of humanity, understood as a complex organism born and living within a wider organism that is our planet Earth. Lately, among the numerous practical facets of this existential awareness, the pursuing of a more balanced interaction with the natural resources emerged [1] due to the spreading worldwide of natural disorders, usually referred to as *climate change* and including: global warming, sea level rise, more violent weather events like storms, rainfalls, etc. In this scenario, energy production and consumption is definitely on the stage due to its dramatic impact on the biosphere, encouraged by a constantly growing world population and a more and more energy-hungry lifestyle. The main concern with conventional fossil fuels is the release in the atmosphere of enormous amounts of CO_2 [1], which is a climate-changing species; however, this is not the only energy production-related environmental concern. *Renewable Energy Sources* (RES), first among them wind and solar, have proved to be a feasible and gentler alternative to conventional high-impact energy sources (coal, oil, natural gas) as they are carbon-free and do not run on exhaustible fuel [2]. For this reason, over the past decades huge efforts have been put into the development of these technologies, from research advances to economical feasibility, from legislative frames to industrial implementation. As a result, the growth of renewables (excluding the traditional use of biomass) has outpaced the rate of increase of energy consumption, allowing for an increase in their share of total final energy consumption up to almost 11% in 2018; however, given the current and planned policies, this share is expected to reach only 15% by 2030 against the figure of 23% suggested by IEA to fulfil the so-called Sustainable Development Goals [3]. In fact, a consistent penetration of these technologies into the current energy system seems to have a long way to go due to economic, technological and socio-cultural issues. Among the RES providing electrical power, *photovoltaic solar* (PV) is the third technology by energy production behind hydropower and wind energy, with a figure of about 443000 GWh delivered in 2017, on the wave of an exponential growth over the last years (see Figure 1.1).

The reasons for this sharp increase of PV deployment lie in the several and desirable advantages that PV technology offers [1, 4, 5], including:

- vast, widely accessible and essentially infinite fuel (PV is renewable);
- waste- and carbon emission-free operation (PV is clean);
- low operating costs (PV is cheap);
- direct, static and wear-free conversion of sunlight into electricity allowing for reliable and long-lasting operation (PV is sustainable);
- noise-free operation (PV is not intrusive);
- ambient temperature operation (PV is safe);
- highly modular (PV is flexible);
- easy to install and integrate in existing infrastructure (PV is flexible).

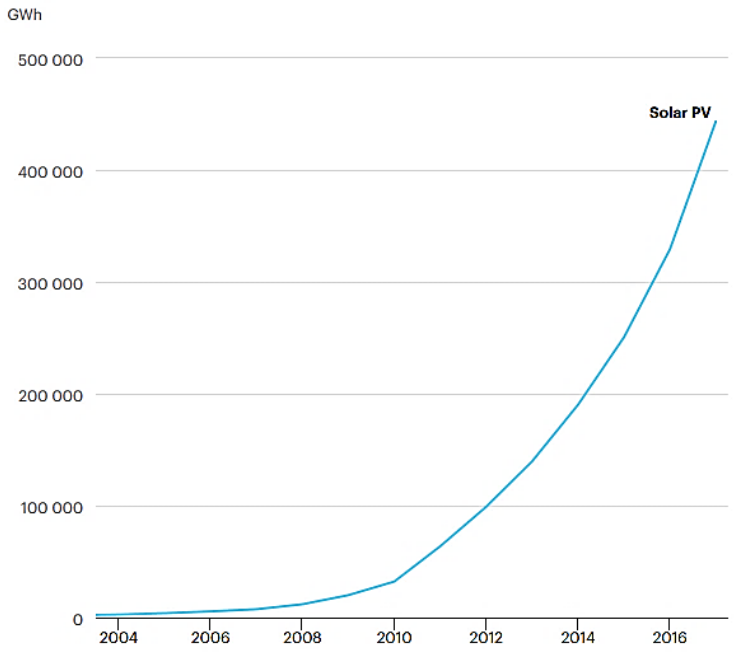

Figure 1.1 Worldwide PV electricity production over the last years [3]

In particular, PV systems can supply electricity directly to a power grid but they can supply electricity also in locations where distribution systems do not exist. PV is highly modular meaning that a PV cell can power small devices such as calculators and wristwatches, a PV module can power water pumps or communications equipment up to satisfying the needs of a single home, and PV arrays can supply electricity to thousands of consumers, households or businesses.

Unfortunately, PV technology shows also few drawbacks:

- low energy density of the fuel, meaning that it requires large areas;
- initial installation costs;
- unpredictable hourly or daily output, that is, the main issue with most RES.

Given this scenario, it is understood how any improvement, even small, in any aspect of PV technology - from manufacturing to physical understanding, from design to operation management - can lead to significant and precious achievements on a global scale, paving the way to a greater share of this technology in the world energy production pie and thus to a more sustainable and liveable world. The way the Object of this work (i.e., PV modelling) can contribute to this goal is explained in Paragraph 1.3, after that a brief explanation on PV basics is given in the next Paragraph.

It must be specified that, for the author, the motivation for research and betterment holds strong even if there was no such environmental emergency or moral drive beneath: in that case, it would be "just" about unravelling science and improving technology, that is, the ultimate embodiment of human curiosity.

1.2 Basic Functioning of a PV Device

The fundamental unit of a PV device is the PV *cell* (1-2 watts). When a number (usually from 36 to 72) of cells are connected, either in series or in parallel (or a mix of both), a PV *panel* or *module* is obtained (tens to hundreds of watts). Several panels make a PV *array* and multiple arrays make a utility-scale PV *plant* (see Figure 1.2) [6].

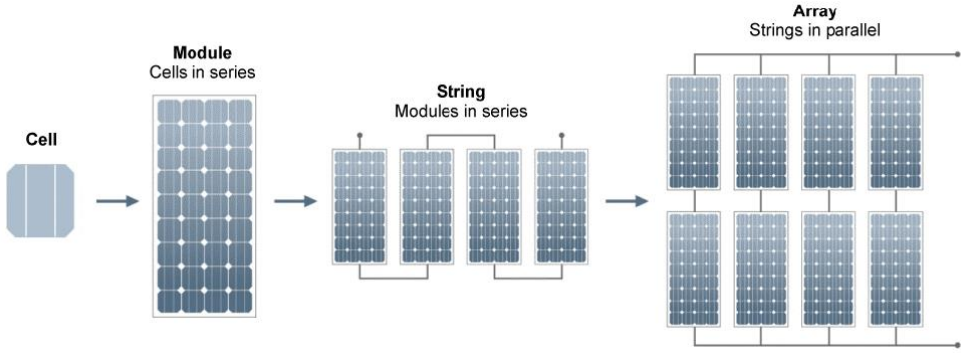

Figure 1.2 PV cell, module and array

Essentially, a PV device delivers at its terminals electric power P, i.e. a flow I of electric charges with electric potential difference V ($P = VI$). This DC current can be fed directly to an energy storage device [1] or to an inverter that converts it into more usable AC current for the loads.

The mechanism by which the abovementioned electric power is generated is made explicit in the name itself of the technology. In fact, the adjective “photovoltaic” is borrowed from a physical effect, the *photovoltaic effect*, and is a self-explaining word: generating electricity (“-voltaic”) from light (“photo-“). When sunlight (theoretically, PV cells can run on any kind of light, even artificial light [1]) strikes a PV cell, the photons that it is made of are partially reflected, partially let pass through (heating up the device) and partially absorbed by the material [5]. These last are the ones whose energy is collected by the PV cell thanks to the special electric properties of the *semiconductor materials* (see Figure 1.3).

Semiconductors show weakly bonded electrons occupying a band of energy called “valence band”; if an incoming photon has enough energy (i.e. greater than a threshold called “bandgap energy” E_g) to break these bonds, the “hit” electron is somewhat free to move in a new energy band called “conduction band” (this is the case for *direct* bandgap materials, otherwise the momentum due to the atomic lattice is also taken into account). A PV cell consists of two layers of semiconductor material, whose surfaces have gone through (different) treatments during manufacturing, called *doping*, that make the surfaces more receptive to the free electrons [5]. The front surface is “n-doped”, becoming a selective contact able to collect the freed electrons in the conduction-band. The movement of the electrons creates an imbalance of electrical charge between the cell’s front and back surfaces and this imbalance creates a voltage potential. When the surfaces are connected to an external *load*, the electrons (i.e., an electric current called *photocurrent*) flow in the circuit and, as they go through the load, they provide usable work. Then, they are restored to the solar cell by the return loop via a second selective contact, i.e. the rear “p-doped” surface, which returns them to the valence band with the same energy that they started

with. The interface between the conduction-band and valence-band selective contacts is called "p-n junction". The electric potential at which the electrons are delivered to the external circuit is always slightly less than the bandgap energy, even if the photons that created it had more energy; that is, the available potential of a solar cell is essentially a characteristic of the material it is made of.

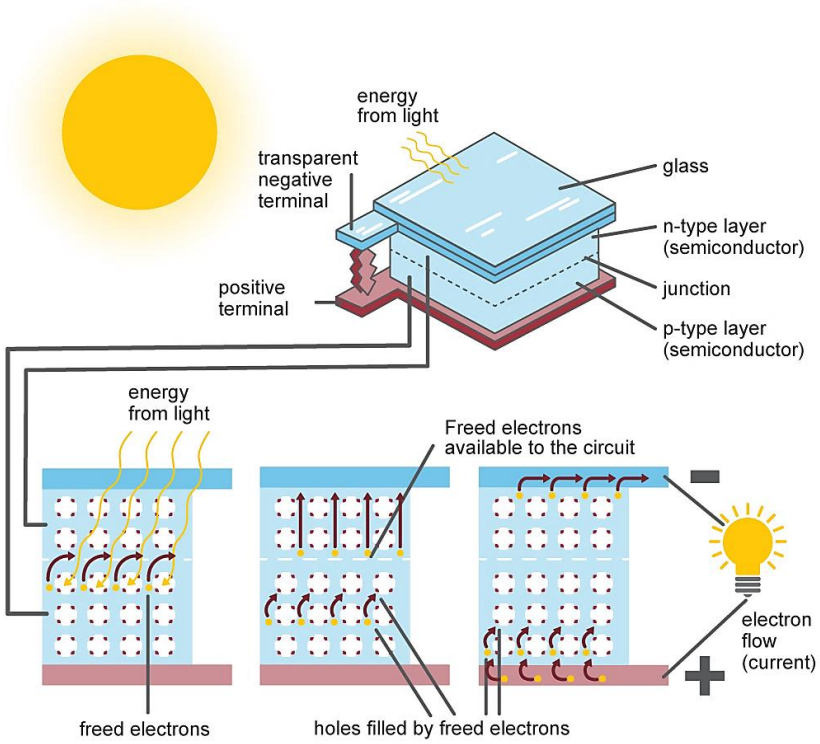

Figure 1.3 Fundamental operating mechanisms of a PV cell [5]

Nowadays, different semiconductor materials are employed in PV industry, with silicon being the most spread and historically the first one used. Usually, solar cells are classified into three *generations*:

- I generation: monocrystalline (mono-Si) and polycrystalline (poly-Si) silicon solar cells;
- II generation: *thin film* solar cells made out of amorphous silicon (a-Si), cadmium telluride (CdTe) or copper-indium-gallium diselenide (CIGS);
- III generation: a number of emerging technologies including organic, quantum dot, perovskite, dye-sensitized solar cells and others.

It is worth mentioning also *multi-junction* solar cells that have multiple p-n junctions made out of different semiconductor materials so that a wider range of bandgap energies is available for photon absorption.

New materials and technologies are tested in the search for cheaper solutions and/or better efficiency. In fact, the efficiency of a PV cell, defined as the ratio of useful delivered power over incoming radiant power, varies by the PV technology (essentially, by the semiconductor material). Commercially available PV modules averaged less than 10% in the mid-1980s, reached 15% around 2015 and now efficiency is about 20% for state-of-the-art modules. Experimental PV cells for niche markets (such as space industry) or research purposes have reached nearly 50% efficiency [5].

The p-n junction

The p-n junction (see Figure 1.4) is the elementary building block not only for PV cells but also for any electronic device based on semiconductors (transistors, LEDs, etc). The reason is that while the surfaces of the two layers are relatively conductive, the junction becomes depleted of charge carriers (through recombination of electrons and holes created by the doping), hence non-conductive, depending on the potential difference between the layers. That is, a p-n junction acts as the electrical equivalent of a check valve, called *diode*, allowing the electric charges to flow in one direction (the junction is *forward biased*) but not in the opposite (the junction is *reverse biased*). A series of microscopic mechanisms occur during the electric flow through the junction, whose macroscopic effect is opposite migrations of electrons and holes from one side to the other (*diffusion*) and *recombination* of the two species in the vicinity of the junction.

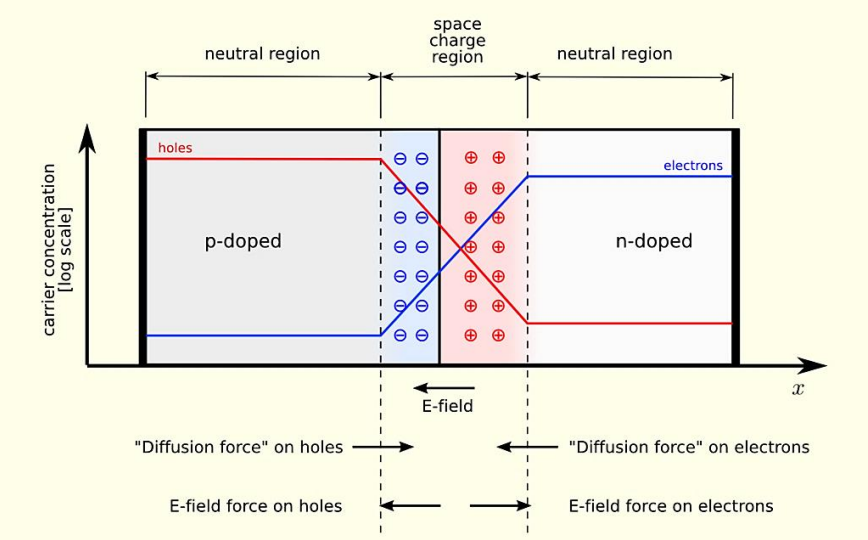

Figure 1.4 The p-n junction

It is understood that the p-n junction is at the heart of any PV device and therefore, it is also at the core of *PV modelling* , which is the Object of this work: in the next Paragraph, the role of PV modelling with respect to the technology challenges is explained and the aim of this study is presented.

1.3 Problem Statement and Aim of This Study

In science and engineering, a model is a representation of a phenomenon or physical system, usually expressed in mathematical, physical and graphical forms. A model facilitates the understanding of the system and provides a tool to simulate or predict its behaviour given certain conditions. When the phenomenon or system to be modelled is complex, a totally comprehensive representation of its functioning is often impossible; as a consequence, usually a model shows a certain level of simplification that is chosen with respect to the purposes it is built for.

Both on research and industry level, effective mathematical PV modelling has gained crucial importance for different reasons and purposes:

- for installers, to evaluate the economic feasibility of a PV system [7], select the most suitable module [8] and then check its status and operativity [4];
- for designers, to predict the performance of a PV system under any weather condition [8, 9, 10];
- for manufacturers, to optimize the fabrication process through the identification of the model parameters [11], especially if these can be determined simply and rapidly [12];
- for researchers, to better understand the physics of a PV cell through the proper interpretation of the model parameters;
- for power electronics engineers, to design efficiently the power inverters through the study of their dynamic behaviour [6, 13, 14];
- for engineers, to simulate the behaviour of Maximum Power Point Trackers (MPPT) [15, 16].

After all, it is well known that predictive performance tools such as models are an important factor in the success of any technology [7]. However, building a PV model that responds accurately and conveniently (i.e., in a reasonable time) to varying ambient conditions (mostly irradiance and temperature) is not straightforward due to the underlying physics and the complex mathematical formulations that describe it. In general, if several experimental measurements can be carried out, the task is made much easier as the goodness of the model can be tuned and validated through real data fitting. Unfortunately, this possibility is not so common as it is a prerogative of research environments. On the industry-commercial level (where the impacts of any improvement are amplified), instead, accurate modelling becomes more complicated. The main reason is that module manufacturers provide performance data only for specific fixed environment conditions, i.e. the Standard Test Conditions (STC) and, sometimes, also for the Nominal Operating Cell Temperature (NOCT) [10] (see Paragraph 2.3 for further details), making it harder to tune multiple-DoF (degrees-of-freedom) systems such as PV models.

For the last decades, different theoretical approaches and numerical methods have been used to develop simulation models and parameters extraction techniques [15]. However, unfortunately, an entirely accurate benchmarking is somewhat elusive since researchers test their models with respect to different PV systems (applied technology, size, location, etc) [11]. The aim of this work is to give a panoramic view on the PV models available in literature, with a novel structure not found (to the knowledge of the author) in any previous review: if the usual approach is pivoted around the *models* themselves, at the core of this work is the effort to provide a reference framework in which the *methodologies* are homogeneously presented and discussed. To prove the importance of a careful choice of such modelling strategies, the most used model is implemented in a software environment, investigated and tested with experimental data.

1.4 Methodology and Structure of the Work

An extensive literature review is at the basis for building the proposed framework, which is presented throughout Chapter 2. In Paragraphs 2.1 and 2.2, the basics of PV modelling are presented, providing a direct correlation between the physical background, the mathematical equations, their graphical representation and the electrical equivalent circuit. These elements constitute the various aspects of a PV model. The main quantities that define it are the *model parameters*, i.e. unknown physical quantities that need to be determined to give mathematical consistency to the model: the methods to *extract* these parameters with only the commercially-available data are presented in 2.3. This parameter extraction is performed at Standard Test Conditions (STC); however, most of the time PV devices operate at different operating conditions than STC. For this reason, the algorithms to account for the effect of the varying irradiance and cell temperature are presented in 2.4. Chapter 2 ends with a review of the performance indices to evaluate the goodness of a model.

In Chapter 3, each model found in literature is presented and discussed in the light of the study conducted in Chapter 2 and a comparison between them is carried out in Chapter 4.

In order to show the importance of the choice of the modelling strategy, thus giving a practical example of application of the proposed framework, two models are implemented and tested: in Chapter 5 they are presented along with a detailed analysis of the behaviour of the parameter extraction algorithm, and in Chapter 6 the models are validated through comparison with experimental data.

The final considerations about the subject are presented in Chapter 7 along with the insights that emerged from the evaluation of the proposed models and strategies. Additionally, possible directions for future work are suggested.

2 PV Modelling Framework

2.1 The I-V Curve and the $I(V)$ Equation

As highlighted at the end of Paragraph 1.2, at the core of a PV cell is the p-n junction or, in other words, a diode. The behaviour of of a diode is described by the *Shockley diode equation* [1]:

$$I_d = I_s \left[e^{\left(\frac{qV_d}{ak_BT_d}\right)} - 1 \right] \tag{2.1}$$

where:

- I_d is the current through the diode,
- I_s is the reverse saturation current,
- q and k_B are physical constants (see Table 2.1),
- T_d is the temperature of the diode,
- a is the diode ideality factor,
- V_d is the voltage across the diode.

It is convenient to introduce a quantity, called *thermal voltage* V_{th}, defined as:

$$V_{th} = \frac{k_B T_c}{q} \tag{2.2}$$

so that the Shockley diode equation (2.1) is written more concisely as:

$$I_d = I_s \left[e^{\left(\frac{V_d}{aV_{th}}\right)} - 1 \right] \tag{2.3}$$

It must be noted that few authors [10, 15, 17] choose to include the ideality factor in the definition of the thermal voltage. In this work, the ideality factor is kept separated in order to evaluate its characteristics and behaviour independently and more explicitly. Expression (2.2) is valid for a single cell; for a panel with N_c cells connected in series, the thermal voltage becomes [10]:

$$V_{th} = \frac{k_B T_c}{q} N_c \tag{2.4}$$

It is worth mentioning that the physical equations have been developed on a cell scale and when scaling up to panels and arrays, certain quantities such as the temperature and the irradiance are implicitly considered uniform across the whole active surface. However, this may not be always the case especially when dealing with arrays; for panels the assumption proves to hold true [14].

From the physical analysis of PV cell, the general expression for the current I delivered by the cell is derived and given by [1]:

$$I = I_{SC} - I_{s1} \left[e^{\left(\frac{V}{V_{th}}\right)} - 1 \right] - I_{s2} \left[e^{\left(\frac{V}{2V_{th}}\right)} - 1 \right] \tag{2.5}$$

where:

- I_{SC} is the short-circuit current,
- T_c is the temperature of the cell,
- V is the voltage at the terminals of the cell.

One can notice that in (2.5) the Shockley equation of *two* diodes appear; the reasons for this will be discussed in the next Paragraph. The saturation currents (usually in the order of 10^{-5} or 10^{-6} A [18, 19]) and are given by rather complex expressions that depend on the solar cell structure (e.g. surface, thickness), material properties (e.g. doping density, surface recombination, minority-carrier diffusivity, etc) and operating conditions (e.g. irradiance and temperature). However, a detailed examination of these terms and their physical meaning is not necessary if one just wants to learn about the solar cell operation [14]. In fact, for this purpose, the mathematical form of Equation (2.5) is sufficient to deduct fundamental information about the PV device.

Table 2.1 Physical constants involved in the PV modeling

Quantity	Symbol	Value
Boltzmann Constant	k_B	1,380649 · 10^{-23} JK^{-1}
Electron Charge	q	1,602177 · 10^{-19} C

It is convenient to represent Equation (2.5) on a cartesian plane where the cell voltage V is plotted on the x-axis and the cell current I is plotted on the y-axis. Figure 2.1 shows the result of such plotting: the represented $I(V)$ curve is usually addressed as “I-V curve” or more simply “IV curve”.

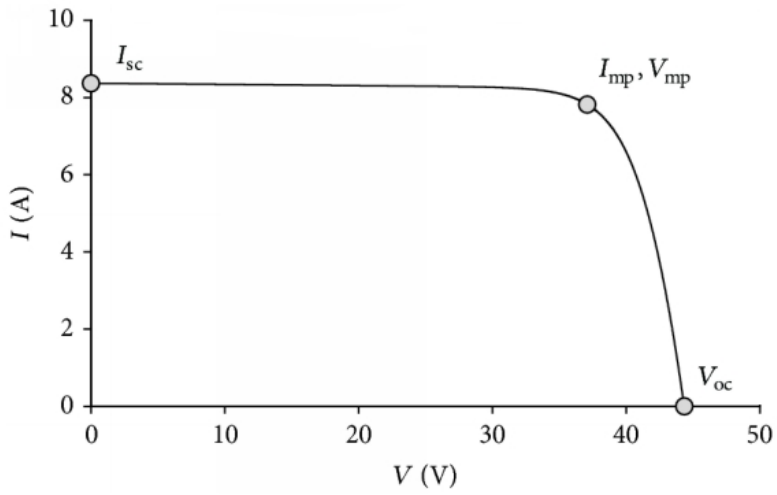

Figure 2.1 The I-V curve plotting the cell current I as function of V

In Figure 2.1 three important figures of merit, also called “three remarkable points” (TRP), are highlighted:

- the *Short-Circuit point* $(0, I_{SC})$, i.e. when the cell is short-circuited as no voltage-dropping load is connected;

- the *Maximum Power Point*, MPP or simply "mp" (V_{MPP}, I_{MPP}), representing the operating conditions for which the maximum power P_{MPP} is extracted from the cell;
- the *Open Circuit point* $(V_{OC}, 0)$, i.e. when the terminals of the cell are not connected and no current is flowing.

At small voltages, the diode current is negligible and the current flowing through the cell is just the short-circuit current, as can be seen when V is set to zero in Equation (2.5). When the applied voltage is high enough, the current flowing through the diodes becomes significant and the net solar cell current drops quickly. This is the reason why the I-V curve shows a characteristic knee-shape around the MPP. The MPP is also of particular interest because it represents the operating (V, I) pair for which the maxium power is extracted from the cell. Given the main purpose of any PV device, i.e. power conversion, often the I-V curve is accompanied by the P-V curve, that is the graph of the power function $P(V) = VI$. Figure 2.2 shows the two curves plotted on the same plane: as expected by definition, the MPP represents the maximum point of the P-V curve.

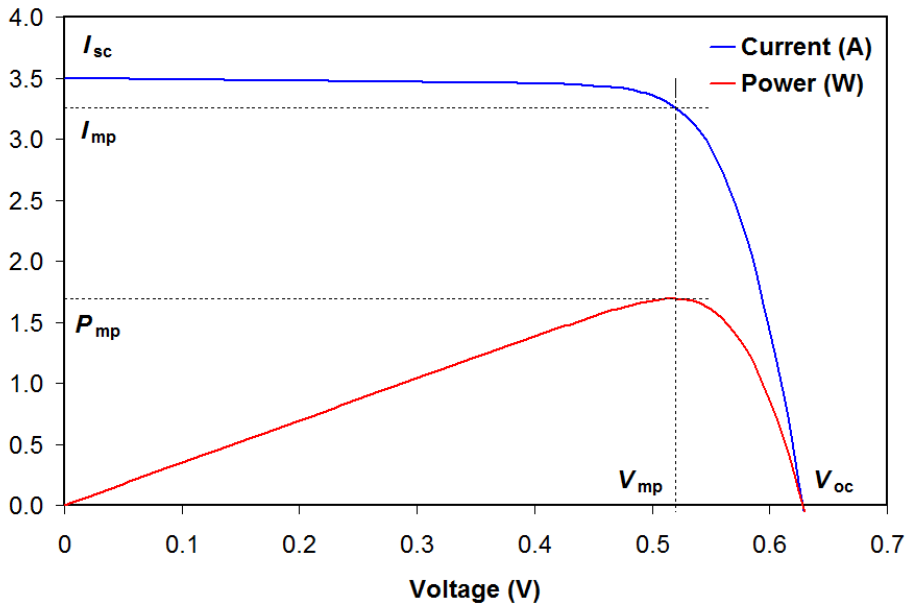

Figure 2.2 Current (blue) and power (red) versus voltage

Ideally, a PV device would convert all the current generated by the incoming photons (i.e. the photocurrent I_{ph}) into usable electric current. However, unavoidable losses occur during the power extraction due to non-idealities. Figure 2.3 shows the graphic representation of such mechanism, providing an interpretation of the shape of a general I-V curve.

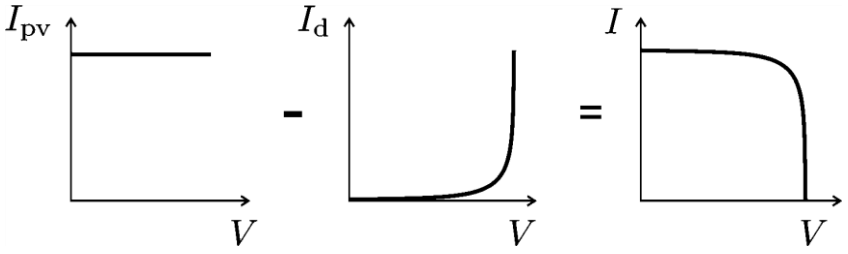

Figure 2.3 The net output current I is not equal to the photocurrent I_{pv} because of the (diode) losses I_d [6]

In fact, Equation (2.5) can be written as:

$$I = I_{ph} - I_{loss} \tag{2.6}$$

with:

$$I_{loss} = \sum_{n=1}^{2} I_{sn}\left[e^{\left(\frac{qV}{nk_BT_c}\right)} - 1\right] \tag{2.7}$$

This means that from a circuital point of view a PV device acts as a current source as long as the *forward bias* of the equivalent diode(s) is not reached, and then *tends* to act as a voltage source once the current starts to be drained through the diode(s); however, the latter case is a strong approximation (see Figure 2.4).

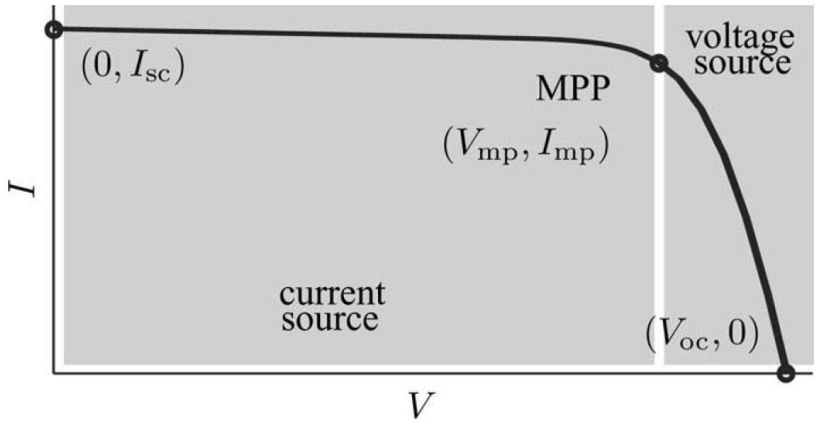

Figure 2.4 Hybrid current/voltage source behaviour [6]

Therefore, a fundamental non-ideality of a PV device is the valve-like behaviour of the p-n junction which is due to its intrinsic diode-nature: for this reason, the natural modelling of a PV device consists of a current source in parallel with two diodes:

$$I = I_{ph} - I_{d1} - I_{d2} \tag{2.8}$$

In the next Paragraph, the diode-based modelling is introduced along with other non-idealities.

2.2 Introduction to the Diode-Based Models

According to Kirchhoff's Law of Currents (KCL), Equations (2.5) and (2.8) represent the equivalent electrical circuit shown in Figure 2.5.

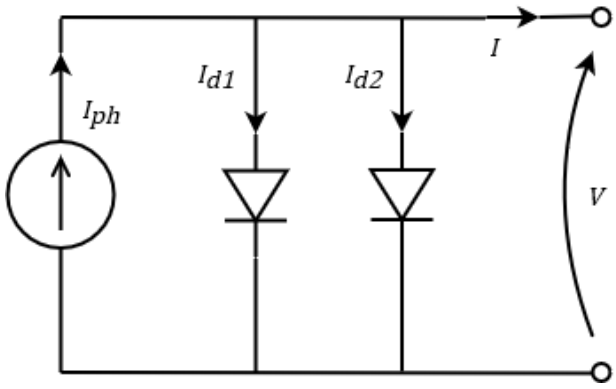

Figure 2.5 Equivalent circuit of Equation (2.8)

Two diodes are present because each of them represents two regions of the cell with different current transport mechanisms: the crystalline region, where *charge diffusion* occurs, and the grain boundary region, where *charge recombination* occurs. In fact, the saturation current of a PV cell is the linear superposition of these two currents.

However, the model shown in Figure 2.5 is practically never used because the presence of two diodes (hence two exponential terms) represents a computational complexity that loses meaning if other physical complexities are not accounted for. In fact, other losses occur during PV cell operation that have a greater impact than that of the distinction between diffusion and recombination currents. For this reason, the simplest PV models feature only one diode whose saturation current and ideality factor are ideally able to account for the effects of both the diodes of Equation (2.5). These models are called "single-diode models" and the simplest of them is the "Ideal Single-Diode Model" (ISDM), featuring only a current source in parallel with a diode. ISDM offers computational advantages however does not account for unavoidable *external* (meaning that are not intrinsic to the p-n junction, as I_d is) losses that can be represented by a lumped series resistance and a lumped parallel (or shunt) resistance: these models are called either "Simplified Single-Diode Model" (SSDM) if only one resistance is present or "Complete Single-Diode Model" (CSDM) if both are used. Figure 2.6 shows how CSDM ("practical PV device") is a natural extension of ISDM ("ideal PV cell").

If both the resistances are allowed in the model, a further step up in the diode complexity is then justifiable: adding a second diode in CSDM one obtains the "Double-Diode Model" (DDM) and if a third diode is added, a "Three-Diode Model" (TDM) is obtained. The third diode accounts for the influence of grain boundaries and leakage current through the *peripheries*. The physical interpretation of the diodes is later reminded in Table 3.1.

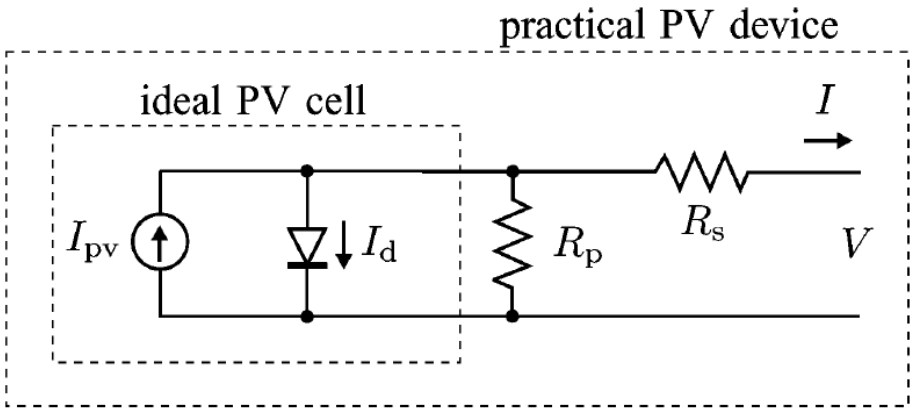

Figure 2.6 Ideal vs real (practical) single-diode models [6]

Each of these diode-based models consists of the equivalent electrical circuit and the related $I(V)$ equation, also called "governing equation" or "characteristic equation"; each of them is presented in detail in Chapter 3. The governing equation features a number of parameters (from 3 up to 9, see Table 2.2), also called "DC parameters" [11], whose values define mathematically the model and characterize physically the device under investigation. The identification of such values is the key step in the model building ("parameter extraction") and in the next Paragraph an overview on the extraction techniques is presented. Once the model is mathematically defined, plotting the I-V curve means solving the characteristic equation $I(V)$ for every $V \in [0, V_{OC}]$ and, in the case the equation is in implicit form (most of the cases), for every $I \in [0, I_{SC}]$. In the latter case, $I = f(V, I)$ therefore a iterative numerical method is used to solve $g(V, I) = I - f(V, I) = 0$ [14].

Table 2.2 General parameters for a diode-based PV electrical model

Symbol	Description
I_{ph}	photocurrent
I_{sn}	reverse saturation current of the n-th diode
a_n	ideality factor of n-th diode
R_s	lumped series resistance
R_p	lumped parallel resistance

Certain model parameters, i.e. the ideality factor and the resistances, deserve a closer look to better understand their meaning and influence on the I-V curve, as shown in the upcoming subsections.

The diode ideality factor a

Given the Shockley diode equation (2.1), a is the *ideality factor* of the diode, also called *quality factor* or *diode constant* and often indicated with "A" or "n". It is characteristic of the semiconductor material of the diode and the manufacturing process it undergoes [9]. The ideality factor is a measure of how closely the diode follows the ideal diode equation, defined for $a = 1$. Defects in the semiconductor are the main reason for a to be higher than 1 [20], with values ranging from 1 at high currents up to 2 at low currents

[21], but in some cases it can be even higher than 2 [11], especially for industrial cells [22]. When the chosen model features only one diode, usually a lays in the range 1-1.5 [6] (see Figure 2.7). The effect of the value of the ideality factor on the I-V curve is illustrated in Figure 2.8 for a SSDM, showing how it affects mainly the knee shape around the MPP, usually referred to as "curvature" of the I-V curve; in [8], the authors pointed out also that its value affects the values of the resistances. The ideality factor is usually used as adjustment parameter to improve the accuracy of the model [6, 7], even though an estimation that is independent from the curve fitting is recommended in [8].

PV technology	n
Si-mono	1.2
Si-poly	1.3
a-Si:H	1.8
a-Si:H tandem	3.3
a-Si:H triple	5.0
CdTe	1.5
CIS	1.5
GaAs	1.3

Figure 2.7 Ideality factor for SDM for various PV technologies [20]

When more than a diode is included in the model, it is important to identify the current transport mechanism of each diode and its domain of action in the solar cell [22]: in general, the diode with $a = 1$ accounts for the diffusion current while that with $a = 2$ represents the recombination current [23].

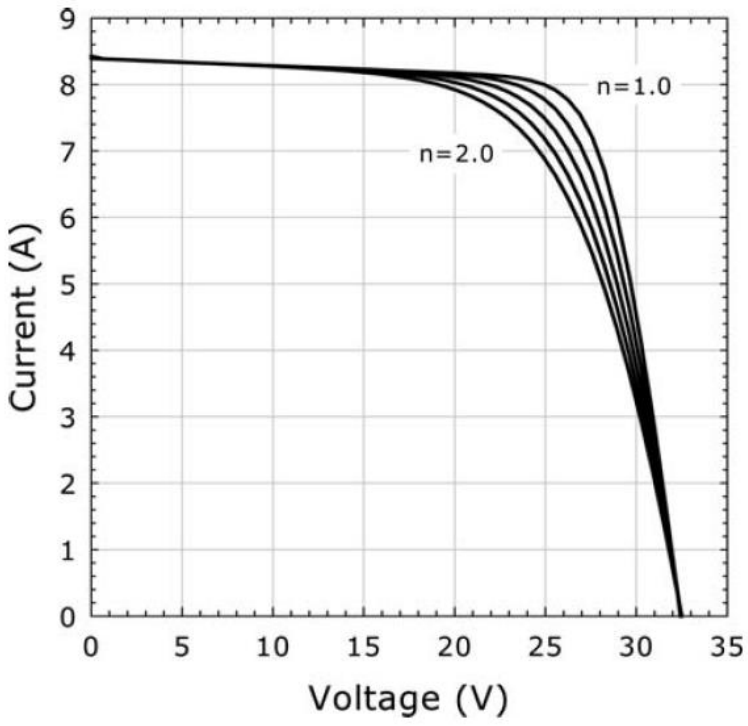

Figure 2.8 Effect of the ideality factor on the I-V curve [20]

The series resistance R_s and the parallel resistance R_p

It is worth highlighting that both the series and parallel resistances do not physically exist [7]. In fact, they represent *lumped* circuit components accouting for phenomena occurring diffusely throughout the cell.

The series resistance R_s represents various mechanisms of ohmic losses that occur along the path of I_{ph}. Mainly, it accounts for the resistivity of [6, 15]:

- the semiconductor material that is not heavily doped;
- the metal grid and the contacts;
- current-collecting wires;

and usually it is found to be lower than 1Ω [24].

The lumped parallel resistance R_p accounts for the unavoidable series of shunts (i.e. high-conductivity paths) forming throughout the large area of semiconductor material that constitutes a PV cell [6, 15]; the order of magnitude of its value goes from 10 up to 10^3 Ω [24].

Both R_s and R_p give an indication of the quality of the semiconductor material, in fact often they are used as manufacturing check and test [6, 25].

According to the general circuit theory, the series resistance has a stronger influence when the device operates in the voltage source region, while the influence of the parallel resistance is more evident in the current source region [6, 25] (*cf.* Figure 2.4). These mechanisms are confirmed also by the mathematical interpretation and value extraction of the two quantities; they are discussed more in detailed in the next Paragraph. In particular, the series resistance has a strong influence on the P_{MPP}, and therefore its evaluation gains even more interest. Instead, the influence of the parallel resistance appears to have a minor impact on the I-V curve.

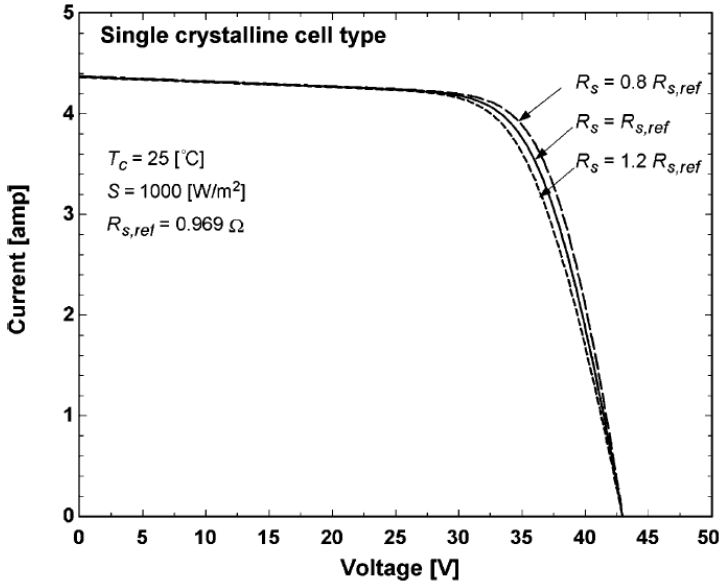

Figure 2.9 Effect of the series resistance R_s on the IV curve at STC [10]

In [9], the authors found that an increase in the series resistance leads to a decrease of the maximum power without affecting the open-circuit voltage nor the short-circuit current (Figure 2.9). Instead, they did not detect significantly noticeable influence of the value of the parallel resistance on the IV characteristics. In [8] the authors found that, when comparing different modules, high values of R_s lead to low values of V_{MPP}, whereas high values of R_p lead to high values of I_{MPP} (Figure 2.10); as a consequence, they deduct that a module with low parallel resistance is unreliable at low irradiance.

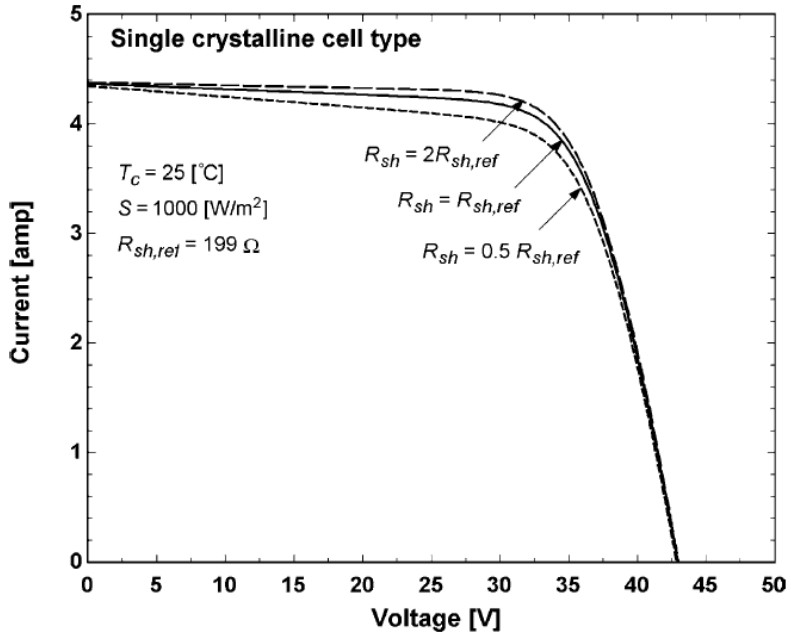

Figure 2.10 Effect of the parallel resistance R_p (R_{sh} in the figure) on the IV curve at STC [10]

2.3 Overview on Parameter Extraction Methods

In order to use a model for simulations or predictions, the model must be mathematically defined, meaning that all the unknown parameters must be identified, i.e. they are given a numerical value. This process is called “parameter extraction” (or identification) and it is crucial since all studies agree that the accuracy of any PV cell model depends mainly on the accuracy of the extracted model parameters [9]. For instance, all the components in the equivalent circuit should be physically realistic, meaning that the corresponding parameters should have a mathematical value that is consistent with the nature of the component (a resistance cannot have a negative value): if this is not true, either the model is not appropriate or significant errors occurred during the extraction [4].

The majority of the parameter extraction methods are based on the features of the I-V curve [9] and they can be classified into two categories: *conventional-analytical* and *metaheuristic* algorithms, where the latter result to be more efficient in dealing with more complicated calculations [23] and are more and more being explored. In this work, metaheuristics have not been considered as the author lacks the background and the competence that are essential to give a trustworthy report on them.

From a mathematical point of view, identifying n parameters means searching the values of n unknowns. Therefore, the main step in parameter extraction consists of setting a number of physically-consistent and analytically-independent constraints equal to the number of the parameters [4, 26]. For instance, five independent equations are needed to be able to find five parameters. These constraints are derived from the I-V curve, by imposing the matching of the modelled curve with the experimental one. If multiple measurements are available, this step is usually sufficient to recover the model parameters (even when they are several). However, as already pointed out in Paragraph 1.3, usually only a limited set of information is commercially-available, and in order to build solid yet widely-applicable methods, authors choose to rely only on this little information [16]. In this scenario, I-V matching is sufficient to recover the parameters only for the simplest models. In fact, since the maximum number of constraints that can be set is limited, for the models of main interest, i.e. those with a medium-high level of complexity, the solving system of equations results to be dependent. In these cases, *iterative* numerical methods and weighted initial guesses on parameters are employed to search for (only) an approximated solution.

Table 2.3 Typical set of STC information provided by the manufacturer (Amerisolar AS-6P30 [27])

ELECTRICAL CHARACTERISTICS AT STC	
Nominal Power (P_{max})	240W
Open Circuit Voltage (V_{OC})	37.7V
Short Circuit Current (I_{SC})	8.57A
Voltage at Nominal Power (V_{mp})	29.9V
Current at Nominal Power (I_{mp})	8.03A
Module Efficiency (%)	14.75

In

Table *2.3* a typical set of data provided by the PV manufacturer is shown: one can notice how little information is given, that is only the values of the three remarkable points (TRP) at the Standard Test Conditions (see Table 2.4); it is also possible to find the same set of values for the Nominal Operating Cell Temperature (NOCT), making for a second useful set of data. It is not impossible that some manufacturers provide also full I-V curves for different irradiance and temperature conditions, making for a precious amount of data for tuning and validation [6], but it is extremely rare.

Table 2.4 Standards for photovoltaics

Quantity	**STC**	**NOCT**
Irradiance	1000 Wm^{-2}	800 Wm^{-2}
Cell Temperature	25 °C	-
Ambient Temperature	-	20°C
Air Mass	1,5	-
Wind Speed	-	1 m/s

The STC information provided by the manufacturer allow to set up to four cartesian constraints on the parameterized I-V curve of the chosen model:

1) matching at the short-circuit point $(0, I_{SC})$:

$$I(0) = I_{SC} \tag{2.9}$$

2) matching at the open-circuit point $(V_{OC}, 0)$:

$$I(V_{OC}) = 0 \tag{2.10}$$

3) matching at the Maximum Power Point (V_{MPP}, I_{MPP}):

$$I(V_{MPP}) = I_{MPP} \tag{2.11}$$

4) first derivative of the power P calculated in MPP equal to zero:

$$\left.\frac{dP}{dV}\right|_{V=V_{MPP}} = 0 \tag{2.12}$$

The last constraint derives from the mathematical definition of the MPP, i.e. the global maximum of the power curve. Considering that $P(V) = V \cdot I(V)$, the left-hand side of (2.12) can be written as [4, 26, 28]:

$$\frac{dP}{dV} = \frac{d}{dV}(VI) = I + V\frac{dI}{dV} \tag{2.13}$$

and substituting (2.13) in (2.12), the fourth constraint can be expressed in terms of I and V as:

$$\left.\frac{dI}{dV}\right|_{V=V_{MPP}} = -\frac{I_{MPP}}{V_{MPP}} \tag{2.14}$$

Equations (2.12) and (2.14) are equivalent and authors use either one or the other. It is worth noting that in [28] the authors make a distinction between the two equations including them both in the solving system of their *five*-parameter model (CSDM), thus obtaining exact analytical solutions (*five* equations): despite the computation did not highlight the issue (the equations led to infinitesimal yet different residuals), this is a conceptual error and it must be avoided. Figure 2.11 shows the graphical interpretation of Equations (2.12) and (2.14), i.e. the slope m of the tangent at the MPP in the P-V plane ($m = 0$) and in the I-V plane $\left(m = -\frac{I_{MPP}}{V_{MPP}}\right)$, respectively.

Usually, these equations are written in normal form:

$$f_i(\boldsymbol{X}) = 0 \tag{2.15}$$

where $\boldsymbol{X}$ is the vector of the unknowns, i.e. the model parameters.

Any system of equations derived from the aforementioned constraints is:

1) *nonlinear,* due to the presence of one or more exponential terms

2) *implicit,* since so are the equations (except for two models, *cf* Paragraph 3.2).

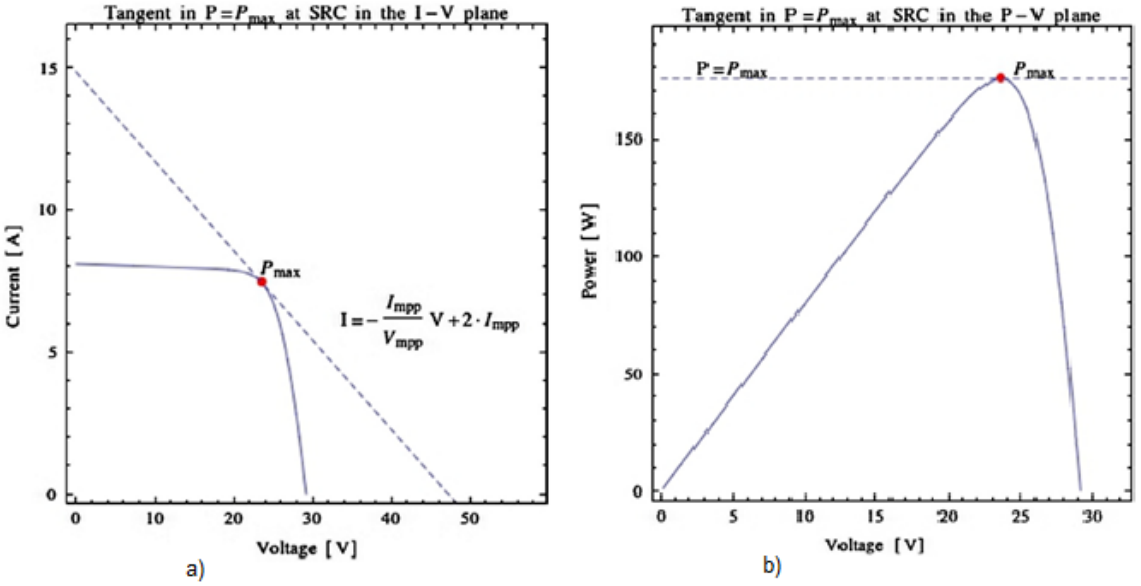

Figure 2.11 (a) Graphical interpretation of Equation (2.14) with the full equation of the tangent and (b) graphical interpretation of Equation (2.12) [28]

For these reasons, numerical *iterative* methods need to be employed to solve these systems; the most used are [4, 28] (see Appendix A.1 for further details):

1) the Newton-Raphson method (NR),

2) a manual trial-and-error routine;

3) the Bisection method.

NR and the Bisection method both need an initial guess and the latter is simpler but converges more slowly than the former; however NR method might not converge at all if the initial guesses are too far from the actual solutions [12, 28].

In [28], Lo Brano et al. suggest to transform the system solution problem in a constrained nonlinear optimization problem. Given the objective function:

$$\Gamma(\boldsymbol{X}_n) = \sum_{i=1}^{n} f_i^2(\boldsymbol{X}_n) \tag{2.16}$$

where $\boldsymbol{X}_n$ is the general vector of the n unknown parameters and $f_i(\boldsymbol{X}_n)$ is the generic implicit function obtained from the solving equations (i.e., constraints) rewritten in the form (2.15), $\Gamma(\boldsymbol{X}_n)$ is fed to a local-minimum finding algorithm given any initial arbitrary value for the n parameters. Usually, this kind of algorithm is based on Generalized Reduced Gradient and is already implemented in any spreadsheet software. Brano et al. claim this approach is more robust, faster and easier than any other numerical method, as it does not need *ad hoc* coding and it is not so sensitive to the initial guesses.

Finally, most common numerical computing softwares such as MATLAB, Python or MS Excel, usually provide a choice for already built-in nonlinear solvers.

Constraints (2.9)-(2.12) are sufficient to determine up to four parameters; for the models featuring more than four parameters, i.e. the most accurate ones, a strategy must be chosen. The main options are:

1) reducing the number of parameters by making weighted assumptions (common in models with several parameters);
2) finding an approximated solution by iterating on initial guesses (common in five-parameter models);
3) setting additional I-V constraints based on the graphical interpretation of the resistances (see next subsection).

Obviously, a mix of the above is also possible.

Sometimes, simplifications are introduced in order to make equations simpler (in some cases they become explicit) thus computations lighter and faster. The two most common simplifications are:

1) photocurrent equal to short-circuit current since the series resistance is usually very low in value [4, 6, 18, 26]:

$$I_{ph} \sim I_{SC} \tag{2.17}$$

or, alternatively [8]:

$$I_{ph} \sim I_{SC} + \frac{I_{SC} R_s}{R_p} \tag{2.18}$$

2) "-1" neglected in the exponential of the Shockley diode equation (2.1), mainly at open-circuit conditions.

Other simplifications are presented throughout Chapter 3.

The third strategy option (graphical interpretation of the resistances) is discussed in the subsection below and it is found to be used also in substitution of the fourth constraint for some four-parameter models.

Once the model parameters are initially determined at STC, the model needs to be further developed to account for the dependence of the parameters on the operating conditions (mainly temperature and irradiance), which is the object of the next Paragraph.

About the resistances R_s and R_p

Few authors have proposed mathematical approaches to determine the resistances independently from the other model parameters; however, in general an evaluation based on experimental data proves to be more reliable [25].

It is possible to approximate the series and shunt resistances from the slopes of the I-V curve at V_{OC} and I_{SC}, respectively (see Figure 2.12) [29]:

$$\left.\frac{dI}{dV}\right|_{V=V_{OC}} \sim -\frac{1}{R_{s0}} \tag{2.19}$$

$$\left.\frac{dI}{dV}\right|_{V=0} \sim -\frac{1}{R_{p0}} \tag{2.20}$$

and use these relations as further constraints [12]. Theoretically, the value of the parallel resistance can be derived even when the cell is not illuminated and power is sourced to the cell since the slope of the curve remains the same. However, in reality, the value of R_p is sensitive to the amount of light hitting the solar cell [30], becoming a key factor at very low irradiance levels [22]. Moreover, R_p is also found to be linked to the position of the MPP to the point that in [14] the authors found this relation to be more reliable in terms of simulation results.

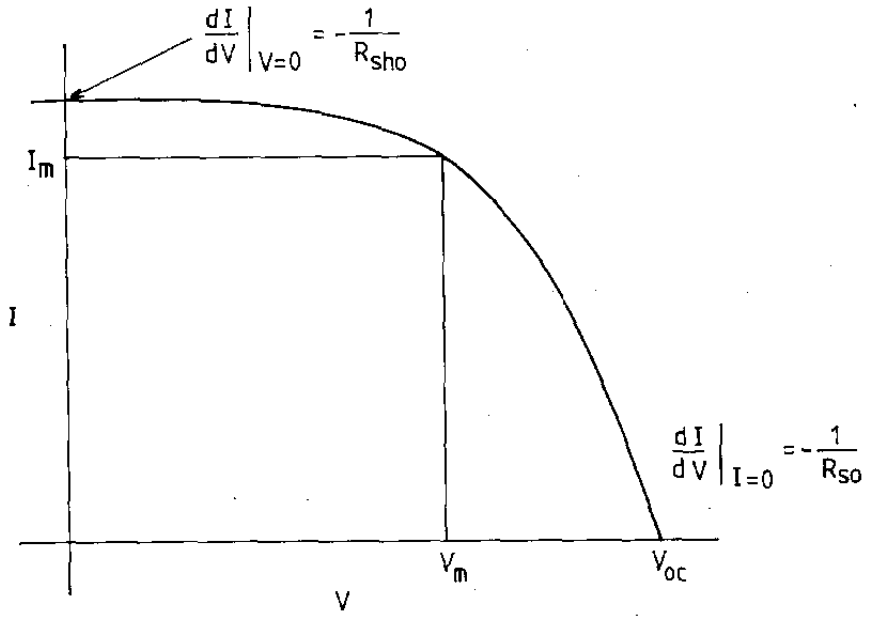

Figure 2.12 Graphical interpretation of series resistance (R_{s0}) and parallel resistance (R_{sh0}) [12]

Some authors suggest to tune the two resistances *separately*, varying R_s in an iterative process until the I–V curve visually fits the experimental data, and then vary R_p in the same way. This is considered a quite poor and inaccurate fitting method, mainly because the resistances should be tuned *simultaneously* if a consistent I-V curve is desired [6]: Villalva et al. suggest to find the "right" pair (R_s, R_p) by matching the MPP in the P-V curve (i.e. by setting Equations (2.11) and (2.12)).

2.4 Dependence on Irradiance and Cell Temperature

A single I-V curve, along its mathematical equation $I(V)$, represents the behaviour of a PV device only for well defined operating conditions, mainly irradiance, cell temperature. However, during normal operation, these conditions vary significantly depending on orientation, location, season, time of the day, cloudiness, dirt, etc. Figure 2.13 shows how greatly the I-V curve of a PV device can vary during a cloudy and a sunny day.

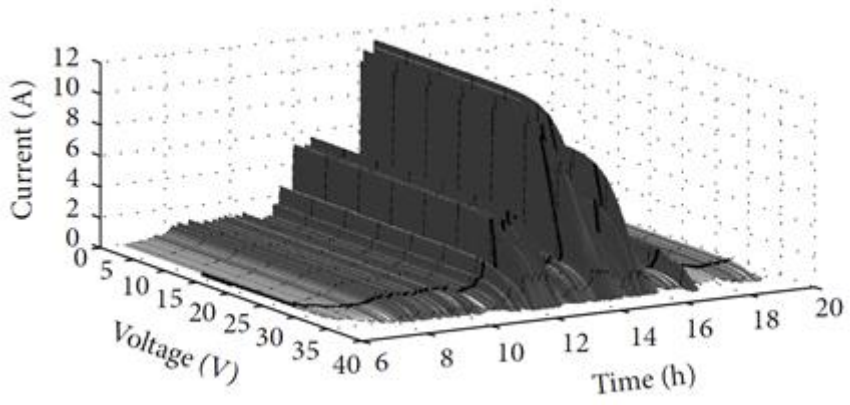

Figure 2.13 I-V curves variation during a cloudy day [29]; the bold line tracks the MPP

Figure 2.14 and Figure 2.15 show the sensitivity of the I-V curve with respect to irradiance and temperature taken separately.

As regards irradiance, the main contribution is given by the photocurrent and this has a clear physical meaning: the more the number of photons hitting the panel (i.e. the irradiance) the more the light-generated current (assuming the spectral distribution does not change). Since this current corresponds mainly to the short-circuit current (*cf.* Equation (2.17)), as the irradiance decreases the curve shifts downwards to lower values of I_{SC}. Consequently, also the (maximum) power delivered and the general performance degrade. Voltage is generally less affected by variations in irradiance.

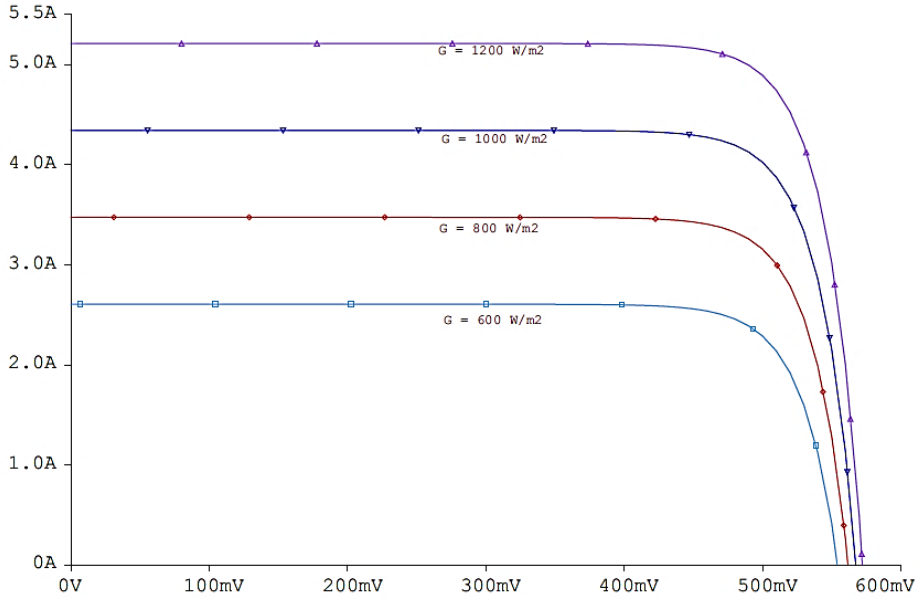

Figure 2.14 Effect of the irradiance G on a computed I-V curve [15]

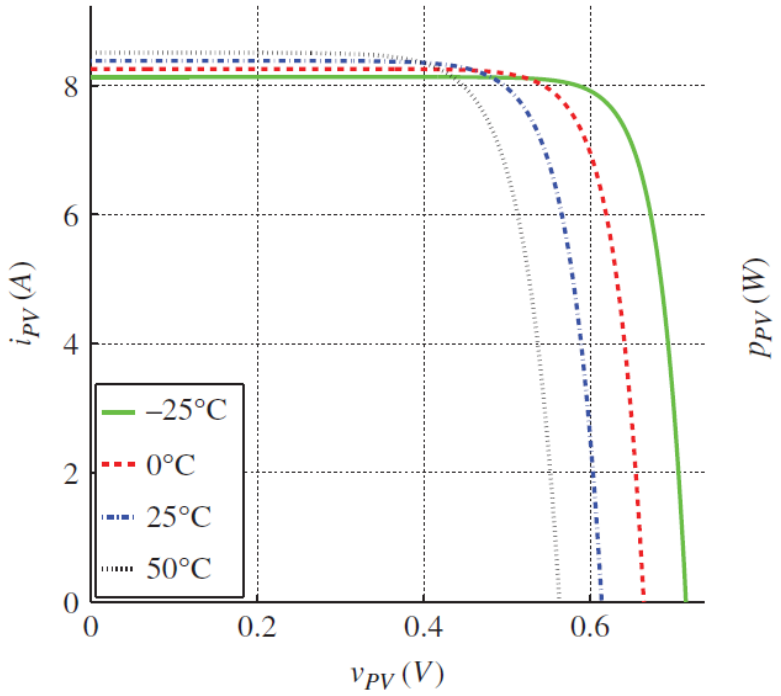

Figure 2.15 Effect of the cell temperature T_c on a computed I-V curve [4]

As regards the (cell) temperature, as it increases, the open-circuit voltage decreases more than the short-circuit increases, leading to a decrease of P_{MPP} and an overall deterioration of the performance (more current is drained through the diode(s)). The reason behind this behaviour lies in the reduction of the bandgap energy of the semiconductor: on the one hand, this means that a larger portion of the incoming photons (photons with lower energy) is involved in the generation of the photocurrent (higher short-circuit current) but on the other hand, a lower bandgap energy implies also higher carrier concentrations that are responsible for the current draining through the diode (the saturation current increases and the open-circuit voltage drops).

Using the data usually provided in the product datasheet allows to extract the model parameters valid *only* when the Standard Test Conditions are met. Therefore, in order for the model to have a theoretical meaning and practical usefulness, it must respond accurately to variations in both solar irradiance G and cell temperature T_c. All the model parameters are affected from changes in irradiance and temperature, even though some are influenced more than others, e.g. the saturation current I_s is heavily dependent on temperature whereas the photocurrent I_{ph} varies significantly with irradiance. Mainly, there are two approaches to evaluate the (G, T_c)-dependence of the model parameters:

- a *theoretical* approach, using equations derived from the physics of the cell;
- an *experimental* approach, using experimental coefficients provided by the manufacturers (this is also the procedure recommended in the International Standard IEC 891).

The former is used mainly in physics research studies whereas the latter finds more interest in the engineering and commercial applications since it provides better results with respect to the purposes. In most cases, a combination of the two approaches is used. The experimental coefficients are called

"temperature coefficients" and express the variation per unit of temperature increase of the three remarkable points (see
Table *2.5*):

- α_T (or K_I) for the short-circuit current,
- β_T (or K_V) for the open-circuit voltage
- γ_T for the power at MPP.

Some manufacturers report also the temperature coefficients for I_{MPP} and V_{MPP} (in the case only one of these is given, the other can be easily derived from γ_T) and some others include also the *irradiance* coefficient on voltage ν_T; unfortunately, these cases are not the standard.

These coefficients can be found in terms of *relative* variation (%/°C) or others *absolute* variation (e.g. V/°C for the voltage); hereinafter relations are developed assuming they are provided in the relative form; formulations for absolute form are derived easily.

Table 2.5 Temperature coefficients provided by the manufacturer (Amerisolar AS-6P30 [27])

TEMPERATURE CHARACTERISTICS	
Temperature Coefficients of P_{max}	-0.43%/°C
Temperature Coefficients of V_{OC}	-0.33%/°C
Temperature Coefficients of I_{SC}	0.056%/°C

It is to be noted that γ_T is always negative, confirming what observed earlier i.e. that the overall performance of the cell decreases with increasing temperature.

In the following, the influence of irradiance and temperature is discussed more in detail, differentiating between three remarkable points and model parameters (a summary is made in Table 2.6). The subscript "ref" indicates known quantities; usually these are the STC values.

Later, the methods to implement these correlations into the chosen model are discussed.

Table 2.6 Level and type of influence of irradiance and temperature on the TRP and the parameters

Quantity	**Dependence on Temperature**		**Dependence on Irradiance**	
I_{SC}	low	linear direct	high	linear direct
P_{MPP}	high	inverse	high	linear direct
V_{OC}	high	inverse	low	nonlinear direct
I_{ph}	low	linear direct	high	linear inverse
I_s	high	nonlinear direct	-	-
a	medium	linear inverse	-	-
R_s	medium	linear direct	-	-
R_p	high	nonlinear inverse	-	-

2.4.1 Dependence of the Three Remarkable Points

1) The Short-Circuit Current I_{SC}

The short-circuit current varies according to [4, 6, 21, 28, 17]:

$$I_{SC}(G,T) = \frac{G}{G_{ref}} I_{SC,ref}\left[1 + \alpha_T\left(T_c - T_{c,ref}\right)\right] \tag{2.21}$$

Since α_T is defined positive, the short-circuit current varies in the same direction as the cell temperature does. This can be due to the increased light absorption (semiconductor bandgaps tend to decrease with temperature) and increased diffusion lengths of the minory carriers [1]. However, the effect of the irradiance is much greater than that of the temperature (see Figure 2.20-c); in fact, values for α_T are generally really low (in the order of 10^{-3}) so that some authors choose to set it to zero and consider the short-circuit dependent only on the irradiance [18].

2) The Maximum Power Point

Paradoxically, the MPP is the point that is given less information about its dependence on the operating conditions. Usually the temperature coefficient on P_{MPP} is provided but those on I_{MPP} and V_{MPP} are rarely found. They update the respective quantity in a similar manner as I_{SC} and V_{OC}:

$$P_{MPP}(T) = P_{MPP,ref}\left[1 + \gamma_T\left(T_c - T_{c,ref}\right)\right] \tag{2.22}$$

$$I_{MPP}(T) = I_{MPP,ref}\left[1 + \delta_T\left(T_c - T_{c,ref}\right)\right] \tag{2.23}$$

$$V_{MPP}(T) = V_{MPP,ref}\left[1 + \omega_T\left(T_c - T_{c,ref}\right)\right] \tag{2.24}$$

3) The Open-Circuit Voltage V_{OC}

Theoretically, V_{OC} varies with temperature according to [30]:

$$V_{OC}(T) = V_{OC,ref}\left(\frac{T_c}{T_{c,ref}}\right) + E_g\left(1 - \frac{T_c}{T_{c,ref}}\right) \tag{2.25}$$

while the irradiance affects the open-circuit voltage according to:

$$V_{OC}(G) = V_{OC,ref} + \frac{N_c a k_B T_c}{q} ln\left(\frac{G}{G_{ref}}\right) \tag{2.26}$$

The open-circuit voltage falls with increasing temperature but increases with higher irradiance. However, the combined effect of increasing irradiance and consequent increasing temperature is a remarkable drop of V_{OC} because the influence of the temperature is far greater [30].

This behaviour is well modelled by the experimental expression for $V_{OC}(G,T)$:

$$V_{OC}(G,T_c) = V_{OC,ref}\left[1 + \beta_T\left(T_c - T_{c,ref}\right)\right]\nu_T \tag{2.27}$$

where β_T is negative (see Table 2.5) and the irradiance coefficient ν_T is positive. When ν_T is provided, it is given in a table from which a fitting polynomial function can be derived [4]. Figure 2.16 shows an example of such fitting: one can notice the little impact of this coefficient (i.e. the impact of

irradiance on V_{OC}) as it assumes values above 0,9 even for really low irradiances – for this reason often it is omitted ($\nu_T = 1$).

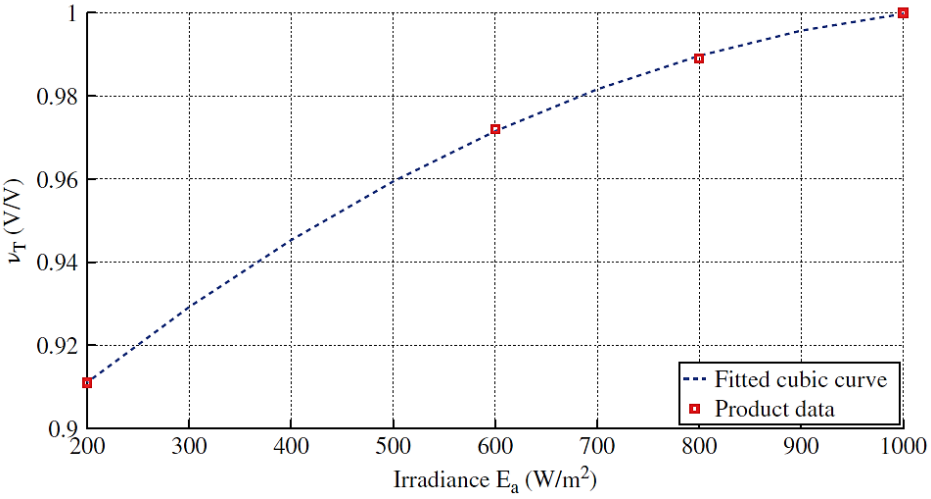

Figure 2.16 Interpolated dependency of ν_T on irradiance [4]

2.4.2 Dependence of the Model Parameters

1) The Photocurrent I_{ph}

As the simplification (2.17) is widely accepted (for ISDM and SSDM-p the approximation is actually an exact equivalence), it results:

$$I_{ph}(G,T_c) = \frac{G}{G_{ref}} I_{SC,ref}\left[1 + \alpha_T\left(T_c - T_{c,ref}\right)\right] \tag{2.28}$$

and the considerations made on the short-circuit apply also to the photocurrent.

2) The saturation current I_s

Also the saturation current varies with temperature (see Figure 2.20-d). Theoretically, its dependence on temperature is given by [6, 8, 18, 31]:

$$I_s(T_c) = D{T_c}^3 e^{-\frac{qE_g}{ak_BT_c}} \tag{2.29}$$

where E_g is the bandgap energy of the semiconductor and the constant D is the *diode diffusion factor* that can be eliminated evaluating $I_{s,ref} = I_s\left(T_{ref}\right)$ (through Equation (2.32)/(2.33)):

$$I_s(T_c) = I_{s,ref}\left(\frac{T_c}{T_{c,ref}}\right)^3 e^{\frac{q}{ak_B}\left(\frac{E_{g,ref}}{T_{c,ref}} - \frac{E_g}{T_c}\right)} \tag{2.30}$$

The bandgap energy shows a weak temperature dependence which can be represented by (for silicon):

$$E_g = E_{g,ref}\left[1 - 0.0002677\left(T_c - T_{c,ref}\right)\right] \tag{2.31}$$

However, only De Soto et al. [10] and Matagne et al. [26] accounted for this dependence whereas other authors considered E_g constant (see Table 2.7).

Table 2.7 Energy bandgap for different PV technologies at STC [10]

PV tech	Si-mono	Si-poly	thin film	a-Si
$\boldsymbol{E_g}$ [eV]	1.12	1.14	1.12	1.6

In the presence of two diodes, a difference can be made between I_{s1} and I_{s2} in (2.29), where for the former $a = 1$ while for the latter $a = 2$ and T_c is elevated to 3/2 instead of 3 [14].

The saturation current is strongly dependent on temperature and it is given by the intrinsic characteristics of the semiconductor, represented by physical parameters such as the coefficient of diffusion of electrons, the lifetime of minority carriers, the intrinsic carrier density, etc. Expressions (2.29)/(2.30) are used often in literature; however, it does not necessarily imply a satisfying match at V_{OC} [6].

Another approach to the saturation current consists in evaluating $I_s(G, T_c)$ from the governing equation $I(V)$ in open-circuit conditions. This is particularly useful for *single-diode* models and represents a simpler and more curve-fitting-oriented approach than (2.30). For SSDM-p and CSDM one can update the saturation current starting from the instantaneous values of $V_{OC}(G, T_c)$ and $I_{ph}(G, T_c)$ [4, 6, 21, 28, 17]:

$$I_s(G, T_c) = \frac{I_{ph}(G, T_c) - \frac{V_{OC}(G, T_c)}{R_p}}{e^{\left[\frac{V_{OC}(G, T_c)}{aV_{th}}\right]} - 1} \tag{2.32}$$

If the model does not feature a parallel resistance (ISDM and SSDM-s), Equation (2.32) becomes:

$$I_s(G, T_c) = \frac{I_{ph}(G, T_c)}{e^{\left[\frac{V_{OC}(G, T_c)}{aV_{th}}\right]} - 1} \tag{2.33}$$

In this approach, it is important not to forget to update also the thermal voltage (*cf.* Definitions (2.2)/(2.4)).

3) The Ideality Factor a

Usually, the ideality factor(s) of the diode(s) is considered temperature-invariant [10]. In reality, it does vary and neglecting its dependence on temperature can lead to model errors [17]. For instance, in [17] and [29] the authors found that the ideality factor of their SSDM-s and CSDM, respectively, decreased with increasing temperature (see Figure 2.17).

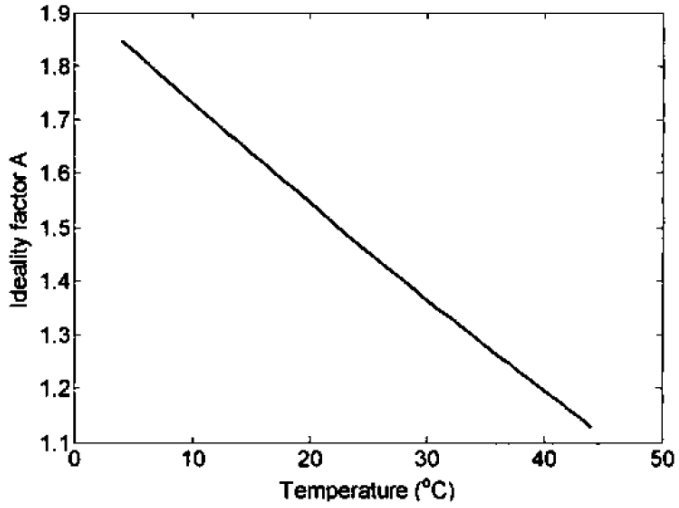

Figure 2.17 Dependency of the ideality factor on cell temperature [17]

As seen in Paragraph 2.2, the ideality factor is strictly connected with the MPP. For this reason, an accurate evaluation of the dependence of a requires complete information on the dependence of V_{MPP}, I_{MPP} on cell temperature through their temperature coefficients;

4) The Resistances R_s and R_p

Like the diode ideality factors, also the resistances are usually considered constant with respect to the cell temperature and irradiance [1, 8, 10]. However this is not true: authors in [29] and [17] found that the series resistance increases with temperature (see Figure 2.18 and Figure 2.20-a) while in [29] and [32] the dependence of parallel resistance on temperature is found to be nonlinear and generally decreasing (see Figure 2.19 and Figure 2.20-b).

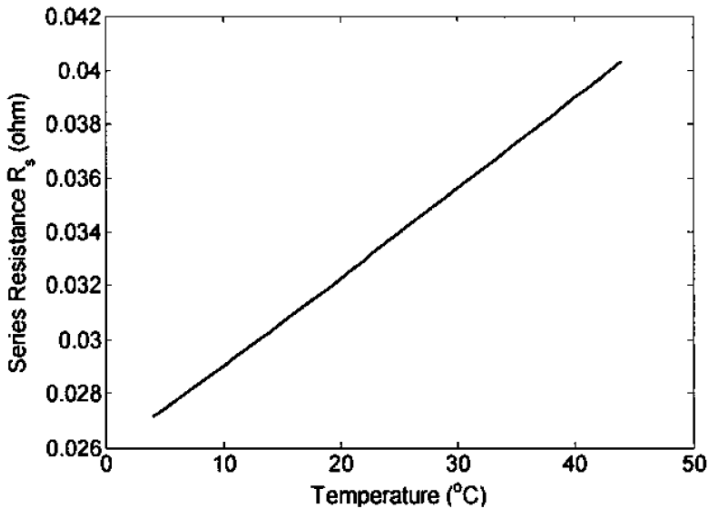

Figure 2.18 Dependence of R_s on temperature in SSDM-s [17]

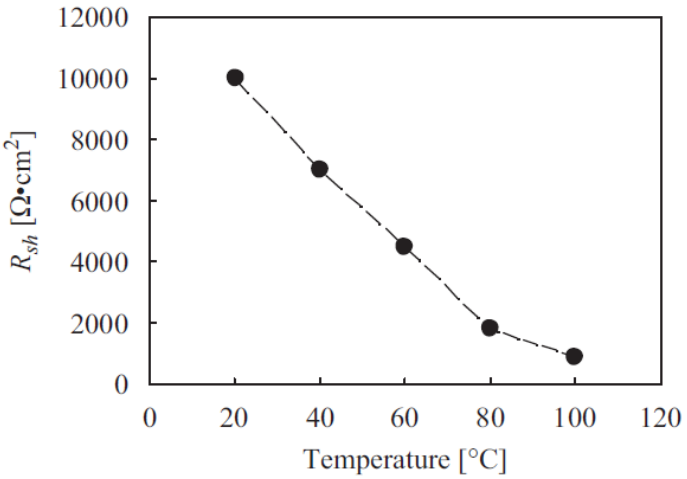

Figure 2.19 Dependence of R_p (R_{sh} in the figure) on temperature in TDM [32]

In [14] and [31] the authors report laws derived from the p-n junction physics:

$$R_s(T_c) = R_{s,ref}\left[1 - K_s\left(T_c - T_{c,ref}\right)\right] \tag{2.34}$$

$$R_p(T_c) = R_{p,ref}e^{-K_p T_c} \tag{2.35}$$

where the coefficients are to be determined experimentally. However,accurate data are required in order to take these effects into account; without them, any additional effort might result meaningless [4].

As regards the influence of irradiance, Lo Brano et al. [7] found that both the resistances of their CSDM are inversely dependent on G and De Soto et al. [10] found the same relation only for R_p, noticing that this effect is more observable in multi-junction cells.

Nevertheless, in [8] it is reported that within the normal operational range of the modules, assuming the resistances independent from temperature does not lead to significant differences in performance results.

In general, the resistances and the ideality factor(s) are considered constant with respect to the operating conditions. This approach is called *Constant-Parameter Modelling* (CPM) by Xiao at al. [17] and it is opposed to the *Adaptive-Parameter Modelling* (APM) that computes R_s, R_p and a for every pair of irradiance and temperature. APM is claimed to lead to significantly better performance with respect to CPM.

2.4.3 Accounting for (G, T_c)-Dependence in the Model Equation

These correlations need to be accounted for in the model equation; two main approaches can be followed, according to the amount of available data:

1) extract the parameters at STC and then update their values independently with the expressions presented in Paragraph 2.4.2; this is the most common approach since it relies on the

information given by manufacturers; the choice of which parameters to consider and which law to use to update them is up to the author and his/her *ad hoc* considerations [4, 7]; often these correlations are used already in the parameter extraction step;

2) perform a parameter extraction for various pairs of temperature and irradiance in order to extract an expression $f_i(G, T_c)$ for each parameter through curve fitting (polynomial or based on the forms presented in Paragraph 2.4.2); this method is less used as TRP coordinates for parameter extraction are evaluated through expressions presented in Paragraph 2.4.1, for which coefficients for MPP are needed but often missing.

In [29], Cubas et al. follow the second approach and extrapolate a polynomial expression for each of their CSDM model parameter as a function of temperature (see Figure 2.20); a is chosen to be temperature-independent. As regards the dependence on irradiance, they assumed that only the photocurrent is affected and update it with Equation (2.21) (with $T_c = const$). The accuracy is claimed to be high since the modelling fits directly the manufacturer's data.

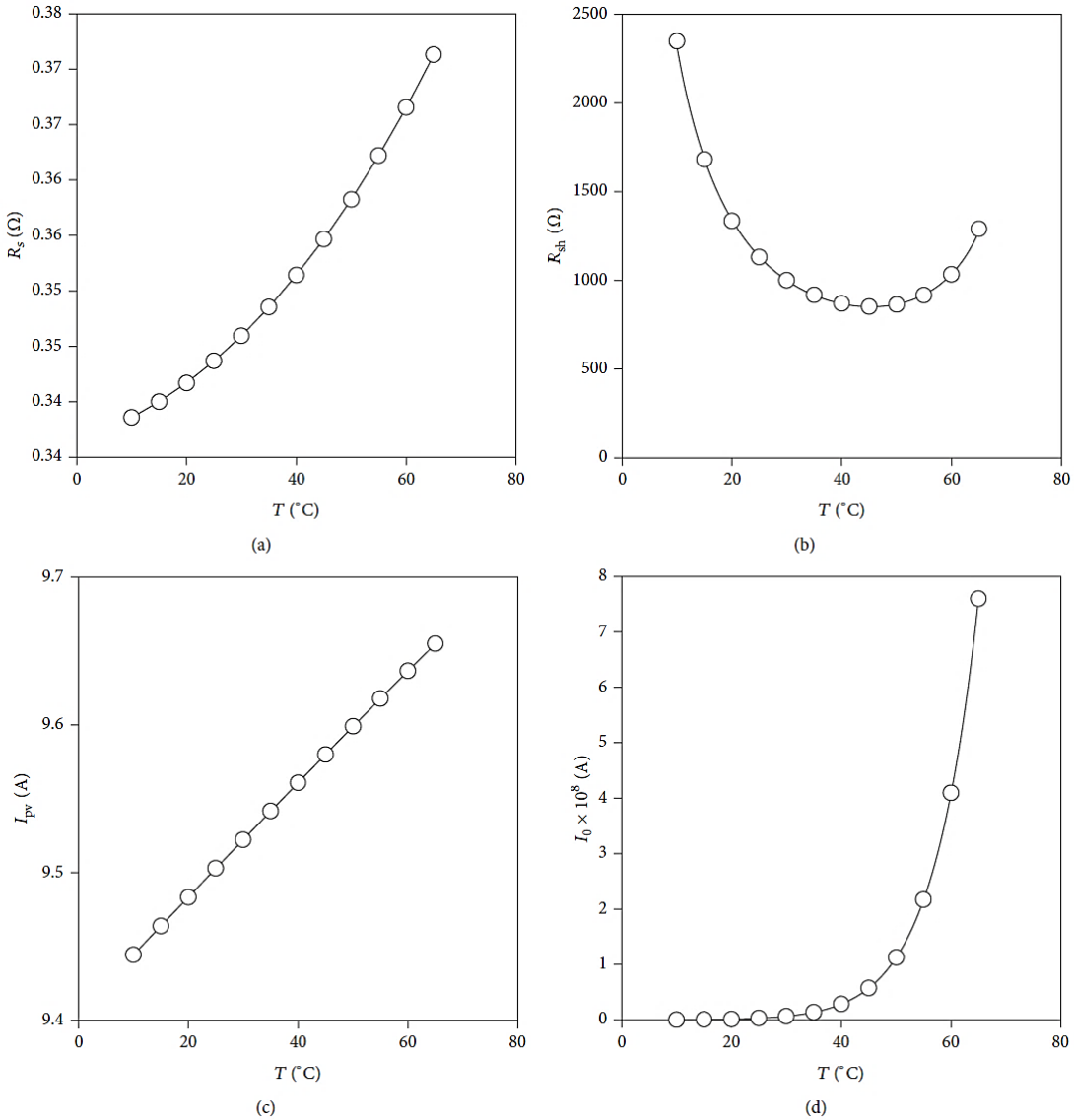

Figure 2.20 Polynomial fit for $R_s(T_c)$, $R_p(T_c)$, $I_{ph}(T_c)$ and $I_s(T_c)$ for CSDM [29]

A similar approach but entirely based on a wide set of experimental measurements (so not applicable if only datasheet data available) is proposed by Hannane et al. in [33] and Habbati et al. in [18]. This method is called Design of Experiments (DoE) and, unlike the methods discussed so far, it is not based on the physical relations between the model quantities. DoE sees the PV device as a black box whose inputs ("factors") and outputs ("responses") are in a mathematical relationship derived solely from experimental data fitting. In the case of PV devices, the mathematical relationship that shows the best fit is a second-grade polynomial [18, 33]:

$$y(G,T_c) = a_0 + a_1 G + a_2 T_c + a_{12} G T_c + a_{11} G^2 + a_{22} T_c^2 \tag{2.36}$$

where the response y is any of the model parameters and the coefficients a_0, a_i, a_{ij}, a_{ii} are the unknowns to be determined from the experimental process. Once $y(G,T_c)$ has been determined for each model parameter, this set of functions can be fed to the chosen model thus enabling it to respond to any pair of operating conditions (G,T_c) in the study domain.

In [18] the authors use this method to compute "only" P_{MPP}, proving that DoE is a useful and simple tool for power predictions as it relates the power directly to ambient conditions, bypassing the model parameters computation. The results show expected trends, i.e. a significant sensitivity of the power to the irradiance versus a low influence of the temperature.

The main drawback of DoE is its statistical nature, meaning that it needs a fairly wide range of measured data for different operating conditions, which usually are not available.

A hybrid approach is followed by Gow et al. in [14] (further details in Paragraph 3.3). Also Humada et al. seem to follow a hybrid approach in [9]. The authors use *only* experimental data to derive expressions for each of the five parameters of their CSDM. These expressions already account for the influence of irradiance G and cell temperature T_c and feature nine experimentally-derived coefficients $C_1 - C_9$; however, the procedure to obtain them is not made explicit and the theoretical background is not clear:

1) $a = \frac{q}{C_1 k_B}$
2) $I_{ph} = (C_2 + C_3 T_c - C_4) G$
3) $I_s = C_5 T_c^3 \exp\left(-\frac{C_6}{T_c}\right)$
4) $R_s = C_7 - \frac{C_8}{T_c} \exp\left(-\frac{T_c}{C_9}\right)$ with $C_7 = R_{s0} = -\left.\frac{dV}{dI}\right|_{V_{oc}}$
5) $R_p = -\left.\frac{dV}{dI}\right|_{I_{sc}}$

It is interesting to notice how these expressions follow closely laws seen earlier in this Chapter, i.e.:

- the dependence of I_{ph} on T_c and G (*cf.* Equation (2.28));
- the dependence of I_s on T_c (*cf.* Equation (2.29));
- the interpretation of the resistances as slopes of the I-V curve;
- the dependence of R_s on T_c.

However, it is not clear if the form of these expressions were set *a priori* or came entirely from the experimental fitting, with the former being more likely to be (they seem to have followed a similar approach to that of Gow et al. in [14]; also, the expressions 4) and 5) resemble closely to the results found by Phang et al. in [24]). In any case, the form of these expressions proved to be a useful and effective approach to the problem of the variation of irradiance and temperature. However, also this method requires an amount of experimental data that is not always available.

Finally, it is worth mentioning that in [26], an attempt to take into account the effects of temperature with a pure mathematical approach was made. Deriving the $I(V)$ expression with respect to temperature, the general thermal behaviour of the cell/model $\frac{\partial I}{\partial T}$ con be made explicit. In the case of the SSDM-s of Matagne et al. [26], the derivative features three new unknowns, that are $\frac{\partial I_{ph}}{\partial T}$, $\frac{\partial I_s}{\partial T}$ and $\frac{\partial R_s}{\partial T}$ (also $\frac{\partial V_{OC}}{\partial T}$ and $\frac{\partial I_{SC}}{\partial T}$ appear, but they correspond to the temperature coefficients taken from the datasheet); however, the constraints applicable to $\frac{\partial I}{\partial T}$ are only two, namely the matching of the open-circuit and short-circuit points (the temperature coefficients of I_{MPP} and V_{MPP} were not provided). As a consequence, the system is dependent and one parameter needs to be arbitrarily chosen: if $\frac{\partial I_s}{\partial T}$ is computed, only the effect of temperature on the saturation current is factored in whereas if $\frac{\partial R_s}{\partial T}$ is chosen, only the effect of temperature on the series resistance is accounted for (this last coefficient proved to have a greater influence on the I-V curve fitting).

2.5 Model Validation and Performance Indices

A good model is a model that is able to predict accurately the performance of the modelled system, i.e. shows an ideally null error when compared with measured data. In the specific case of a PV model, it is desirable that the model is able to fit the experimental I-V curve fully (i.e. for virtually every point of the curve) and does so also under various environmental conditions. Therefore, it is hard to define a single parameter as a reference to evaluate the goodness of the investigated model or compare different models. For these reasons, different performance-evaluating methods can be found in literature and the choice of which of these is more appropriate depends on the specific purpose of the modelling.

It is interesting to note that some of these indices (such as the area error rate) can be also used as target functions for parameter extraction through optimization.

Distance from (or Error on) MPP

When a full I-V set is not available for validation, many authors choose to compare the value of the maximum power P_{MPP} as in many cases it is the main figure of interest. For instance, in commercial applications it is used as a reference to tune the other components of the system, and it is the main target of MPPT optimization algorithms [4]. However, if the fourth constraint has been used to extract the model parameters, i.e. that V_{MPP} is actually the global maximum of the $P(V)$ curve (see Equation (2.12)), then this term of comparison loses its validity as the perfect match at MPP is set by default. For

instance, parameter identification for ISDM does not imply that the MPP is necessarily the maximum of the power function, whereas for SSDM-s it is exactly so (see Figure 2.21).

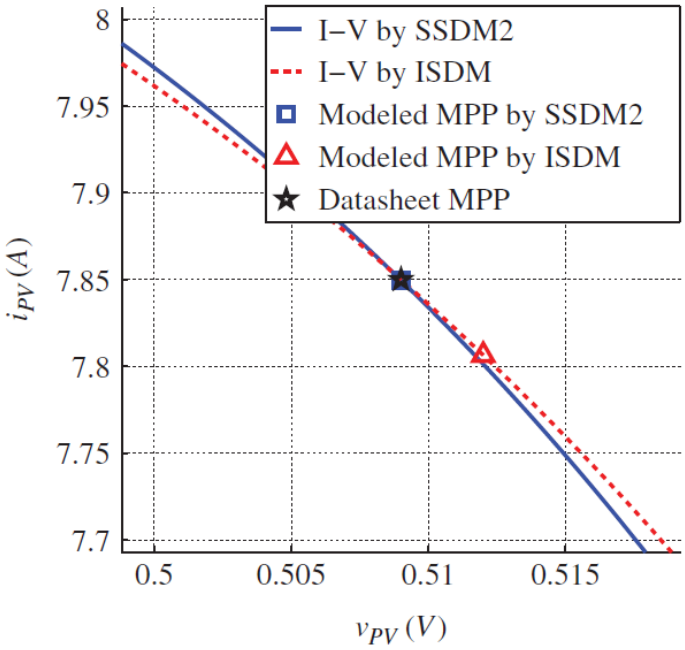

Figure 2.21 Deviation from true MPP for ISDM and SSDM-s

Therefore, if the fourth constraint is not employed, the cartesian distance D_{MPP} from the true MPP in the P-V plot can be used as a measure of the model accuracy. Also this parameter can be normalized and calculated as [4]:

$$D_{MPP} = \sqrt{\left(\frac{\widetilde{P_{MPP}}}{P_{MPP}} - 1\right)^2 + \left(\frac{\widetilde{V_{MPP}}}{V_{MPP}} - 1\right)^2} \tag{2.37}$$

where the tilde marks the computed quantities. It is also possible to evaluate a model comparing separately the computed P_{MPP} and V_{MPP} with the experimental ones [17, 19] and in this case the term used is “error” rather than “distance”.

Root-Mean-Square Deviation

In general, if a complete dataset can be obtained either from experimental measurements or from the manufacturer, the model accuracy can be evaluated through the Root-Mean-Square Deviation (RMSD) [4]:

$$RMSD_I = \sqrt{\frac{\sum_j^N \left(\widetilde{I_j} - I_j\right)^2}{N}} \tag{2.38}$$

where the tilde marks the points computed from the model versus the N experimental (or anyhow available) values. An RMSD for the power curve can be defined analogously.

Since the output ratings of solar cells vary greatly from one to another due to the differences in size and materials, a *Normalized* RMSD (NRMSD) can be employed so that different devices can be compared more accurately:

$$NRMSD_I = \frac{RMSD_I}{I_{SC}} \tag{2.39}$$

Similarly, a NRMSD can be defined for the output power where the reference for normalization would be the P_{MPP}.

Absolute Current Error (or Deviation)

For each of the TRP, an absolute and relative (with respect to the measured value) error can be computed. For example, for the short-circuit current:

$$\varepsilon = \widetilde{I_{SC}} - I_{SC} \qquad\qquad \varepsilon_{\%} = \frac{\varepsilon}{I_{SC}} \tag{2.40}$$

Eventually, these errors can be computed for every point of the I-V curve. Like D_{MPP}, the absolute error on current should be null in correspondence of the Three Remarkable Points if the first three constraints have been used in the parameter extraction (see Figure 2.22).

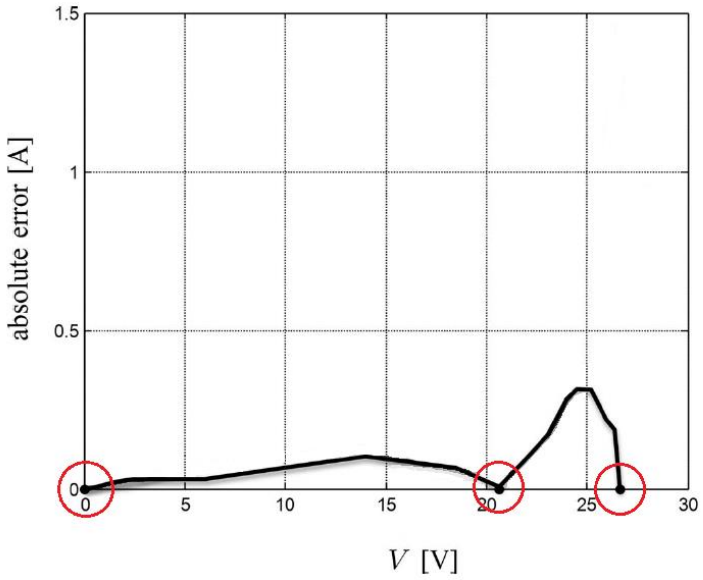

Figure 2.22 Current absolute error between the experimental I-V points and the computed points for CSDM in [6]

Area Error Rate

In [34], the authors use the parameter "area error rate" $\Delta A_{\%}$, defined as the difference of the area subtended by the computed I-V curve A_{comp} and the area subtended by the experimental I-V curve A_{exp}, divided by the latter (see Figure 2.23):

$$\Delta A_{\%} = \frac{A_{comp} - A_{exp}}{A_{exp}} \tag{2.41}$$

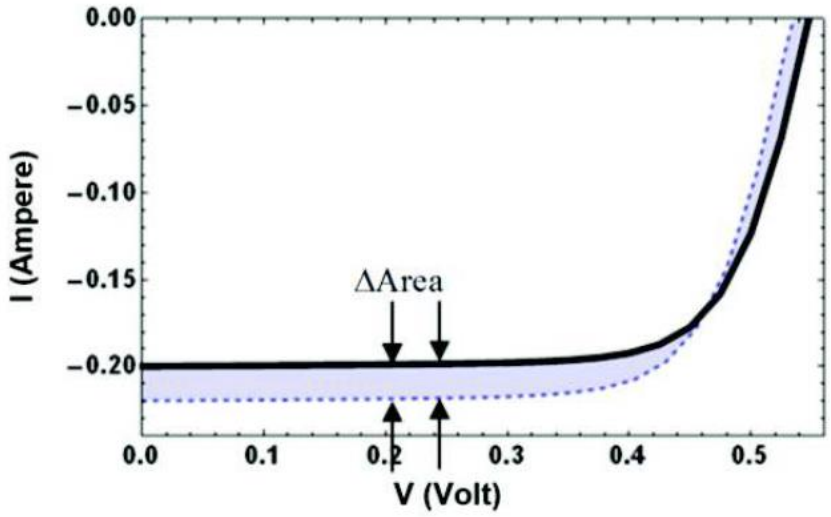

Figure 2.23 Area error rate between experimental and computed curves [34]

From their work on CSDM and DDM, the area error rate is found to be dependent mainly on the values of the series resistance and the ideality factor(s).

Visual Fitting

Strictly related to the concepts of RMSD, absolute errors and area error rate is the visual fitting of the computed I-V curve to the measured one. Clearly, this is an approximate and limited evaluation method. Nevertheless, it is often proposed by authors as it offers the undeniable advantage of being immediate and straightforward. Also, it can give insights about the possible flaws of the model (e.g. the evaluation of the slopes in the current-source and voltage-source regions can tell about the resistances). However, visual fitting should be always associated with numerical data such as the indices presented before.

Computing Time

In parallel to the accuracy of the model, i.e. how closely it fits and predicts the real data, one should be able to evaluate also the computing time of the model. Precisely, a distinction could be made between the time necessary to extract the parameters at STC and the time the model needs to produce an I-V curve for a given pair of irradiance and temperature. Either quantities are crucial to any of the purposes for PV modelling presented in Paragraph 1.3. The reasons are trivial: a 1%-more-accurate but 10%-slower model might not be appealing for PV system designers as well as a 10%-faster but 1%-less-accurate model might be useless for matter physics researchers. Nevertheless, no explicit evaluation in this sense was found in any work reviewed, i.e. no author reported the numerical computing time of his/her model; rather, only qualitative evaluations were expressed such as “faster than …” or “slower than …”. Clearly, these do not constitute a valid reference for a proper evaluation of the speed of the model: more data-based attention to computing time is herein suggested for future works.

3 PV Models

3.1 Overview

As already introduced in Paragraph 2.2, a criterion to categorize the available PV models is the number of diodes present in the equivalent circuit: single-diode, double-diode and three-diode models. Table 3.1 summarizes the physical interpretation of each diode.

Table 3.1 Physical interpretation of the PV model diodes

Diode	Represented Phenomena	a (typical)
D_1	diffusion (and recombination in the quasi-neutral regions)	1
D_2	recombination in the space-charge regions	2
D_3	recombination in the defect regions, grain boundaries, etc	>2

An alternative and almost equivalent criterion is the number of unknown parameters featured in the $I(V)$ equation (see *Table 3.2*) [15]: three-parameter (3-p), four-parameter (4-p), five-parameter (5-p), seven-parameter (7-p) and nine-parameters (9-p) models. The electric losses and all the non-idealities are taken into account with the addition of a series resistance (R_s) and a parallel resistance, also called shunt resistance (R_p or R_{sh}).

Table 3.2 General parameters for a diode-based PV electrical model

Symbol	Description
I_{ph}	photocurrent
I_{sn}	reverse saturation current of the n-th diode
a_n	ideality factor of n-th diode
R_s	lumped series resistance
R_p	lumped parallel resistance

In the following, each of these models is presented along with:

- the equivalent electrical circuit,
- the governing equation $I(V)$ derived from Kirchhoff's laws,
- the most common parameter extraction strategies (detailed equations are reported in Appendix A.2).

In general, the number of the parameters is directly related to the model accuracy [9] and more accurate models are more suitable for applications at low-irradiance conditions [12, 23] and multicrystalline cells. Some authors report that it is not possible to calculate the I-V characteristics precisely by using a conventional single-diode model [32]. Both resistances must be included for a realistic representation of the device; however, the parallel resistance is often neglected [8] and the series resistance turns the $I(V)$ equation in implicit form which is harder to deal with (*cf.* Chapter 2.3).

Finally, It should be noted that all these models are *static* models meaning that the dynamics regarding the time response are not accounted for [4].

3.2 Single-Diode Models

3.2.1 Ideal Single-Diode Model (3-p)

The equivalent circuit of the Ideal Single-Diode Model is shown in Figure 3.1. According to Kirchhoff's Law of Currents (KCL), the current I at the terminals of the cell is given by:

$$I = I_{ph} - I_d \tag{3.1}$$

Applying Kirchhoff's Law of Voltages (KVL) to the circuit, the voltage at the terminals of the cell V results equal to the voltage across the diode V_d:

$$V_d = V \tag{3.2}$$

Substituting (2.3) and (3.2) in (3.1), the governing equation $I(V)$ of the ISDM is obtained:

$$I = I_{ph} - I_s \left[e^{\left(\frac{V}{aV_{th}}\right)} - 1 \right] \tag{3.3}$$

Since the parameters to be identified to define (3.3) are three (I_{ph}, I_s, a), this model is also called "three-parameter (or 3-p) model" [4, 15].

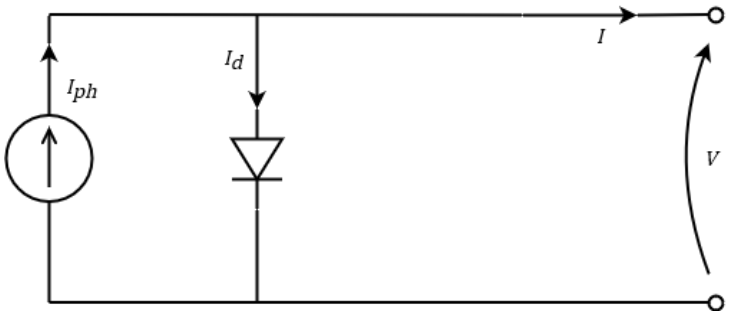

Figure 3.1 Equivalent circuit of an Ideal Single-Diode Model (ISDM)

Parameter Extraction for ISDM

Given the number of unknowns, the first three constraints discussed in Chapter 2.3 are sufficient to completely define ISDM. Applying Equations (2.9)-(2.11) to (3.3), the following is obtained:

1) matching of the Short-Circuit point $(0, I_{SC})$:

$$I_{SC} = I_{ph} \tag{3.4}$$

2) matching of the Open-Circuit point $(V_{OC}, 0)$:

$$0 = I_{ph} - I_s \left[e^{\left(\frac{V_{OC}}{aV_{th}}\right)} - 1 \right] \tag{3.5}$$

3) matching of the Maximum Power Point (V_{MPP}, I_{MPP}):

$$I_{MPP} = I_{ph} - I_s \left[e^{\left(\frac{V_{MPP}}{aV_{th}}\right)} - 1 \right] \tag{3.6}$$

As discussed in Chapter 2.3, the system of Equations (3.4)-(3.6) is nonlinear therefore a numerical method is used to solve it. Nevertheless, an approximated analytical solution can be obtained if one choose to neglect the "-1" next to the exponential. In fact, substituting (3.4) in (3.5) a simpler relation between I_s and a is obtained:

$$I_s = I_{SC} e^{\left(\frac{-V_{OC}}{aV_{th}}\right)} \tag{3.7}$$

Substituting (3.4) and (3.7) in (3.6) an explicit expression for a can be obtained:

$$a = \frac{V_{MPP} - V_{OC}}{V_{th}} \left[ln\left(1 - \frac{I_{MPP}}{I_{SC}}\right) \right]^{-1} \tag{3.8}$$

The value of a computed with (3.8) is then used to evaluate I_s with (3.7).

Once the reference parameters are computed, they can be used in Equations (2.28), (2.33) and (2.27) to evaluate the variations with irradiance and temperature. ISDM is almost never used as its desired simplicity unfortunately does not deliver accurate results (see Paragraph 4.1).

3.2.2 Simplified Single-Diode Models (4-p)

In the Complete Single-Diode Model (CSDM), the series and shunt resistances represent the non-idealities of the real PV cell. A middle ground between the ISDM and the CSDM is represented by the Simplified Single-Diode Models (SSDM) in which only one type of resistance is featured. Mathematically, this is equivalent to setting either the series resistance to zero or the parallel resistance to infinite in the CSDM. In this context, let's refer to the model with only the series resistance as SSDM-s, while the model with the parallel resistance is indicated with SSDM-p.

Simplified Single-Diode Model with R_p

The equivalent circuit of SSDM-p is shown in Figure 3.2. Differently than ISDM, the balance of the currents according to KCL is:

$$I = I_{ph} - I_d - I_{R_p} \tag{3.9}$$

KVL gives the same result as ISDM (Equation (3.2)), therefore:

$$I_{R_p} = \frac{V_d}{R_p} = \frac{V}{R_p} \tag{3.10}$$

according to Ohm's law. Substituting (2.3) and (3.10) in (3.9), the governing equation for SSDM-p becomes:

$$I(V) = I_{ph} - I_s\left[e^{\left(\frac{V}{aV_{th}}\right)} - 1\right] - \frac{V}{R_p} \tag{3.11}$$

Equation (3.11) features four unknown parameters (I_{ph}, I_s, a, R_p), one more with respect to the ISDM, i.e. the resistance R_p. For this reason, this model is also called "four-parameter (4-p) model" [4, 15].

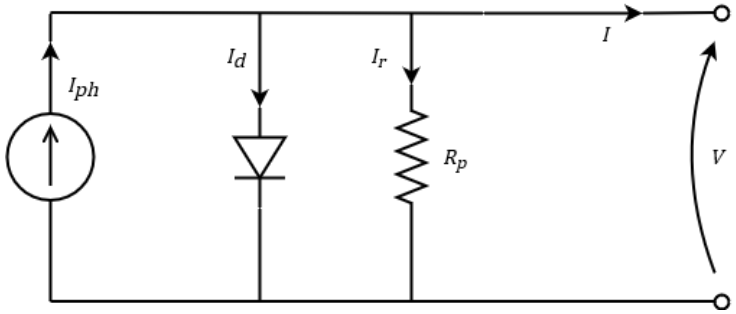

Figure 3.2 Equivalent circuit of a Simplified Single-Diode Model with parallel resistance R_p (SSDM-p)

Parameter Extraction for SSDM-p

Given the number of unknowns, all the four constraints discussed in Chapter 2.3 are sufficient to completely define SSDM-p. Using a system solver for these four equations, all the unknowns can be determined. If a ISDM has tried before, its parameters can be used to initialize a and I_s [4]. The detailed equations are reported in Appendix A.2.

Once the reference parameters are computed, they can be used in Equations (2.28), (2.33) and (2.27) to evaluate the variations with irradiance and temperature.

Simplified Single-Diode Model with R_s

The equivalent circuit of SSDM-s is shown in Figure 3.3. The balance of the currents in SSDM-s is the same as in ISDM, given by (3.1). However, the presence of R_s modifies the output of KVL so that the voltage across the diode V_d is not equal anymore to the voltage at the terminals of the cell V; Equation (3.2) modifies into:

$$V_d = V + V_{R_s} = V + IR_s \tag{3.12}$$

Substituting (3.12) in (2.3) and then in (3.1), the governing equation for SSDM-s is obtained:

$$I = I_{ph} - I_s\left[e^{\left(\frac{V+IR_s}{aV_{th}}\right)} - 1\right] \tag{3.13}$$

It must be noted that this expression of the I-V characteristics is in implicit form as the current I appears also on the right side of the equation.

Like SSDM-p, SSDM-s features four unknown parameters (I_{ph}, I_s, a, R_s), therefore also this model can be addressed as "four-parameter (4-p) model" [4, 15].

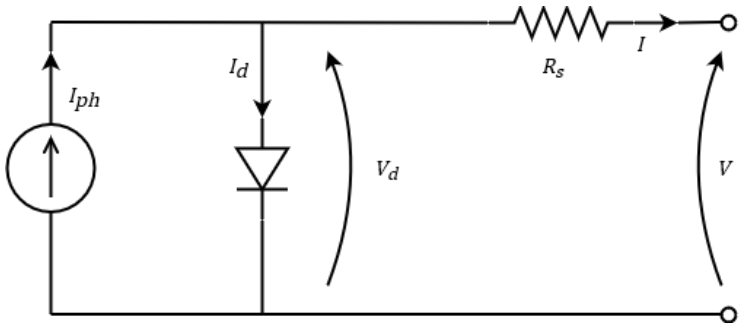

Figure 3.3 Equivalent circuit of a Simplified Single-Diode Model with series resistance (SSDM-s)

Parameter Extraction for SSDM-s

As for SSDM-p, all the four constraints discussed in Chapter 2.3 are sufficient to completely define SSDM-s. However, the presence of the series resistance makes the calculations harder for the following three reasons [4]:

1) both the series resistance R_s and the terminal current I appear inside an exponential term;
2) the $I(V)$ characteristics is in implicit form;
3) the photocurrent I_{ph} is not simply equal to the short-circuit current I_{SC} (*cf.* (3.4) and (2.17)) since the series resistance causes a residual voltage at the short-circuit condition.

In the following, a series of strategies from literature is presented.

In [26], the authors apply the constraints (2.9)-(2.12) directly to (3.13) as seen in ISDM and SSDM-p. The system of four nonlinear equations is then solved iterating only on a and R_s while I_{ph} and I_s are determined by verification of the remaining two equations.

In [4], the authors suggest to remove the coupling $I = f(V, I)$ and turn (3.13) into the explicit form $V = g(I)$:

$$V = aV_{th} ln\left(\frac{I_{ph} + I_s - I}{I_s}\right) - IR_s \tag{3.14}$$

Then, the first three constraints are set on (3.13) while the fourth is derived from (3.14). The system is then solved numerically with the NR method. As discussed, a way to simplify the parameter identification is assuming the photocurrent to be equal to the short-circuit current [4, 18] or, alternatively neglecting the term "-1" in (3.13). Xiao et al. [4] found no difference in the values of the parameters calculated with and without these simplifications.

In [21], I_{ph} is directly evaluated through (2.28), I_s through (2.30) and R_s through (2.19). An initial guess for a is set to 1.3 and the solution is found by NR approximations.

In [17] the authors evaluate I_{ph} and I_s already in dependence with the cell temperature; then they substitute Equation (2.33) into Equation (3.13) calculated in the MPP, obtaining a relation between R_s and a:

$$R_s = \frac{aV_{th}ln\left[\left(1-\frac{I_{MPP}}{I_{ph}}\right)e^{\frac{V_{OC}}{aV_{th}}}+\frac{I_{MPP}}{I_{ph}}\right]-V_{MPP}}{I_{MPP}} \tag{3.15}$$

Then, R_s and a are evaluated by minimizing the quantity (*cf.* Constraint (2.14)):

$$\left.\frac{dI}{dV}\right|_{V=V_{MPP}}+\frac{I_{MPP}}{V_{MPP}} \tag{3.16}$$

through numerical methods. The authors implement this loop for every temperature level as R_s and a are not considered temperature-constant: this is a perfect example of *Adaptive Parameter Modeling* (APM).

In [1], [18] and [19], despite the presented model is a CSDM, the authors choose to neglect the influence of the parallel resistance R_p because usually it assumes really high values (see last term of Equation (3.19)). Doing so, *de facto* they treat their CSDM as a SSDM-s with four unknowns. Also here I_{ph} is evaluated through Equation (2.28) and I_s through Equation (2.29). Then, R_s is evaluated as the slope of the curve in open-circuit condition as discussed in Chapter 2.2:

$$R_s = -\left.\frac{dV}{dI}\right|_{V=V_{OC}} \sim \frac{V_{OC}-V_{MPP}}{I_{MPP}} \tag{3.17}$$

where the approximation is due to the asymptotic behaviour of the I-V curve in $[V_{MPP}, V_{OC}]$. The last unknown, the ideality factor a, is evaluated from the matching of the MPP and the short-circuit point, leading to:

$$a = \frac{V_{MPP}+R_sI_{MPP}-V_{OC}}{V_{th}ln\left(\frac{I_{SC}-I_{MPP}}{I_{SC}}\right)} \tag{3.18}$$

It is important to note that in (3.18) the authors neglected the "-1" that appears next to the exponential term as this last is much greater.

3.2.3 Complete Single-Diode Model (5-p)

The equivalent circuit of the Complete Single-Diode Model is presented in Figure 3.4. KCL and KVL give the Equations (3.9) and (3.12) respectively, with (3.10) being valid too. Therefore, the governing equation for a CSDM is:

$$I = I_{ph} - I_s\left[e^{\left(\frac{V+IR_s}{aV_{th}}\right)}-1\right]-\frac{V+IR_s}{R_p} \tag{3.19}$$

Like for SSDM-s, $I(V)$ for CSDM is in implicit form. Equation (3.19) features five unknown parameters $(I_{ph}, I_s, a, R_s, R_p)$, hence this model is also called "five-parameter (5-p) model" [4, 15].

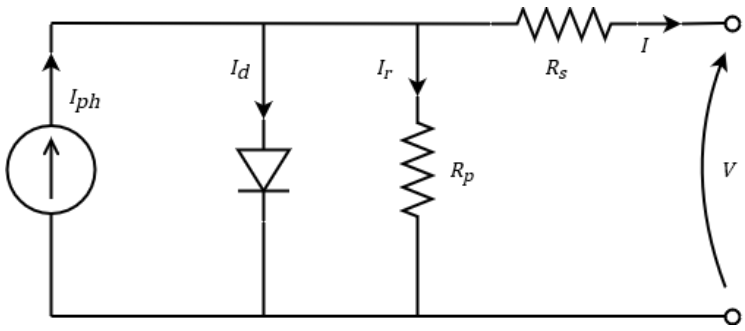

Figure 3.4 Equivalent circuit of a Complete Single-Diode Model (CSDM)

Parameter Extraction for CSDM

The *four* constraints (2.9)-(2.12) are insufficient to recover the *five* unknown parameters, making it impossible to aim to an exact analytical solution for CSDM. For this reason, in [4] the authors recommend to adopt this model only when the full I-V dataset is available for modelling and the curve-fitting performance is critically important for simulation, otherwise the significant effort involved in using this model might be wasted [19] if the simpler models already match the data from the manufacturer to a satisfying level [4]. On the other hand, it is the most widely employed and studied model, as it offers a desirable balance between accuracy and complexity.

Numerous methods have been developed to solve the problem of the fifth piece of information. The most common approach is to set the four constraints (the explicit expressions are reported in Appendix A.2.4, Equations (A.18)-(A.21)) and then make some initial estimation with regard to:

1) any of the parameters, or
2) any particular characteristic of the I-V curve.

In the first case, generally the ideality factor is the parameter chosen to be initialized since the sensitivity of the I-V curve to a is relatively limited (*cf.* Figure 2.8) [29]. The initial value is picked in the range (1, 1.5) and then iterations on it are carried out to improve the accuracy of the model. Once a has been estimated, explicit expressions for the remaining four parameters I_{ph}, I_s, R_s and R_p can be derived from the constraints equations with help of simplifications; among the most used are:

$$I_{ph} \sim I_{SC} \tag{3.20}$$

$$e^{\left(\frac{I_{SC}R_s}{aV_{th}}\right)} \ll e^{\left(\frac{V_{OC}}{aV_{th}}\right)} \tag{3.21}$$

$$\frac{I_s}{aV_{th}} e^{\left(\frac{I_{SC}R_s}{aV_{th}}\right)} \ll \frac{1}{R_p} \tag{3.22}$$

It is worth noting that in [16], following the abovementioned approach (a initialized plus simplifications) the authors derive explicit expressions for *all* the five parameters employing the Lambert W-function (details in Appendix A.2.4); this function allows to solve implicit equations featuring exponentials.

In the second case, it is common to use the slope of the I-V curve at short-circuit and open-circuit points, measured or estimated, to evaluate the parallel and series resistances [28, 29] as discussed at the end of Paragraph 2.3. In these cases, the constraints on the TRP are integrated by equations (2.19) and (2.20). An example is found in [7]; the parameters are then found through a double process of trial and error for R_s and a, with the second process nested into the first.

In [10], the fifth equation is derived from the temperature coefficient of V_{OC}. In fact, for temperatures within 10K from STC, V_{OC} can be considered linearly dependent on the temperature T:

$$\beta_T = \left.\frac{dV}{dT}\right|_{V=V_{OC}} \sim \frac{V_{OC,ref} - V_{OC}}{T_{c,ref} - T_c} \tag{3.23}$$

where V_{OC} is evaluated from the open-circuit constraint (2.10), knowing $I_{ph}(T_c)$ and $I_s(T_c)$ (R_p and a are considered constant).

In [8], Carrero et al. make the approximation (2.18), evaluate I_s and I_s through Equation (2.29) and (2.28), respectively, and consider the resistances temperature-independent.

In [35], I_{ph} is evaluated through (2.28) and the constraints on the TRP are set; from these, a direct expression for $I_s(T_c)$ is derived using (2.30) and neglecting R_p and the term "-1". Then, R_p is made explicit from the third constraint and an iteration on R_s is carried out starting from $R_s = 0$ until the MPP is matched.

In [6], the authors find the parameters of their CSDM as follows:

- initially $I_{ph} \sim I_{SC}$, then I_{ph} is updated from R_s and R_p;
- a chosen arbitrarily;
- I_s evaluated from (2.33) ($R_p \to \infty$);
- R_s and R_p from the matching of the MPP by iteration.

The core of their parameter extraction is the last point, i.e. the search for the resistances by iteration. The initial value of R_s can be set to zero while the initial value of R_p can be set as follows:

$$R_{p,min} = \frac{V_{MPP}}{I_{SC} - I_{MPP}} - \frac{V_{OC} - V_{MPP}}{I_{MPP}} \tag{3.24}$$

which corresponds to the slope of the line segment between the short-circuit point and the MPP. Besides, once the pair (R_s, R_p) assume reasonable values, the value of I_{ph} can be tuned according to:

$$I_{ph} = \frac{R_p + R_s}{R_p} I_{SC} \tag{3.25}$$

Once the model is defined and validated, the authors suggest that it can be further improved tuning the ideality factor.

In [20], the authors set all the four constraints and consider Equation (2.28) as the fifth equation (dependence of I_{ph} on irradiance and temperature). The parameters are found by iterations through NR method setting an initial value for the ideality factor.

In [24], the authors use simplifications (3.21), (3.22) and:

$$1 + \frac{R_s}{R_p} \sim 1 \tag{3.26}$$

$$\frac{I_s}{aV_{th}} e^{\left(\frac{V_{OC}}{aV_{th}}\right)} \gg \frac{1}{R_p} \tag{3.27}$$

to derive explicit expressions for each of the five parameters. Given the simplifications, the authors calculated the error contours on each parameter and found that it depends on the width of the values range of the resistances, being it as low as 1% if lower and upper limitations are set on R_s and R_p, respectively (see Figure 3.5).

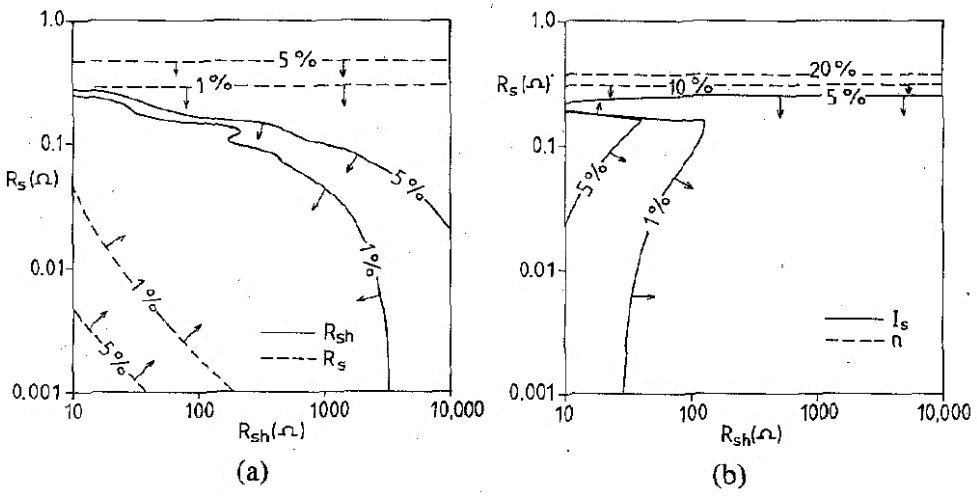

Figure 3.5 Error contours of R_p (R_{sh}) and R_s (a) and I_s and a (n) in the model of Chan et al. [12]

Finally, as already seen at the end of Paragraph 2.4, Humada et al. in [3] derive an expression for each parameter directly as function of irradiance and temperature. However, this approach requires an amount of experimental data usually not provided by the manufacturer.

3.3 Double-Diode Model (7-p)

The equivalent circuit of the Double-Diode Model is shown in Figure 3.6. KCL modifies as follows:

$$I = I_{ph} - I_{d1} - I_{d2} - I_{R_p} \tag{3.28}$$

whereas (3.10) and (3.12) are still valid, being $V_d = V_{d1} = V_{d2}$, and (2.3) applies for each diode. The governing equation for DDM results to be:

$$I = I_{ph} - I_{s1}\left[e^{\left(\frac{V+IR_s}{a_1 V_{th}}\right)} - 1\right] - I_{s2}\left[e^{\left(\frac{V+IR_s}{a_2 V_{th}}\right)} - 1\right] - \frac{V + IR_s}{R_p} \tag{3.29}$$

Also Equation (3.29) is in implicit form and the number of unknown parameters increases to seven because of the two added tuning parameters for the second diode: $I_{ph}, I_{s1}, a_1, I_{s2}, a_2, R_s, R_p$. This model can be called also "seven-parameter (7-p) model". It is worth reminding that I_{d1} represents the diffusion current while I_{d2} the recombination current; usually, I_{s2} is found to be 3-7 orders of magnitude larger than I_{s1} [13].

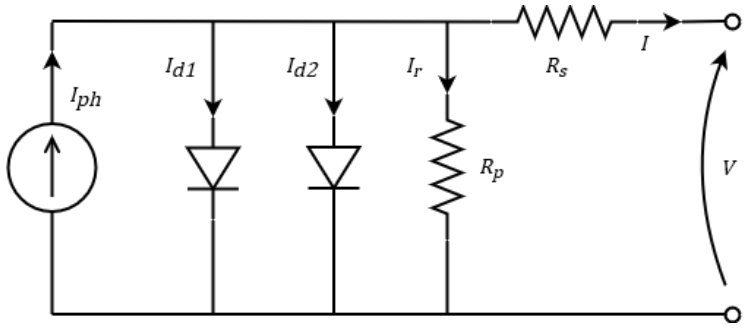

Figure 3.6 Equivalent circuit of a Double-Diode Model (DDM)

It is worth mentioning that in [22], the authors introduce a variation of the standard DDM, called Modified Double Diode Model (MDDM), featuring an additional resistance in series with the second diode (see Figure 3.7). This second resistance takes into account the effect of grain boundary region since the resistivity here is higher than that within the crystallites [23], in fact R_{s2} is found to be one order of magnitude higher than R_s [22]. A consequence is that an enlargement of crystallite size can enhance directly the performance of the cell.

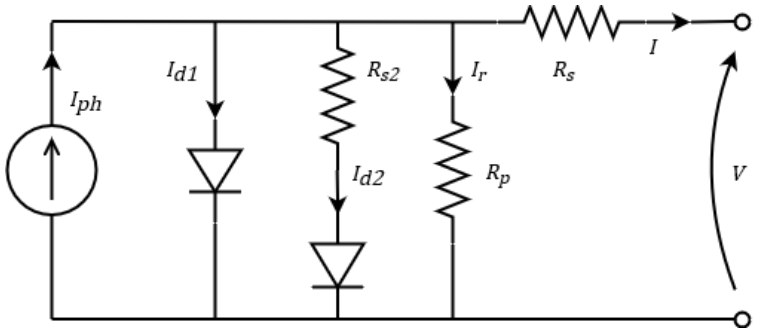

Figure 3.7 Equivalent circuit of a Modified Double-Diode Model (MDDM)

Parameter Extraction for DDM

This model is commonly considered to be more comprehensive as it simulates the PV cell output characteristics with more accuracy thanks to the two added tuning parameters (literature reports that this model shows its "superiority" especially at low-voltage bias [4, 12]). However, it is not commonly used due to its computational complexity (see the implicit form and the presence of two exponential terms). In fact, an improper tuning of the parameters can cancel the claimed advantage of accuracy. Moreover, parameter identification is quite sensitive to the initial conditions [4]. To reduce the complexity, some restricting assumptions can be made [11]. The most common of these simplifications is:

$$a_1 = 1, \qquad a_2 = 2 \tag{3.30}$$

This assumption decreases by 2 the number of unknowns and is based on the approximation of Shockley-Read-Hall recombination in space-charge layer of the photodiode (*cf.* Equation (2.1)). Unfortunately, this approximation not always holds true from a physical point of view [4, 13, 15, 22] and still requires numerical iterations to solve mathematically the model.

In [12], assumption (3.30) is made and the constraints on the TRP are set together with Equations (2.19) and (2.20): an independent system of five equations in five unknowns is obtained and solved with a NR iteration. However, to overcome the problems linked to this numerical method and the complexity of the equations, the authors introduce simplifications analogous to (3.21)-(3.27) and through few manipulations they find either a quadratic or cubic equation in R_s. Once R_s has been computed, all the other parameters are evaluated through the other four exact equations. The results obtained from the "quadratic" and "cubic" solutions are then compared the results of the "accurate" solution: although the quadratic solution shows a problematic 19.7% error on I_{s2}, the cubic solution is affected by errors all within 4%. The analysis of the error contours showed that these solutions have a wide range of validity provided the series resistance and the irradiance are not both high.

In [13], in order to make the computation of the parameters of the DDM lighter, the authors:

- assume $a_1 = 1$ (one unknown less);
- choose arbitrarily $a_2 \geq 1.2$ (one unknown less);
- assume $I_{s1} = I_{s2}$ (one unknown less);
- make explicit two parameters (I_{ph}, I_s) as function of the other parameters.

Then, they use a simple iterative method based on the matching of the MPP to compute the values of the two resistance based on the same reasoning followed by Villalva et al. in [6] (see parameter extraction of CSDM). Results show that their 4-parameter double-diode model is simple and fast yet accurate.

In [14], the authors make use of the NR method and the Levenberg/Marquardt algorithm to obtain the values of the five parameters (approximation (3.30) is used) through curve fitting. Since both these algorithms are crucially sensitive to the initial guesses of the unknowns, a thorough evaluation of these is made through a cascade of different iterations, where the next algorithm takes over if the previous

failed to deliver physically-acceptable initial values. It is worth noting that R_p was evaluated in relation to the MPP rather than the slope of the I-V curve at the short-circuit point (*cf.* Paragraph 2.3). Successively, a *set* of I-V curves were sampled in order to derive the experimental laws describing the variation of the parameters with respect to irradiance starting from the dependences on temperature found in literature. The so-obtained equations feature 13 constants.

In [34], the authors use the so-called *iterative injection extraction method*, whose aim is reducing to zero the area error rate $\Delta A_{\%}$ defined in Paragraph 2.5. Since $\Delta A_{\%}$ is found to be dependent on the deviation of R_s, a_1 and a_2 from their real values, the parameter extraction consists of finding the values of these three parameters for which the area error rate is minimal (see Figure 3.8); the other four parameters ($R_p, I_{ph}, I_{s1}, I_{s2}$) are then deduced. Unfortunately, the authors did not test the method for different irradiances and temperatures.

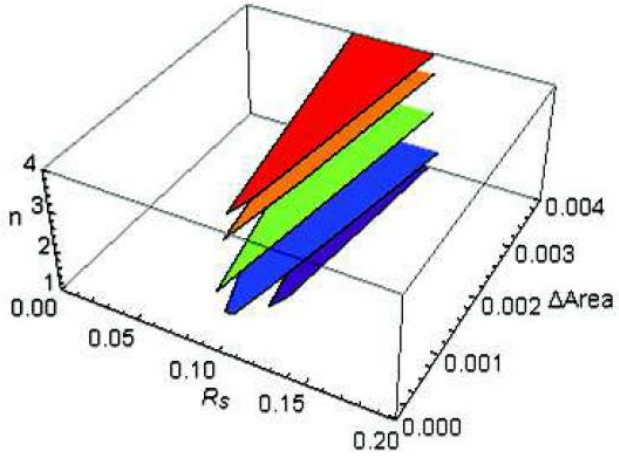

Figure 3.8 $\Delta A_{\%}$ as function of series resistance and (one) ideality factor (colors are used just to make the figures clearer) [34]

Finally, it is worth noting that in in [22] the authors allow for variable diode ideality factors for their MDDM, representing the reality more accurately. This model features 8 unknown parameters that the authors find through optimization of RMSD. The comparison between MDDM and CSDM shows a better fit (χ^2) of the former by two orders of magnitude.

3.4 Three-Diode Model (9-p)

The equivalent circuit of a Three-Diode Model is presented in Figure 3.9. The balance of currents is:

$$I = I_{ph} - I_{d1} - I_{d2} - I_{d3} - I_{R_p} \tag{3.31}$$

Equations (3.10) and (3.12) also apply, being $V_d = V_{d1} = V_{d2} = V_{d3}$, and (2.3) modifies for each diode accordingly. The governing equation for TDM is:

$$I = I_{ph} - I_{s1}\left[e^{\left(\frac{V+IR_s}{a_1 V_{th}}\right)} - 1\right] - I_{s2}\left[e^{\left(\frac{V+IR_s}{a_2 V_{th}}\right)} - 1\right] - I_{s3}\left[e^{\left(\frac{V+IR_s}{a_3 V_{th}}\right)} - 1\right] - \frac{V + IR_s}{R_p} \quad (3.32)$$

Also Equation (3.32) is in implicit form and the number of unknown parameters increases to nine because of the two added tuning parameters for the third diode: $I_{ph}, I_{s1}, a_1, I_{s2}, a_2, I_{s3}, a_3, R_s, R_p$. This model can be called also "nine-parameter (9-p) model". I_{d1} represents the diffusion current, I_{d2} the recombination current and I_{d3} the current due to recombination in the defect regions, grain boundaries, etc [23].

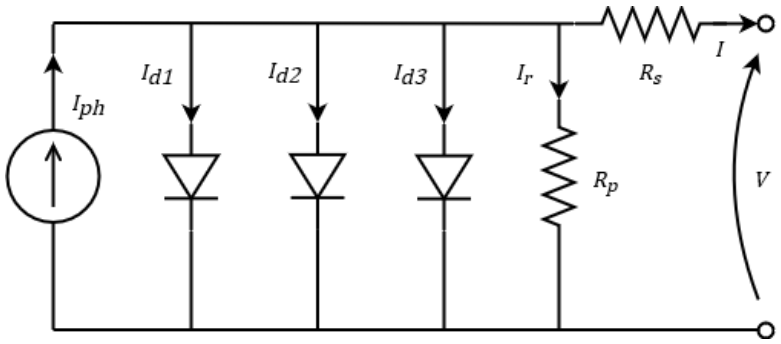

Figure 3.9 Equivalent circuit of a Three-Diode Model (TDM)

Parameter Extraction for TDM

Due to the number of unknowns, only metaheuristics algorithms are found to be employed to find the parameters of TDM.

In [23], Allam et al. set approximation (3.30) while the ideality factor of the third diode remains an unknown, $a_3 > 2$. Doing so, their TDM features 7 unknowns instead of 9. Then, the authors use the Moth-Flame Optimization to minimize the objective function, chosen to be the RMSD of the output current I.

Few Considerations

In general, the circuit models herein presented are based on assumptions that may not always be valid. The main assumption is that of linearity, i.e. that the current flowing through the cell is a superposition of two currents, with no second-order interaction between them. Other simplifying assumptions include the material parameters assumed to be insensitive to changes in either voltage or irradiance, and the minority-carrier concentrations at the edges of the space-charge regions assumed to be dependent on the junction bias and independent of irradiance. These assumptions may not be accurate [12].

However, the models do generally fit experimental I-V characteristics fairly accurately, and can provide a very useful tool in assessing cell performance provided the model parameters are easily obtainable. This might imply that, although not explicitly account for, the abovementioned aspects are actually included and somehow distributed among the tuning parameters.

Finally, it is worth noting that the modelling could be *significantly* improved if manufacturers were to provide at least two I-V curves and/or two sets of coordinates of the TRP, one for low irradiance and one for high irradiance conditions [10], or the values of the resistances [8].

4 Model Comparison

Unfortunately, it is not straightforward nor possible to conduct a meaningful, useful and exhaustive model comparison based on the heterogeneous studies reviewed. The reasons are mainly two:

1) lacking of *common reference frames* such as same PV module and same experimental data for validation;
2) lacking of *numerical results*; for instance, as pointed out before, often it is preferred to show *visual* results and the computing time is practically never reported.

As regards the first point, it is worth noting that in [8] Carrero et al. acknowledge the problem of comparing different panels based only on datasheet information, suggesting to scale each panel's I-V curve in normalized axis with respect to I_{SC} and V_{OC} at STC. By doing so, the influence of the various parameters can be evaluated more properly.

As regards the second point, also reporting comparisons made *within* the studies could be misleading as numerical results are incomplete. Besides, a crucial aspect to factor in when comparing models is the sensitivity to varying irradiance and temperature as it involves multiple heavy calculations: it is clear how a meaningful evaluation of such aspect is practically impossible if the computing time is lacking.

Nevertheless, it is possible to compare carefully-chosen set of results so that general trends and useful conclusions can be outlined. For instance, it is true that there is always a trade-off between the model simplicity and the model accuracy [4], i.e. between computing time and reliability of results. On the other hand, not always more accurate, hence more complicated, is desirable: for example in MPPT applications in space technology a more robust thus simpler algorithm is preferred over a super-accurate yet fragile one [29].

In the following, comparisons based on different selected aspects of PV modelling are presented.

4.1 Comparison between Single-Diode Models

Among the single-diode models, ISDM and CSDM represents the two extremes as ISDM is overly simple while CSDM requires careful considerations for parameter extraction. In fact, it can be said that CSDM stands out among single-diode models because its solving system of equations is dependent while all the others can be represented by an independent system. However, this mathematical complication is rewarded by a widely accepted superiority in terms of accuracy and robustness. Therefore, if medium-level computations are not an issue, CSDM should be preferred over the other single-diode models. If, on the contrary, computational simplicity is to be preferred, the following considerations about ISDM and the two SSDM apply.

The advantages of ISDM lie in the straightforward parameterization process allowing for potentially fast simulation speed. However it shows a deviation from the true MPP due to the low number of tuning parameters (the fourth constraint cannot be set). Instead, the two SSDM have the advantage of accuracy

at all three significant points and a straightforward modelling process. However, the initial values are critical for the success of the parameter identification for these models, and SSDM-p might show an inconsistent negative value for the resistance.

In light of these considerations, in [4] a simple algorithm is suggested to choose among these single-diode model:

- ISDM is initialized and parameterized;
- D_{MPP} is calculated and if it is acceptable then ISDM is selected;
- if not, the parameters of ISDM are used as initial values for the parameterization of SSDMp;
- if R_p is positive and the NRMSD (if applicable) is acceptable, then SSDMp is selected;
- if not, the parameters of SSDM-p are used as initial values for the parameterization of SSDM-s, which in the end results to be the selected model.

SSDM-p is considered before SSDM-s because it is simpler since it governing equation $I(V)$ is not implicit.

It is worth noting that, in reality, SSDM-s can be considered an interesting alternative to CSDM also in terms of accuracy. In fact, as seen in Paragraph 3.2.2, parameter extraction for SSDM-s can be carefully tuned to obtain excellent results. For instance, in [26] the matching between experimental data and computations by SSDMs around the knee of the I-V curve is found to be sensitive to the dependence of the series resistance on temperature $\left(\frac{\partial R_S}{\partial T}\right)$: if that piece of information is correctly retrieved, the authors claim that the model is highly accurate. Also in [21], the authors find excellent correspondence between their SSDMs and the manufacturer's data for a multicrystalline PV module (notably well modelled by complicated models such as DDM and TDM – see Paragraph 4.3), for different irradiance and temperature values.

4.2 Comparison Based on the Number of Diodes

When evaluating the number of diodes, CSDM is to be taken as reference for the single-diode models as it features both the resistances like its "contestants" DDM and TDM do.

First of all, CSDM appears to be the most widely used choice to simulate PV power systems as it offers the most reasonable trade-off between simplicity and accuracy [4, 6, 9, 15]: therefore, the "battlefield" between CSDM, DDM and TDM is the accuracy of the representation of the physical phenomena occurring inside a PV cell.

In fact, the single-diode models assume that the recombination losses in the depletion region are negligible if not completely absent, while in a real PV cell these losses can be significant [13]. When compared to experimental data, DDM exhibits similar results to CSDM at STC (see Figure 4.1, where SEM is CSDM, CDEM is DDM with both the ideality factors constant, 1VDEM is DDM with one ideality factor constant and 2VDEM is DDM with both the factors variable). This is because both the models use the similar MPP matching alogorithm. However, at low irradiance more accurate results are obtained by

the DDM, especially in the proximity of V_{OC}, suggesting that the DDM provides a better tool to evaluate the performance during shading [1, 12]. In general, DDM seems to show little sensitivity to irradiance when compared to CSDM (and SSDM-s) while they react well to temperature variations (while SSDM-s shows poor performance). In [12], after a detailed analysis on error contours, the authors deducted that if the ideality factor of CSDM is close either to 1 or to 2, it can be a valid representation of the combined effects of the two lumped diodes of DDM.

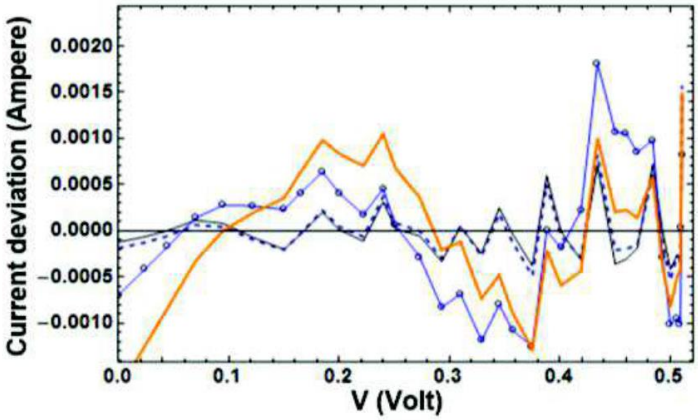

Figure 4.1 Comparison between CSDM and different DDM [34]:
SEM ( ), CDEM (—), 1VDEM (- - - -) , 2VDEM (—)

A proof of the these considerations is provided in [13], where the authors compare directly SSDMS-s ("R_s-model"), CSDM ("R_p-model") and DDM, both on monocrystalline (Shell Solar SQ150-PC) and polycrystalline (Kyocera KC 200GT) modules. Figure 4.2 shows the relative errors between measured and simulated quantities for each of models for different irradiances; it must be pointed out that this SSDM-s was originally developed on another module and the third constraint on it was not set. From the comparison few things can be highlighted:

- DDM always performs better than the others;
- CSDM shows issues at low irradiances;
- SSDM-s performs better than CSDM on V_{OC} but worse on P_{MPP};
- the technology does not have a clear one-direction effect.

Similar trends have been found with respect to different temperatures (not herein reported).

Finally, TDM seems to relate to DDM in the same way DDM relates to CSDM that is, the third diode improves the accuracy and the sensitivity to variations in the operating conditions (see Figure 4.3). The improved accuracy of DDM and TDM is especially marked and useful when modelling relatively complicated materials such as polycrystalline silicon cells [4, 14, 15, 23, 28] and when dealing with small size PV cells (reasearch), since these cells are affected by greater leakage current through peripheries [32]. Losses in multi-crystalline cells are often put in relation with grain boundaries, where recombination is likely to take place [22]. On the other hand, DDM and TDM are very sensitive to the initial conditions and can lead to inconsistent results if not properly guided by an initial estimate of the parameters [7].

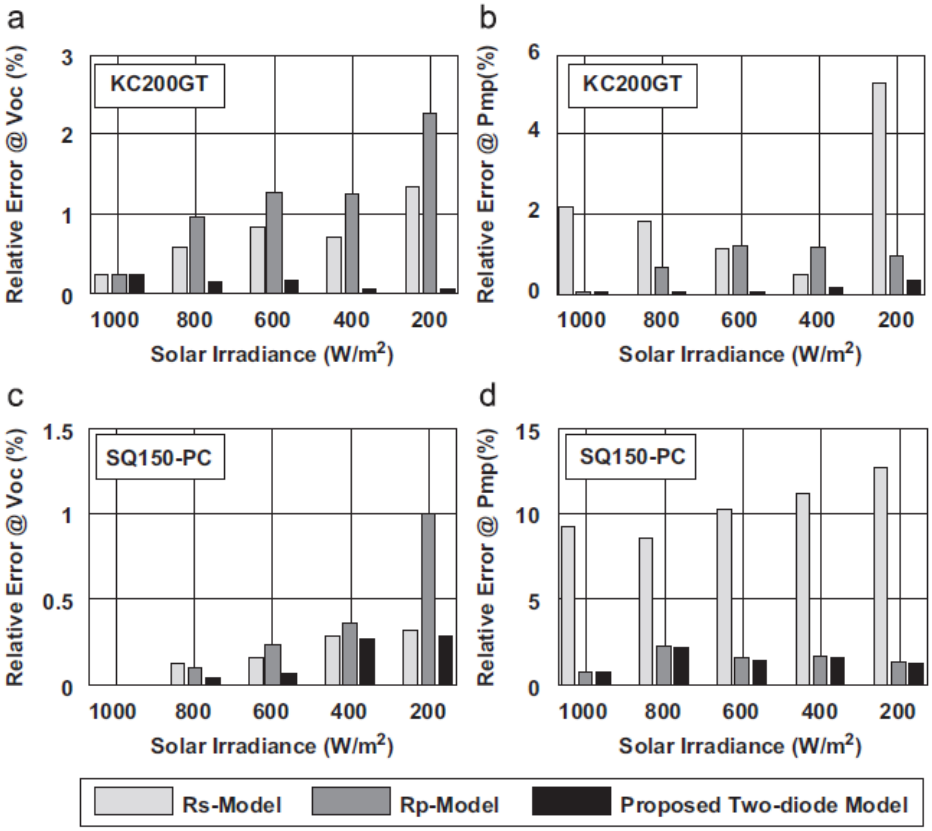

Figure 4.2 Relative error for SSDM-s, CSDM and DDM for mono- and poly-crystalline panels [13]

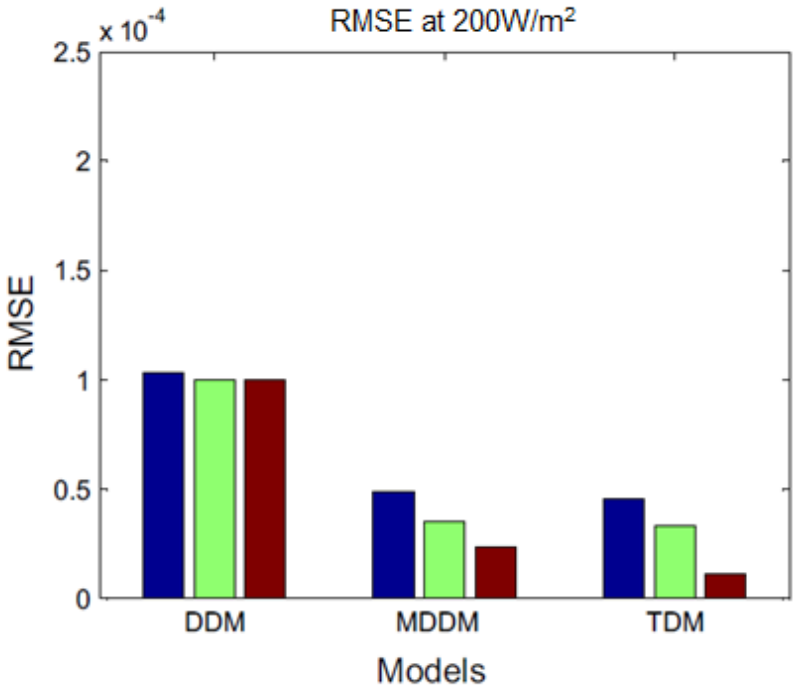

Figure 4.3 RMSE (RMSD) comparison between TDM, DDM and MDDM using three different heuristic algorithms (represented by the different colors) [23]

4.3 Further Aspects

Obviously, there are also other aspects that are worth to be thoroughly evaluated and compared. Each of these could be object of an entire focused study however, herein only a mention is given for the reasons stated at the beginning of this Chapter.

Of particular interest is the strategy to account for irradiance and temperature variations as it is understood the impact it has on the ability of the model to predict the performance of a PV system and to give precious hints about its components behaviour with varying operating conditions.

In this sense, the approach followed in [17], i.e. the Adaptive Parameter Modelling (APM), proves to be superior with respect to Constant Parameter Modelling (CPM) both on the theoretical and practical level. In fact, assuming a number of parameters to be independent from the operating conditions is widely accepted to be a simplification that does not reproduce the reality. A proof comes from simulations results as APM shows constant (null) error independently from the temperature while CPM shows a clear dependence (see Figure 4.4). Nevertheless, it is worth noting that only a 0.03 W error gap on 40 W is found over a 60°C range in CPM: once again, the evaluation of the computing time of the two approaches is essential for an exhaustive and meaningful comparison.

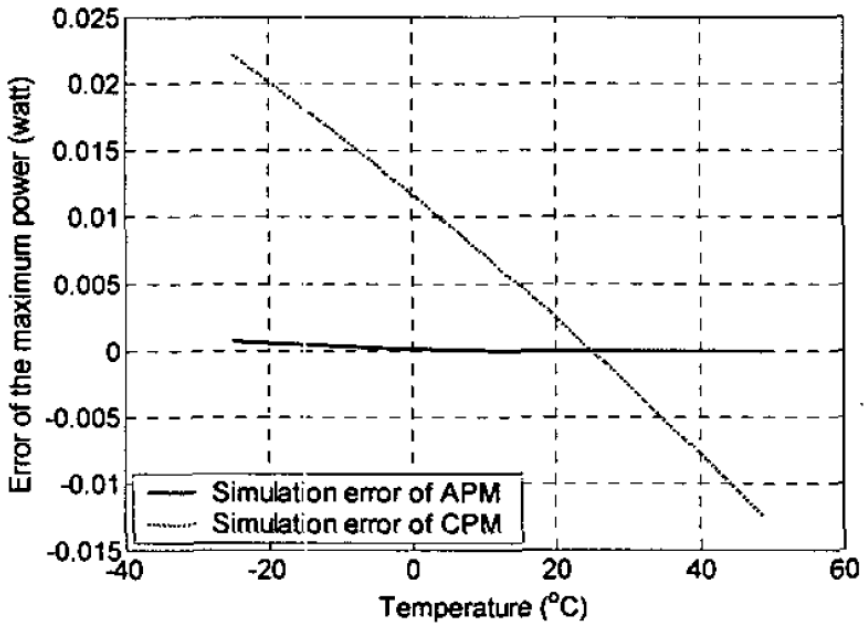

Figure 4.4 Error on P_{MPP} (40W) as function of temperature for APM vs CPM [17]: it is to be noted as CPM shows null error only at STC

Another important level of comparison is the PV technology. For instance, as already pointed out, more complicated models such as DDM and TDM are more suitable for polycrystalline modules (as discussed in the previous Paragraph) that are increasingly gaining attention thanks to their lower cost [32].

Table *4.1* shows percentage errors for SSDM-s [19] and CSDM [17] for different technologies: as expected, both perform better with monocrystalline and thin film rather than polycrystalline.

Table 4.1 Performance results for SSDMs and CSDM found in literature

	Average Error on P_{MPP} [%]		**Average Error on V_{MPP} [%]**	
	SSDM-s [19]	*CSDM* [17]	*SSDM-s* [19]	*CSDM* [17]
monocrystalline	0,36	0,02	1,44	0,34
polycrystalline	0,89	0,15	2,34	1,44
thin film	-	0,02	-	0,34

Also in [13], SSDM-s, CSDM and DDM show to perform at best (meaning that give the lowest relative errors) with monocrystalline modules. However, they give the worst results with thin-film technology, with polycrystalline standing in the middle. Besides, this trends are more marked for SSDM-s rather than CSDM and DDM, with DDM giving always the lowest relative errors.

5 Proposed Models and Methodology

In this study, the Complete Single-Diode Model (CSDM) featuring 5 parameters is investigated. This model has been chosen because, despite the wide literature available on it for the reasons seen in the Chapter 4, poor reference is found (to the knowledge of the author) on the different strategies to account for varying operating conditions (*cf.* Paragraph 2.4) for this model. In this study, a CSDM with Adaptive Parameter Modelling (APM) and a CSDM with Constant Parameter Modelling (CPM) are implemented, investigated and compared. Moreover, a study on the effect of the parameter initial guesses on the parameter extraction performance is conducted. The proposed models make use only of the datasheet information.

5.1 Proposed APM and CPM Models

The $I(V)$ equation and the equivalent circuit of CSDM have been presented in Paragraph 3.2.3 and are reported here for simplicity:

$$I = I_{ph} - I_s\left[e^{\left(\frac{V+IR_s}{aV_{th}}\right)} - 1\right] - \frac{V + IR_s}{R_p} \tag{5.1}$$

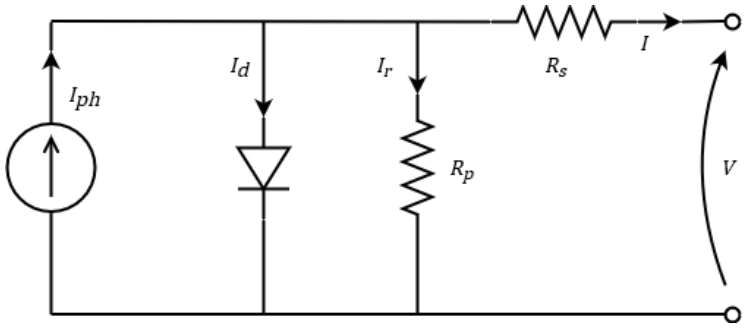

Figure 5.1 Equivalent circuit of a Complete Single-Diode Model (CSDM)

Adaptive Parameter Modelling CSDM

In the proposed APM model, the TRP are computed for the given cell temperature T_c and irradiance G according to Equations (2.21)-(2.24) and (2.27).

$$I_{SC}(G, T_c) = \frac{G}{G_{ref}} I_{SC,ref}\left[1 + \alpha_T\left(T_c - T_{c,ref}\right)\right] \tag{5.2}$$

$$P_{MPP}(T_c) = P_{MPP,ref}\left[1 + \gamma_T\left(T_c - T_{c,ref}\right)\right] \tag{5.3}$$

$$I_{MPP}(T_c) = I_{MPP,ref}\left[1 + \delta_T\left(T_c - T_{c,ref}\right)\right] \tag{5.4}$$

$$V_{MPP}(T_c) = V_{MPP,ref}\left[1 + \omega_T\left(T_c - T_{c,ref}\right)\right] \tag{5.5}$$

$$V_{OC}(G, T_c) = V_{OC,ref}\left[1 + \beta_T\left(T_c - T_{c,ref}\right)\right]\nu_T \tag{5.6}$$

With this approach, the irradiance affects only the short-circuit current ($\nu_T = 1$), and literature shows that this is a reasonable assumption.

Once the TRP are updated, a parameter extraction is performed for the given pair (G, T_c) so that *all* model parameters are *adapted* to the operating conditions. The details about the parameter extraction process are presented in Paragraph 5.2. It is to be noted that this model does not need a preliminary evaluation at STC.

Constant Parameter Modelling CSDM

In the proposed CPM model, a preliminary one-timer parameter extraction is performed at STC. The obtained model parameters are used as reference to build the model's response to any irradiance and any temperature; the photocurrent I_{ph} is updated through Equation (2.28) while the saturation current I_s is updated with Equation (2.30):

$$I_{ph}(G, T_c) = \frac{G}{G_{ref}} I_{SC,ref}\left[1 + \alpha_T\left(T_c - T_{c,ref}\right)\right] \tag{5.7}$$

$$I_s(T_c) = I_{s,ref}\left(\frac{T_c}{T_{c,ref}}\right)^3 e^{\frac{qE_g}{ak_B}\left(\frac{1}{T_{c,ref}} - \frac{1}{T_c}\right)} \tag{5.8}$$

With this approach, the following assumptions are made:

1. the irradiance affects only the photocurrent,
2. the ideality factor and the resistances are constant with respect to both the irradiance and the temperature.

As for APM, the first assumption is reasonably acceptable while the second one is more questionable, as seen in Paragraph 2.4.2 (*cf. Figure 2.17-2.21*).

5.2 Parameter Extraction Algorithm

In APM the parameter extraction is performed for every level of irradiance and temperature, while in CPM it is performed once to extract the STC parameter upon which the irradiance-temperature response is built: either model, the parameter extraction is (differently) fundamental.

The models are implemented in a Python [36] script developed *ad-hoc* on the Jupyter Notebook (a multi-language online execution environment) for fast and effective visualization and parameterization. In this software environment, the solving constraints (2.9)-(2.12) are set without any simplification (they are expressed explicitly in Equations (A.18)-(A.21) in Appendix A.2.4). The function `fsolve` (SciPy package) finds their solutions applying the Newton-Raphson method on the corresponding functions, i.e. the four solving equations are set in the form:

$$\begin{cases} f_1(\boldsymbol{X}) = 0 \\ f_2(\boldsymbol{X}) = 0 \\ f_3(\boldsymbol{X}) = 0 \\ f_4(\boldsymbol{X}) = 0 \end{cases} \tag{5.9}$$

where $\boldsymbol{X}$ is the vector of the unknowns, i.e. the model parameters. Since the `fsolve` function runs only when a independent system is fed to it (i.e. a number of equations equal to the number of unknowns), one out of the 5 parameters must be set fixed, as discussed in Paragraphs 2.3 and 3.2.3: the ideality factor has been chosen as fixed parameter (therefore, $\boldsymbol{X} = [I_{ph}, I_s, R_s, R_p]$) because of the limited range of values that it proved to assume according to the reviewed literature. In fact, as this range is limited, the ideality factor can still be evaluated through an iteration loop. The `fsolve` function tries to find the solution vector $\boldsymbol{X}_{sol}$ that minimizes the residuals of system (5.9). In order to do this, it needs an initial guess for each of the unknowns and, as explained in Appendix A.1.1, this is crucial for the accuracy of the performance and for the execution time. If the initial guesses are too far from the actual solution, the algorithm diverges and fails returning no solution. For this reason, an evaluation of the initial guesses has been conducted as follows:

- I_{ph} is set equal to I_{SC};
- I_s is evaluated through Equation (2.33) for every a:

$$I_s(G,T) = \frac{I_{ph}(G,T)}{e^{\left[\frac{V_{OC}(G,T)}{aV_{th}}\right]} - 1} \tag{5.10}$$

- R_p is evaluated through Equation (3.24):

$$R_{p,min} = \frac{V_{MPP}}{I_{SC} - I_{MPP}} - \frac{V_{OC} - V_{MPP}}{I_{MPP}} \tag{5.11}$$

- R_s is set to zero.

At the beginning, the loop on a was set in the range [1.0, 2.0] with 0.01 steps, according to the physical background presented in the previous Chapters. The performance index of the extraction over the a-loop was chosen to be the RMSD on the residuals of system (5.9), as natural extension of the NR-based `fsolve` algorithm itself:

$$RMSD_{PE} = \sqrt{\frac{\sum_i^4 f_i^2(\boldsymbol{X})}{4}} \tag{5.12}$$

$RMSD_{PE}$ is used as selection criterion to choose between the various solutions, meaning that the selected solutions (a_{sol}, $\boldsymbol{X}_{sol}$) are those for which $RMSD_{PE}$ is minimum. Also, a physical-consistency constraint is set on the solutions, i.e. that all of the parameters must be non-negative.

After various trials, a_{sol} showed to lie always below 1.55 : this result is consistent with the results obtained from other authors, who indicated a to lie in the range [1.0, 1.5] (*cf.* Paragraph 2.2). For this

reason, the loop on the ideality factor was reset to [1.0, 1.55] as looping showed to be the main time-consuming factor (see computing time analysis further on).

During manual trials, another factor was highlighted to impact the extraction results, i.e. the initial guess on the series resistance. For this reason, a second loop on $R_{s,in}$ was set outer of the loop on a, in the range [0, 0.15] with 0.01 steps. It is worth to note that while the loop on a sets a fixed model parameter, the loop on R_s sets "only" its *initial* guess $R_{s,in}$.

A performance analysis was conducted and the results are shown in Figure 5.2: the size and the color intensity of the circles measure the goodness of the extraction performance as they are proportional to the opposite of the order of magnitude of $RMSD_{PE}$ (i.e., the larger the circle and the darker the color, the smaller the $RMSD_{PE}$), for the corresponding pair of ideality factor (fixed) and initial guess on the series resistance.

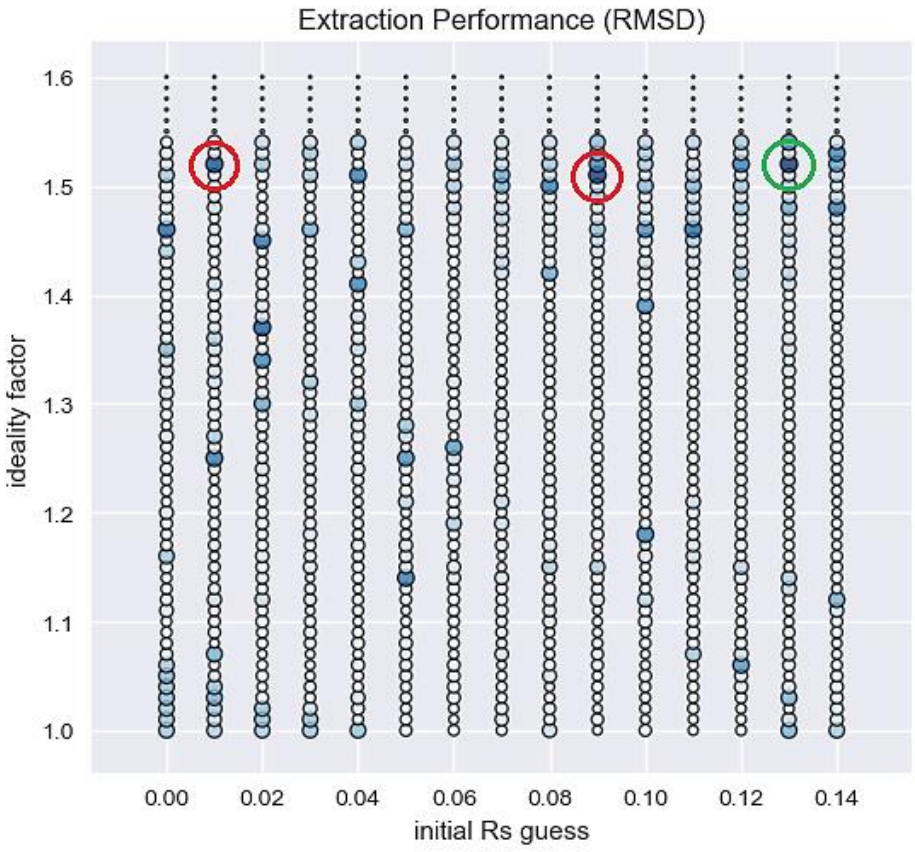

Figure 5.2 $RMSD_{PE}$ for all the combinations $(R_{s,in}, a)$ in the extraction algorithm: the color intensity and the size of the circles are proportional to $-log_{10}(RMSD_{PE})$

A first clear result is the confirmation that for $a > 1.55$ the performance drops significantly. The loop-nested selection criterion on minimum $RMSD_{PE}$ picked the solution highlighted with the green sign ($a = 1.52$, $R_{s,in} = 0.13$); however, from the picture it is clear that other solutions give a similar $RMSD_{PE}$ (red signs) but are discarded as they perform slightly worse. Yet, the red solution on the left would have been found significantly earlier than the others (as it comes first in the $R_{s,in}$ loop). All this put to question:

- whether to "extend" the minimum $RMSD_{PE}$ *value* criterion to a minimum *range*. However, this would require either 1) a human analysis of the selected range, which is reasonable for CPM (one initial extraction) but is unthinkable for APM (constant extraction) or 2) a second selecting criterion;
- if there is a correlation between a and $R_{s,in}$ with respect to $RMSD_{PE}$ (for instance, from Figure 5.2 it seems that no matter $R_{s,in}$, a_{sol} lies tightly around 1.52);
- to what extent it is convenient to set wide and detailed (stepped) loops to search for the best numerical $RMSD_{PE}$ value, i.e. what is the acceptance level on the fitness of the constraints.

In order to address this issues, it is convenient to plot the results of Figure 5.2 in another way: Figure 5.3 plots the vertical trends of Figure 5.2, i.e. it shows the order of magnitude of $RMSD_{PE}$ as function of a for a given $R_{s,in}$.

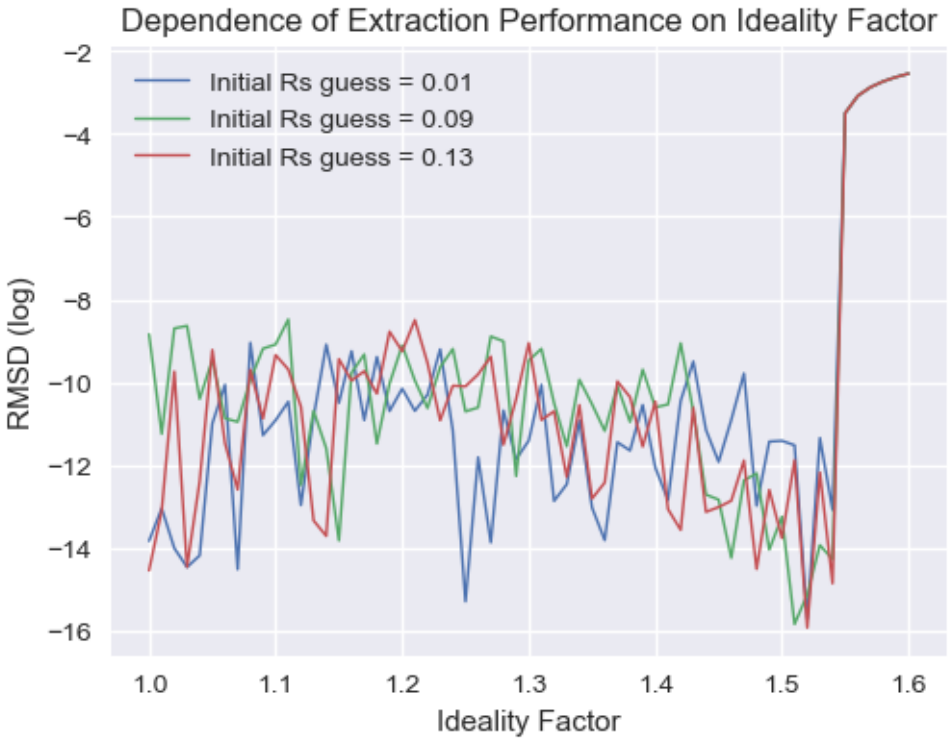

Figure 5.3 Dependence of $log_{10}(RMSD_{PE})$ on ideality factor a for different $R_{s,in}$

Considering that the three displayed $R_{s,in}$ values are exactly those highlighted in Figure 5.2, the following can be noticed:

- as suspected, there is a solution convergence around 1.52 where the gaps between the three $RMSD_{PE}$ are minimal (and in the domain of 10^{-16}!);
- this convergence zone is dangerously close to the divergence zone, i.e. the abovementioned $a > 1.55$, meaning that on the one hand, a slightly too conservative upper boundary on the a-loop could cut out the best solutions and on the other, a too loose upper boundary would be inefficient time-wise;

- overall, the plots show similar trends apart from a couple of zones, that are [1.00, 1.05] and 1.25, where $R_{s,in} = 0.09$ shows an interesting valley;
- other two areas of accumulation for possible solutions appear in the range [1.0, 1.1] (except for $R_{s,in} = 0.09$) and around 1.15: here, if on the one hand the $RMSD_{PE}$ is about two orders of magnitude higher than the selected solution, on the other hand it is still extremely low ($\sim 10^{-14}$) and it "appears" significantly earlier in the a-loop (i.e. faster execution time).

The insights brought into light by Figure 5.2 and Figure 5.3 suggest that the best fit on the constraint equations (that is, the best match at TRP and the MPP as actual maximum of the power curve) might not be truthful. From a mathematical point of view, this is expectable as the system is dependent. Even if a loop on one of the unknowns is set (herein it was chosen a, but can be any of the others), simulating a fifth equation, a *real* fifth piece of information is still missing. This means that the *numerical best* fit on the TRP might not be the actual best fit on the real PV device. This will emerge clearly in the simulations presented in Chapter 6.

A further level of analysis can be carried out with respect to the computing (or execution) time of the parameter extraction algorithm. Figure 5.4 shows its dependence on the upper boundaries for the a-loop and the $R_{s,in}$-loop: the influence of each upper limit is evaluated setting the other at its lowest in order to reduce the mutual influence.

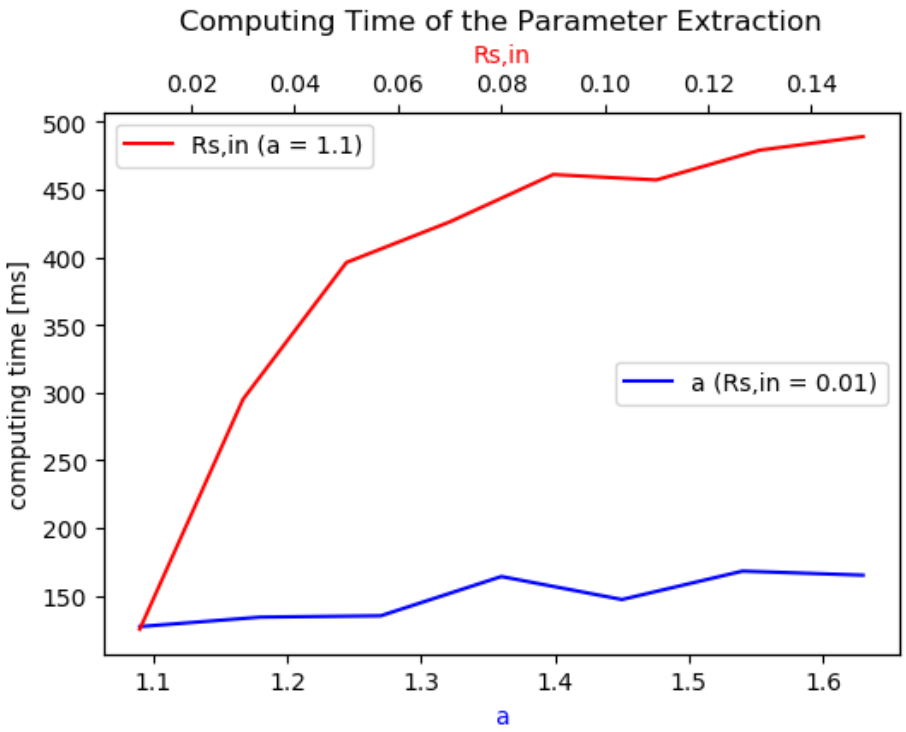

Figure 5.4 Computing time as function of the loops upper boundaries

From the figure, $R_{s,in,max}$ appears to have a nonlinear influence and stronger than that of a_{max}, which appears to be almost constant. Both the behaviours appear to be counterintuitive as an increase in the upper boundary of a loop should "simply" increase linearly the computing time. When they are set both on higher values, the behaviour appears to be a superimposition of the trends shown in Figure 5.4: as a reference, for $a_{max} = 1.2$ and $R_{s,in,max} = 0.1$ the computing time is around 500 ms while for $a_{max} = 1.55$ and $R_{s,in,max} = 0.15$ it jumps to 900 ms (*cf.* also Table 6.3). The reason might lie in the trial-and-error structure of the `fsolve` function.

As comparison, CPM never goes over 10 ms to return its model parameters, as it does not have to perform a numerical approximation for every pair (G, T_c).

As a conclusion, these analysis bring into question to what extent the fitting of the constraints can be sacrificed for the sake of model simplicity, solidness and usefulness. In fact, one can argue about making a difference between a $RMSD_{PE}$ in the order of 10^{-16} and one of 10^{-14} if the irradiance and the temperature values fed to the model are inevitably affected by uncertainties that have a significantly higher impact on the model performance. Even the experimental equations such as (2.21) introduce an error greater than those observed in Figure 5.3 by orders of magnitude.

In Chapter 6, the effect of the loops on a and $R_{s,in}$ are further (visually) investigated in terms of I-V curve fitting. Along with this, also the effect of measurement uncertainty and of a modified $RMSD_{PE}$ are explored, as explained in the Paragraph 5.3.

Finally, either the chosen model is APM or CPM, for sure a careful design and a preliminary evaluation of the extraction process is herein suggested in order to highlight behaviours that are specific to the module and the solving algorithm, so to optimize the results and the extraction process itself.

5.3 Code Implementation

As already mentioned, the models have been implemented in a Python script. The code features a degree of parameterization as it allows to:

- sweep within the uncertainty range on irradiance and temperature;
- set the degree of dirtiness of the module (*cf.* Appendix A.3.2);
- choose the upper limit on the $R_{s,in}$-loop, $R_{s,in,max}$;
- choose the upper limit on the a-loop, a_{max} ;

Once the model parameter are extracted, the code computes and plots the I-V curve applying the `fsolve` function to Equation (5.1) in the range [0, V_{OC}]. Then, it computes and plots the power curve, extracting the coordinates of the MPP.

The computed values are then used to evaluate the model with respect to the experimental values according to a number of criteria discussed in Paragraph 2.5, that are:

- the RMSD and NRMSD on current and power,
- absolute and relative errors on the TRP,
- the distance from the MPP.

The flowchart of the code algorithm is shown in Figure 5.5.

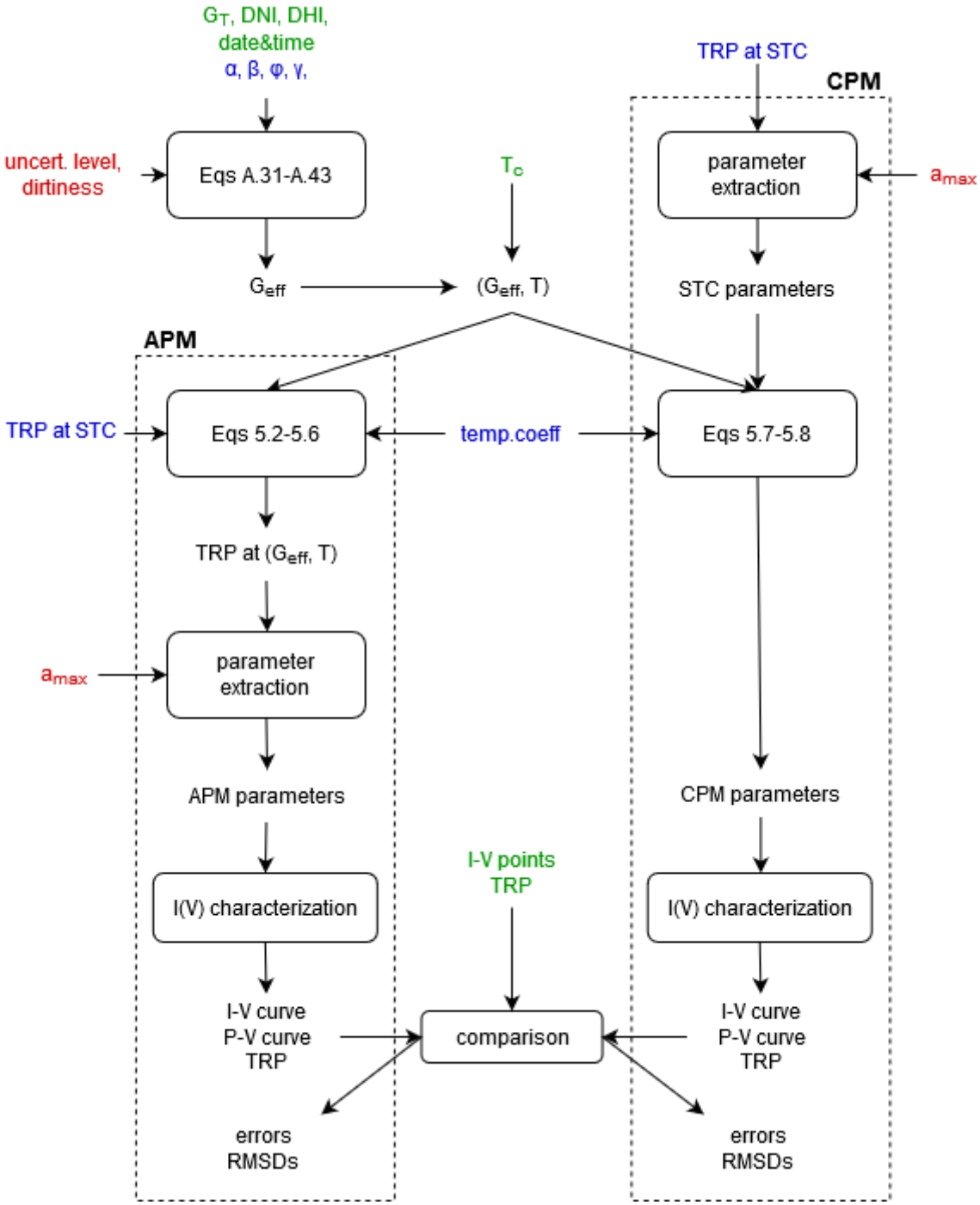

Figure 5.5 Flowchart of the implemented code. Blue quantities are taken from the datasheet, green ones from the measured dataset and red one are user's inputs

6 Evaluation of the Proposed Models

In this Chapter, the proposed models are tested and evaluated by comparison of their results with experimental data. A preliminary parameter extraction is performed at STC to initialize CPM. Then, the models are compared and discussed in a series of simulations with varying irradiance and temperature.

6.1 Experimental Data

The experimental data to validate the models has been taken from the publicly available database of the National Renewable Energy Laboratory (NREL) [37]. The models have been tested on the monocrystalline silicon module of the NREL PV system located in Cocoa, Florida (USA); the datasheet data is shown in Table 6.1 and the mounting details in Table 6.2. It must be noted that the datasheet values are not the actual manufacturer's values (also, the module model and manufacturer are not mentioned) but those measured in NREL facilities, according to standards IEC 60904-3 (TRP) and IEC 61215/61646 (temperature coefficients) [37].

Table 6.1 Datasheet values for the tested mono-Si module

Quantity	**Symbol**	**Value**	**Unit**
Short-Circuit Current	I_{SC}	5.127	A
Open-Circuit Voltage	V_{OC}	22.06	V
Voltage at MPP	V_{MPP}	17.58	V
Current at MPP	I_{MPP}	4.724	A
Power at MPP	P_{MPP}	83.04	W
Temperature Coefficient on I_{SC}	α_T	0.05	%/°C
Temperature Coefficient on V_{OC}	β_T	-0.34	%/°C
Temperature Coefficient on I_{MPP}	δ_T	0.01	%/°C
Temperature Coefficient on V_{MPP}	ε_T	-0.43	%/°C
Temperature Coefficient on P_{MPP}	γ_T	-0.42	%/°C

Table 6.2 Mounting details

Quantity	**Symbol**	**Value**	**Unit**
Azimuth	α	0	°
Slope (Tilt)	β	28.5	°
Latitude	φ	28.39	°
Longitude	λ	-80.46	°
Timezone	ET	UTC-5 (-4 in DST)	

The dataset is provided as a *.csv* file and it features a series of values sampled every 5 minutes; each of these values is associated with an uncertainty level (details on measurements, quality and

uncertainty assessments are described in the Manual provided with the datasets [37]). The data of interest for this study are: the date and time, the Plane-Of-Array (POA) irradiance, the Direct Normal Irradiance (DNI), the Diffuse Horizontal Irradiance (DHI), the back-surface module temperature, the coordinates of the MPP and the sampled (V, I) points; the number of the I-V points vary from 181 to 189. It must be noted that while I_{SC} and V_{OC} are taken from the I-V dataset, most of the times the MPP coordinates are not included in this dataset, suggesting that they are recorded by a separate measurement (like an MPPT). The effective irradiance reaching the module has been computed taking into account both the uncertainty on the measurements and the dirtiness on the module (details are reported in Appendix A.3). Finally, despite the significant and precious amount of precise data provided in the datasets, the I-V curve at STC has not been reported nor measured, unfortunately.

6.2 Parameter Extraction at STC

A preliminary parameter extraction is carried out at STC. Since the measurements were executed in a laboratory, the dirtiness is neglected (model set to '`clean`'). Given the doubts emerged in Paragraph 5.2, the upper loop boundaries $R_{s,in,max}$ and a_{max} are explored in different combinations. The results of the parameter extractions are shown in Table 6.3.

Table 6.3 Parameter extraction results for different pairs of $(R_{s,in,max}, a_{max})$

$R_{s,in,max}$	a_{max}	comp. time [ms]	Iph [A]	Is [A]	a	Rs [Ω]	Rp [Ω]
0.05	1.2	285	5.139	1.03e-09	1.07	0.35	150
0.10	1.2	365	5.136	4.07e-09	1.14	0.32	177
0.15	1.2	420	5.136	4.07e-09	1.14	0.32	177
0.05	1.55	415	5.127	7.79e-07	1.52	0.19	3023
0.10	1.55	590	5.127	7.01e-07	1.51	0.19	2129
0.15	1.55	749	5.127	7.79e-07	1.52	0.19	3023

As expected from the analysis discussed in Paragraph 5.2, the solutions appear to converge around two sets of values depending on a_{max} (*cf.* Figure 5.3): one with $a = 1.52$ and the other with $a = 1.14$, where the former features higher I_s and R_p and lower R_s than the latter. These differences are visible in the I-V curves produced by the two sets (see Figure 6.1). However, as expected, the errors on the TRP are *exactly the same* if the physical quantities are considered with a precision of 10^{-4} (the $RMSD_{PE}$ for the two sets is in the orders of 10^{-14} - 10^{-16}!). The performance of the extraction algorithm is excellent as the errors are practically null, showing a perfect match with experimental data (see Table 6.4).

Despite the difference in the $RMSD_{PE}$ for the two sets is minimal, the differences of the model parameters for the two sets (especially a, R_s and R_p) are crucial as they have clear physical meaning (as seen in Paragraph 2.2): this means that, with respect to the model with $a = 1.14$, the model with

$a = 1.52$ inteprets the real PV module as better fabricated in the assembly (low dissipation through the resistances) but with a poorer semiconductor material (high ideality factor). This is the fifth piece of information that is missing: in fact, if an I-V dataset at STC was available, the RMSD *on the curve* (i.e. the curve fitting) would have selected the set that best matched the shape of the actual PV device.

Table 6.4 Model errors at STC for every tested pair $(R_{s,in,max}, a_{max})$

Quantity	Measured	Computed	Absolute Error	Relative Error (%)
Isc	5.127	5.1270	0.0000	0.00
Voc	22.060	22.0600	0.0000	0.00
Pmpp	83.040	83.0479	0.0079	0.01
Vmpp	17.580	17.5773	-0.0027	-0.02
Impp	4.724	4.7247	0.0007	0.02

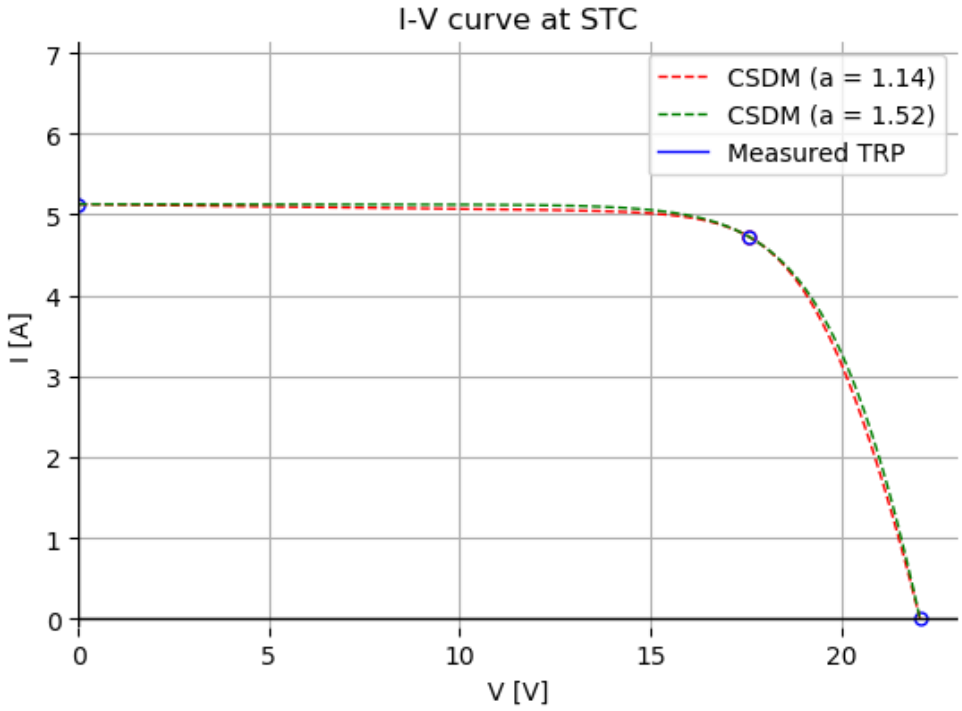

Figure 6.1 Modelled I-V curves at STC, the blue dots are the measured TRP

Nevertheless, a criterion to choose between the two sets of parameters must be chosen. In fact, if on the one hand APM does not need to be initialized at STC, on the other hand for CPM the choice is crucial because, in later evaluations with varying irradiance and temperature, a, R_s, R_p are the same as at STC. In reality, also for APM this evaluation is crucial as it gives an hint on which pair $(R_{s,in,max}, a_{max})$ is best to feed to it. One can argue about the computing time as criterion; however, as the extraction at STC is a one-timer for CPM, higher computing times can be serenely accepted for the sake of the accuracy of the model parameters. Depending on the availability of the producers, a check with the

manufacturing process could give hints on which set best represents the actual physics of the module. Alternatively, depending on the purposes of the modelling, hints could come from a statistical evaluation of the (location-specific) temperature range that will be fed to the model, on the basis of the results from literature presented in Paragraph 2.4.2.

In this study, for the sake of research, the set with $a = 1.52$ is chosen to produce reference values for CPM, while lower values of a_{max} (possibly leading to sets closer to that with $a = 1.14$ at STC) will be fed to APM, as for this model the computing time gains importance. This choice will produce results that confirm the insights gained so far.

6.3 Behaviour with Varying Operating Conditions

Once CPM has been initialized at STC, both the models are ready to be tested with varying operating conditions (irradiance and cell temperature).

The following is taken as default:

- the uncertainties on irradiance and temperature are neglected (meaning that the center value of the uncertainty range is considered);
- the panel surface is considered clean; however, a low degree of dirtiness can be considered as the NREL maintenance checks detected sporadically the presence of light soiling on modules [37];
- for APM, $a_{max} = 1.2$ and $R_{s,in,max} = 0.15$.

Three levels of irradiance and temperature levels are investigated: high, medium and low. It must be noted that mixed combinations (e.g. high irradiance and low temperature) were hard to find in the measurement dataset, except for low irradiance and high temperature (shading during summer days).

High irradiance, high temperature

Figure 6.2 shows the performance of the models for the 11th April with $G = 1071\ \mathrm{W/m^2}$ ($G_{eff} = 1049\ \mathrm{W/m^2}$, $\theta_s = 12.3°$) and $T_c = 56.3\ ℃$. The following can be noticed:

- the I-V curves of the models are almost superimposable ($NRMSD_I$ is 1.24% for APM while for CPM is 1.82%), except for the slopes in the current-source and voltage-source areas as they feature significantly different values for R_p and R_s, respectively; this behaviour has been already highlighted at STC and was expected for the design choices explained at the very end of Paragraph 6.2;
- the higher deviation is registered on the currents (at SC and MPP about 1.5%) while there is virtually no error on the voltages (0.3% at OC and MPP for CPM, 0.2% and 0.01% for APM);
- despite the similar results, APM runs in 265 ms versus the 3 ms taken from CPM.

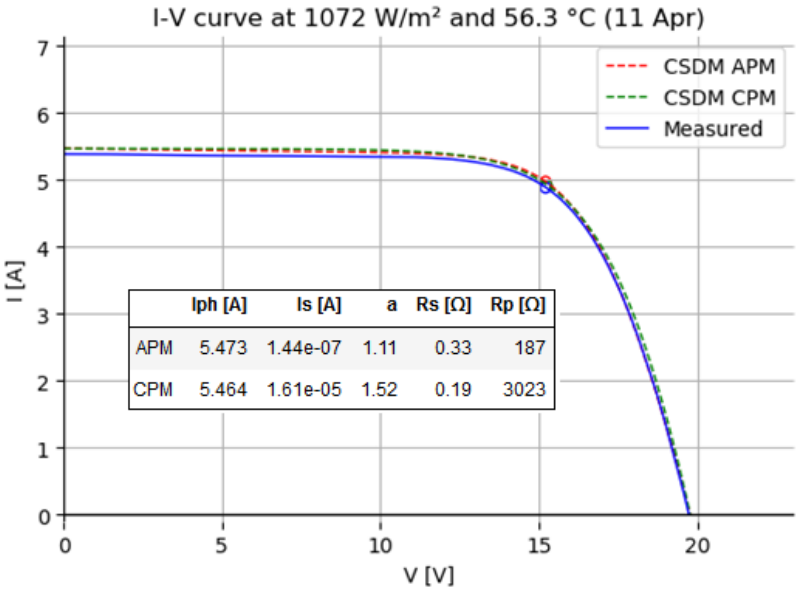

Figure 6.2 I-V curves for high irradiance and high temperature

The second point suggests that the models are actually performing very good except for an offset along the y-axis, i.e. the currents. In fact, if the sensitivity of pyranometers to temperature [38] is considered (the distance of the operating temperature from the calibration temperature, i.e. 20 °C, is significant), the results show a quasi-perfect match.

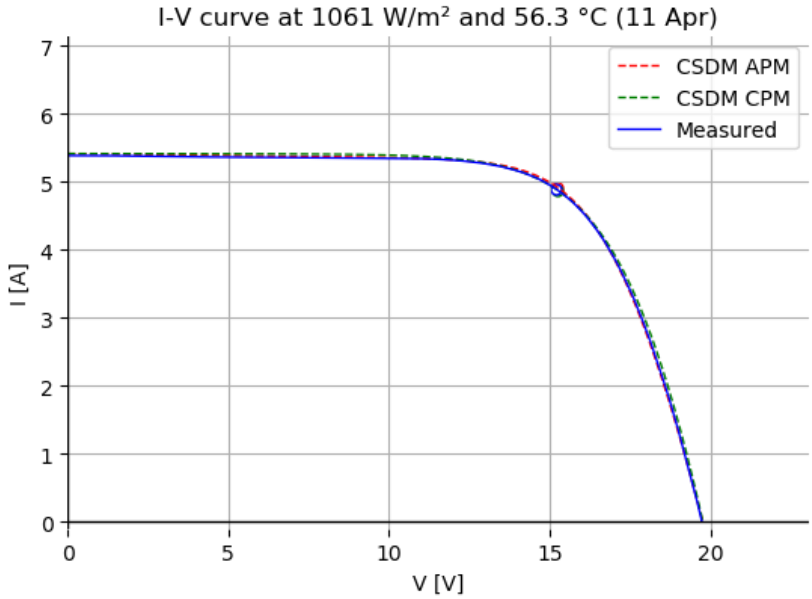

Figure 6.3 Models match with uncertainty-adjusted irradiance

Figure 6.3 shows the models performance for the same moment but with G evaluated in the middle point of its lower half uncertainty range: $NRMSD_I$ drops to 0.45%-0.02 A for APM and 1.00%-0.05 A for CPM. The computing times and the model parameters did not change, except for I_{ph} (as expected).

Medium irradiance, medium temperature

Figure 6.4 shows the performance of the models for the 17th February with $G = 622\ \mathrm{W/m^2}$ ($G_{eff} = 594\ \mathrm{W/m^2}$, $\theta_s = 48.7°$) and $T_c = 26.2\ °\mathrm{C}$. The match is certainly satisfying even if CPM shows a non-neglectable -1.8% deviation from V_{MPP}. Overall, APM performs better as it follows more tightly the shape of the measured I-V curve ($NRMSD_I$ is 1.02% for APM and 2.33% for CPM). This might suggest that, from a physics point of view, the real PV module is better modelled by the set with $a = 1.14$ at STC (see previous Paragraph). In light of this consideration, it is reasonable to ascribe the higher gap for CPM not to the Constant-Parameter approach itself, rather to the design choice to initialize it with the set of STC parameter with $a = 1.52$. In fact, if CPM is initialized with the other set, it returns the same model parameters as APM (see Figure 6.5) with an average gap in the errors in the order of the tenth of %.

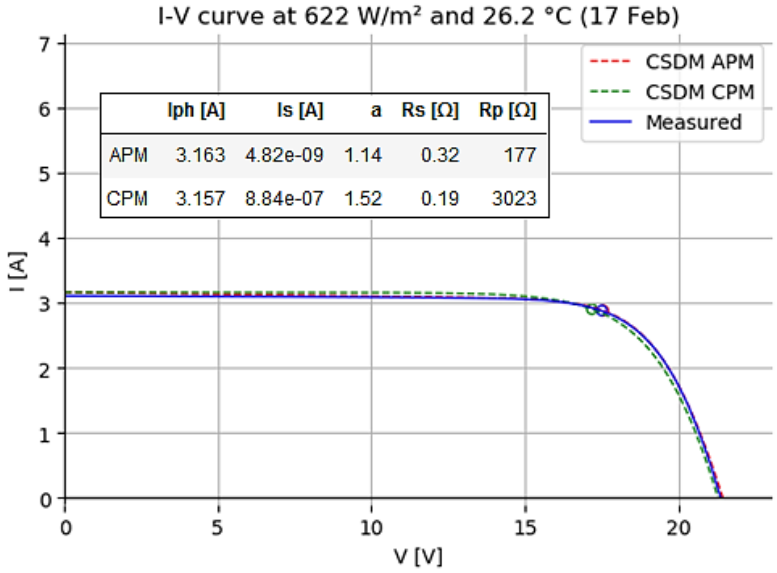

Figure 6.4 I-V curves for medium irradiance and medium temperature

In this case, for both the models all the errors fall below 0.4% except for I_{SC} (1.8%). However, it is worth noting that, since I_{SC} is lower due to the irradiance, relative higher percentage errors on the currents and (therefore, on the power) hide absolute errors that are still quite low. For instance, the absolute error on I_{SC} is 0.05 A and a $NRMSD_I$ of 1.05% means $RMSD_I = 0.03\ A$. The absolute error on the P_{MPP} is 0.14 W. APM performed in 385 ms and CPM in 3 ms.

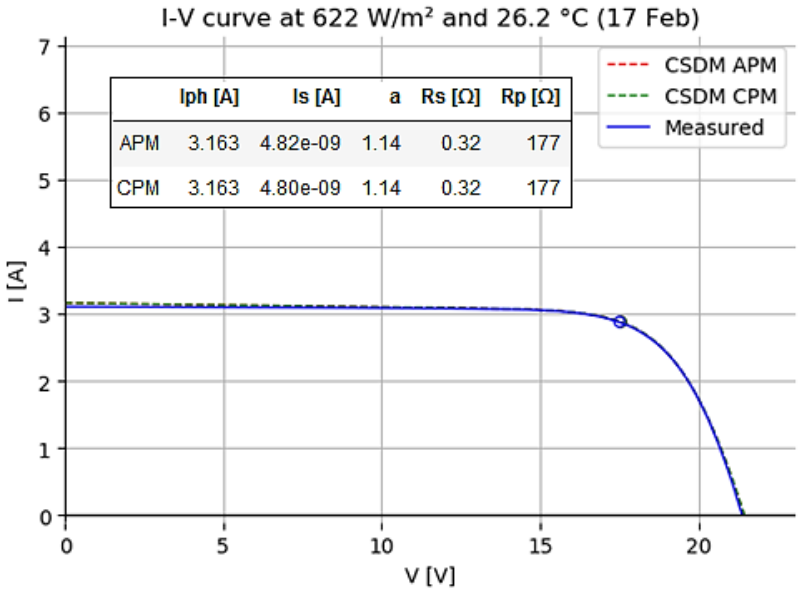

Figure 6.5 CPM is initialized with the other STC parameters set

Low irradiance, low temperature

Figure 6.6 shows the performance of the models for the 8th February with $G_{POA} = 287\ \mathrm{W/m^2}$ ($G_{eff} = 247\ \mathrm{W/m^2}$, $\theta_s = 67.4°$) and $T_c = 11.5\ °\mathrm{C}$.

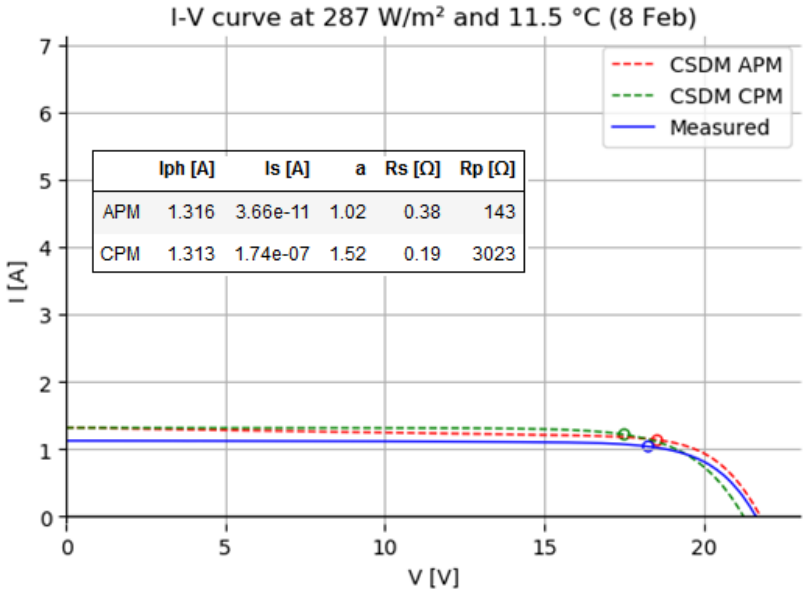

Figure 6.6 I-V curves for low irradiance and low temperature

It is clear that both the models are affected by a non-neglectable mismatch, both in the current and voltage domain. This was expected as CSDM is known to perform worse at low irradiance, as seen in Chapter 4. In particular, as APM shows a better fit of the shape despite the offset, the first choice for the STC parameter set to initialize CPM proves again to be the wrong one, as seen in the previous test.

$NRMSD_I$ is as high as 16.3% for APM and 19.7% for CPM. Errors on the TRP are high on the currents and power (about 21% and 16%, respectively) but lower on the voltages, with CPM performing significantly worse (-3.85% vs 1,72% on V_{MPP}). However, as 11.5°C is fairly far from the calibration temperature of the pyranometer (the sensitivity is more emphasized for temperatures below the reference [38]), the irradiance can be adjusted to the lower value in the uncertainty range. Figure 6.7 shows the effect of this correction with the CPM re-initialized with the correct set. Despite the error on I_{SC} is still considerable and the $NRMSD_I$ are still high (about 8%), a significant improvement is registered at the MPP, with CPM performing slightly better (-0.36% vs 1.48% on V_{MPP}). This suggests that a possible source of inaccuracy might be the evaluation of the photcurrent through Equation (2.28). The absolute errors on the P_{MPP} are around 1.7 W and APM performs in 600 ms while CPM in 2 ms.

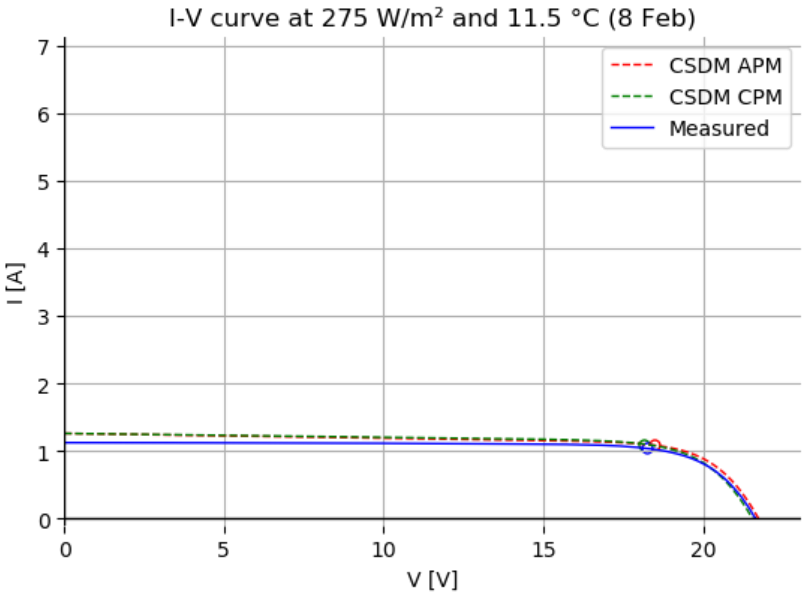

Figure 6.7 Models match with uncertainty-adjusted irradiance

Finally, if a low level of dirtiness is considered, $NRMSD_I$ falls to 2.85% (0.03 A) for APM and 3.79% (0.04 A) for CPM. Also the errors on the MPP drop, with CPM performing better than APM (see Table 6.5 and Table 6.6).

Table 6.5 Errors for CPM in low irradiance and temperature

Quantity	Measured	Computed	Absolute Error	Relative Error (%)
Isc	1.1205	1.1926	0.0721	6.44
Voc	21.6270	21.4766	-0.1504	-0.70
Pmpp	18.9362	18.7902	-0.1460	-0.77
Vmpp	18.2170	18.1229	-0.0941	-0.52
Impp	1.0395	1.0368	-0.0027	-0.26

Table 6.6 Errors for APM in low irradiance and temperature

Quantity	Measured	Computed	Absolute Error	Relative Error (%)
Isc	1.1205	1.1926	0.0721	6.44
Voc	21.6270	21.6730	0.0460	0.21
Pmpp	18.9362	18.8169	-0.1193	-0.63
Vmpp	18.2170	18.4405	0.2235	1.23
Impp	1.0395	1.0204	-0.0191	-1.84

Low irradiance, high temperature

Figure 6.8 shows the performance of the models for the 6th August with $G = 108\ \mathrm{W/m^2}$ ($G_{eff} = 96\ \mathrm{W/m^2}$, $\theta_s = 80.0°$) and $T_c = 37.7\ °\mathrm{C}$, with CPM initialized correctly and the irradiance evaluated at the higer quarter point in the uncertainty range.

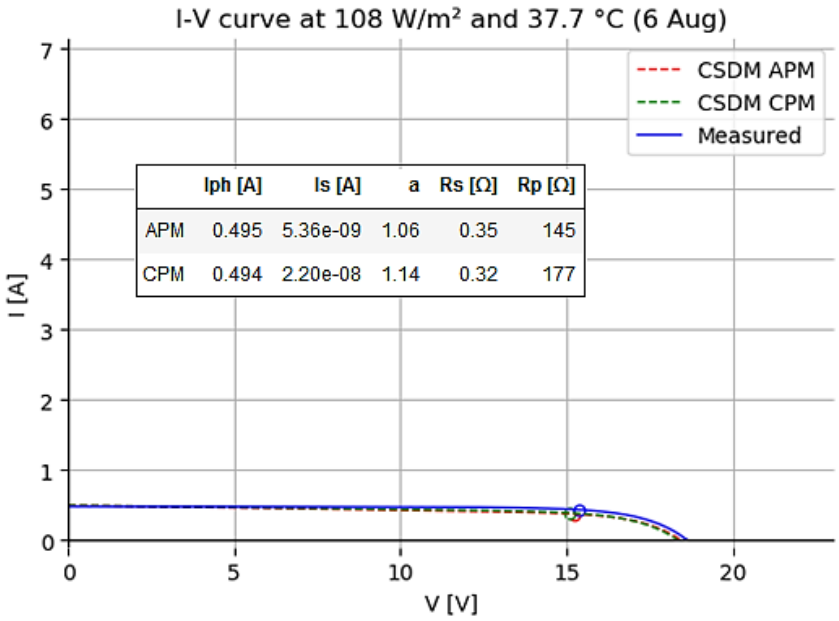

Figure 6.8 I-V curves for low irradiance and high temperature

Despite the severe conditions, the models continue to perform fairly good, with an $NRMSD_I$ of 9.15% (0.044 A) for APM and 8.15% (0.039 A) for CPM. The highest errors are registered at P_{MPP} (higher for APM with -14.9% and -0.99 W) due to the error on the I_{MPP} (same order of magnitude as P_{MPP}) while in V_{MPP} there is a -0.93% (-0.14 V) deviation for APM and -1.92% (-0.29 V) for CPM.

Conclusions

Overall, the comparison with the experimental data showed a very good predictive performance of the proposed models. As suspected from the parameter extraction analysis, the set of model parameters showing the best $RMSD_{PE}$ did not prove to represent the actual physics of the module, whereas the second best set showed to follow tightly the shape of the experimental I-V curves, especially at middle-lower irradiances and temperatures. This influenced the comparison between APM (guided towards the correct set) and CPM (initialized with the wrong set). When the models share the same parameter basis (i.e. a_{max} is the same), APM showed to perform almost always better than CPM although the differences were minimal and sometimes CPM perfomed better than APM, especially at low irradiances. This might not justify the significantly larger amount of computing time required by APM with respect to CPM (up to 200 times more).

The influence of the uncertainty on the irradiance and the effect of the dirtiness on the module proved to be able to justify possible mismatches, especially at low irradiance. This is confirmed by a generally perfect match in the voltage domain versus a positive offset along the current-axis.

Finally, analysing the variations of the parameters of APM, the following can be noticed:

- the ideality factor a seems to show a nonlinear mixed dependency on temperature and irradiance, with a clear drop at low irradiances;
- the series resistance R_s does not show clear trends;
- the parallel resistance R_p seems to increase both with irradiance and temperature, where the former dependency is stronger than the latter.

However, to properly evaluate these trends, datasets with mixed levels of irradiances and temperatures are needed; this is not trivial given the real behaviour of modules and its dependency on the climate profile of the location where the available data come from (it is unlikely to have high irradiance and low temperatures in Florida).

7 Conclusions and Further Developments

In this study, a reference framework for PV modelling has been presented and two different Complete Single-Diode Models have been investigated.

The preliminary literature review and the built framework showed that different physical approaches and analytical strategies have been suggested as numerous aspects need to be considered when modelling a PV device, such as the availability of experimental data and the behaviour of the models with respect to varying irradiance and temperature. In the light of these considerations, the Complete Single Diode Model (CSDM) featuring 5 model parameters proved to represent the best compromise between simplicity and accuracy. However, since its solving system of equations is dependent, the parameter extraction is affected by a certain level of arbitrariness in the design choices. Therefore, in order to provide additional results for further developments, this model has been chosen for implementation and evaluation. In particular, two different strategies to account for dependence on irradiance and temperature have been investigated, i.e. Constant-Parameter Modelling (CPM) and Adaptive-Parameter Modelling (APM).

For the purpose, an ad-hoc script was developed in Python, featuring a degree of parameterization to allow for the investigation of the extraction process, of the influence of uncertainties on irradiance and temperature and the dirtiness of the PV device surface. The analysis of the parameter extraction algorithm based on the matching of the Three Remarkable Points showed that a reasoned design is crucial in terms of accuracy of the results due to the dependent nature of the solving system of equations. In particular, a loop on the ideality factor was set to compensate the missing fifth constraint. However, the width of the range on this loop proved to affect heavily the computing time (crucial for APM) without offering a guaranteed trade-off in terms of accuracy of the extracted parameters. This put to question to what extent the default selection criterion (i.e. the minimum RMSD on the constraints) should be considered, as the simulations showed that the second best set of parameters modelled more realistically the physics of the tested PV device: by setting a wider range of the loop on the ideality factor, thus supposedly increasing the chances to find the best solution, the actual better set is discarded. Mathematically, this is due to the lack of a *real* fifth physical constraint that brings in information about the shape of the I-V curve. This issue was considered also in light of the order of magnitude of the errors introduced by the empirical formulas for irradiance and temperature and the measurement uncertainties.

These effects have been investigated through simulations and comparison with measured data. Both the models proved to match almost perfectly the measured data in any operating condition, showing expected issues at low irradiance. However, these were never too severe and could be justified by taking into account the measurement uncertainties.

As regards the comparison between the two approaches to varying operating conditions, on the one hand the results showed that APM provides almost always better results than CPM and on the other hand, that CPM is sensitive to the preliminary parameter extraction at STC: if it is not conducted properly (e.g. for the abovementioned issue on the shape of the curve) it could cause CPM to mismatch sensibly from reality. However, if CPM is well initialized, it requires hundreds of times less computing time to

produce as accurate results as APM (differences lie in the tenth or hundrenth per cent). This could be crucial if the model is employed, for instance, in MPPT algorithms or in space applications. Moreover, APM is based on the availability of the temperature coefficients on the current and voltage at MPP, which is not to be taken for granted. Overall, CPM appears to be more rigid and sensitive yet simpler and faster, while APM is more refined but slower and possibly non-implementable.

The good results delivered by the models proposed in this study are based on the previous investigations conducted by the scientific community (for instance, the evaluation of the initial guesses for the parameter extraction). Another piece of investigation has been herein conducted providing useful insights about the design of the parameter extraction and the differences between APM and CPM. In this sense, further developments include:

- investigation of a mixed model between the proposed APM and CPM: this model would update the photocurrent and the saturation current as CPM does through empirical formulas, and numerically extracts the resistances exploiting only two constraints (at short-circuit and open-circuit), thus avoiding the necessity for temperature coefficients on current and voltage at MPP (the ideality factor is looped),
- a more detailed analysis of the variations of a, R_s and R_p with irradiance and temperature, with the use of the APM model,
- validation of the proposed models for PV technologies other than monocrystalline silicon,
- extension of the parameter extraction analysis to more complex models such as the Double-Diode Model,
- comparison and, possibly, integration with metaheuristic methods.

References

[1] A. Luque and S. Hegedus, Handbook of Photovoltaic Science and Engineering, John Wiley & Sons, 2011.

[2] N. Long and K. Steinberger, "Renewable Energy is Key to Fight Climate Change," Natural Resources Defense Council, 26 07 2016. [Online]. Available: https://www.nrdc.org/experts/noah-long/renewable-energy-key-fighting-climate-change. [Accessed 04 07 2020].

[3] International Energy Agency, "Data & Statistics," [Online]. Available: https://www.iea.org/data-and-statistics/. [Accessed 04 07 2020].

[4] W. Xiao, Photovoltaic Power System: Modeling, Design and Control, John Wiley & Sons, 2017.

[5] U.S. Energy Information Administration, "Solar explained - Photovoltaics and electricity," 28 05 2020. [Online]. Available: https://www.eia.gov/energyexplained/solar/photovoltaics-and-electricity.php. [Accessed 04 07 2020].

[6] M. G. Villalva, J. R. Gazoli and E. R. Filho, "Comprehensive Approach to Modeling and Simulation of Photovoltaic Arrays," *IEEE Transactions on Power Electronics,* vol. 25, no. 5, pp. 1198-1208, 2009.

[7] V. Lo Brano, A. Orioli, G. Ciulla and A. Di Gangi, "An improved five-parameter model for photovoltaic modules," *Solar Energy Materials & Solar Cells,* vol. 94, no. 8, pp. 1358-1370, 2010.

[8] C. Carrero, J. Amador and S. Arnaltes, "A single procedure for helping PV designers to select silicon PV modules and evaluate the loss resistances," *Renewable Energy,* vol. 32, pp. 2579-2589, 2007.

[9] A. M. Humada, S. Y. Darweesh, K. G. Mohammed, M. Kamil and et al, "Modeling of PV system and parameter extraction based on experimental data: review and investigation," *Solar Energy,* no. 199, pp. 742-760, 2020.

[10] W. De Soto, S. Klein and W. Beckman, "Improvement and validation of a model for photovoltaic array performance," *Solar Energy,* no. 80, pp. 78-88, 2006.

[11] A. M. Humada, M. Hojabri, S. Mekhilef and H. M. Hamada, "Solar cell parameters extraction based on single and double-diode model: a review," *Renewable and Sustainable Energy Reviews,* no. 56, pp. 494-509, 2016.

[12] D. S. H. Chan and J. C. H. Phang, "Analytical Methods for the Extraction of Solar-Cell Single- and Double-Diode Model Parameters from I-V Characteristics," *IEEE Transactions on Electron Devices,* vol. 34, no. 2, 1987.

[13] K. Ishaque, Z. Salam and H. Taheri, "Simple, fast and accurate two-diode model for photovoltaic modules," *Solar Energy Materials & Solar Cells,* no. 95, pp. 586-594, 2011.

[14] J. Gow and C. Manning, "Development of a photovoltaic array model for use in power-electronics simulation studies," *IEE Proceedings - Electric Power Applications ,* vol. 146, no. 2, pp. 193-200, 1999.

[15] M. N. I. Sarkar, "Effect of various model parameters on solar photovoltaic cell simulation: a SPICE analysis," *Renewables: Wind, Water and Solar,* vol. 3, no. 3, 2016.

[16] J. Cubas, S. Pindado and C. de Manuel, "Explicit Expressions for Solar Panel Equivalent Circuit Parameters Based on Analytical Formulation and the Lambert W-Function," *Energies,* no. 7, pp. 4098-4115, 2014.

[17] W. Xiao, W. G. Dunford and A. Capel, "A Novel Modeling Method for Photovoltaic Cells," in *35th Annual IEEE Power Electronics Specialists Conference*, Aachen, Germany, 2004.

[18] A. Habbati, Y. Ramdani, F. Moulay and K. Medles, "Irradiance and temperature impact on photovoltaic power by Design of Experiments," *Revue Roumaine des Sciences Techniques Serie Electrotechnique et Energetique,* vol. 58, pp. 284-294, 2013.

[19] R. Zieba Falama, A. Dadjé and N. Dyongyang, "A new analytical modeling method for photovoltaic solar cells based on derivative power function," *Journal of Fundamental and Applied Sciences,* 2016.

[20] P. Cuce and E. Cuce, "A novel model of photovoltaic modules for parameter estimation and thermodynamic assessment," *International Journal of Low-Carbon Technologies,* vol. 7, no. 2, pp. 159-165, 2012.

[21] G. Walker, "Evaluating MPPT converter topologies using a MATLAB PV model," *Journal of Electrical & Electronics Engineering,* Vols. 21-1, pp. 49-56.

[22] A. Kassis and M. Saad, "Analysis of multi-crystalline silicon solar cells at low illumination levels using a modified two-diode model," *Solar Energy Materials and Solar Cells,* vol. 94, pp. 2018-2112, 2010.

[23] D. Allam, D. Yousri and M. Eteiba, "Parameters extraction of the three diode model for the multi-crystalline solar cell/module using Moth-Flame Optimization Algorithm," *Energy Conversion and Management,* vol. 123, pp. 535-548, 2016.

[24] J. Phang, D. Chan and J. Phillips, "Accurate analytical method for the extraction of solar cell model parameters," *ELectronics Letters,* vol. 20, no. 10, pp. 406-408, 1984.

[25] J. Cabestany and X. Castaner, "A simple solar cell series resistance measurement method," *Revue de Physique Appliquée,* vol. 18, pp. 565-567, 1983.

[26] E. Matagne, R. Chenni and R. El Bachtiri, "A photovoltaic cell model based on nominal data only," in *CPE-POWERENG*, Setubal (PT), 2007.

[27] Amerisolar, "Amerisolar AS-6P30 Solar Module," [Online]. Available: http://www.weamerisolar.com/english/product/pro1/257.html.

[28] V. Lo Brano and G. Ciulla, "An efficient analytical approach for obtaining a five parameters model of photovoltaic modules using only reference data," *Applied Energy,* no. 111, pp. 894-903, 2013.

[29] J. Cubas, S. Pindado and A. Sanz-Andrés, "Accurate Simulation of MPPT Methods Performance When Applied to Commercial Photovoltaic Panels," *The Scientific World Journal,* 2015.

[30] S. A. A. Mustafa, "Modeling combined effect of temperature, Irradiance, series resistance and shunt resistor on solar cell by MATLAB/Simulink," *International Journal of Latest Technology in Engineering, Management & Applied Science,* vol. VI, June 2017.

[31] N. Veissid and A. Andrade, "The I-V Silicon Solar Cell Characteristic Parameters Temperature Dependence. An Experimental Study using the Standard Deviation Method," in *10th European Photovoltaic Solar Energy Conference* , Lisbon, Portugal, 1991.

[32] K. Nishioka, N. Sakitani, Y. Uraoka and T. Fuyuki, "Analysis of multicristalline silicon solar cells by modified 3-diode equivalent circuit model taking leakage current through periphery into consideration," *Solar Energy Materials and Solar Cells,* vol. 91, pp. 1222-1227, 2007.

[33] F. Hannane, H. Elmossaoui, T. Nguyen, P. Petit, M. Aillerie and J. Charles, "Forecasting the PV panel operating conditions using the Design of Experiments method," *Energy Procedia,* no. 36, pp. 479-487, 2013.

[34] S. Yadir, H. Amiry, R. Bendaoud, A. El Hassnaoui, A. Obbadi and M. Benhmida, "Physical parameters extraction by a new method using solar cell models with various ideality factors," in *27th International Conference on Microelectronics*, Casablanca, Morocco, 2015.

[35] A. Habbati, Y. Ramdani and F. Moulay, "A detailed modeling of photovoltaic module using MATLAB," *NRIAG Journal of Astronomy and Geophysics,* no. 3, pp. 53-61, 2014.

[36] Python. [Online]. Available: https://www.python.org/.

[37] W. Marion, A. Anderberg, C. Deline and et al., "User's Manual for Data for Validating Models for PV Module Performance," NREL, April 2014. [Online]. Available: https://www.nrel.gov/docs/fy14osti/61610.pdf.

[38] M. Korevaar, "The Importance of Pyranometer Temperature Response," Kipp&Zonen, 9 March 2015. [Online]. Available: https://www.kippzonen.com/News/582/The-Importance-of-Pyranometer-Temperature-Response.

Appendices

A.1 Numerical Methods for Nonlinear Equations

A.1.1 Newton-Raphson Method

The Newton-Raphson (NR) method, also known simply as Newton's method, is a root-finding algorithm of a real-valued function $f(x)$. It starts from an initial guess x_0 of the root and finds successively better approximations by the iteration:

$$x_{n+1} = x_n - \frac{f(x_n)}{f'(x_n)} \tag{A.1}$$

The point $(x_{n+1}, 0)$ is the intersection of the x-axis and the tangent to the function in $(x_n, f(x_n))$, meaning that the improved guess is the root of the linear approximation at the previous point (see Figure A.1). For this reason it also called method of the tangents. The iteration is repeated until the desired level of accuracy is achieved. NR method can be extended to vectorial functions and systems of equations.

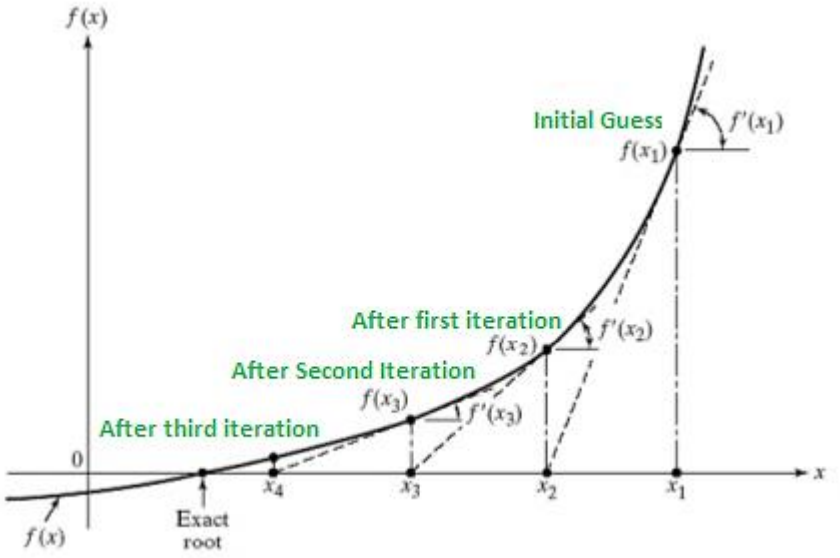

Figure A.1 The graphical interpretation of the Newton-Raphson method

A.1.2 Trial-and-Error Routine

A manual trial-and-error routine can be implemented in widely available software environments such as MATLAB, Python or MS Excel [7]. In general, if n parameters are to be determined with $k < n$ equations, then $(n - k + 1)$ parameters are initially guessed and the others are calculated by means of $k - 1$ equations. One of the $(n - k + 1)$ remaining equations is used to calculate one of the parameter initially guessed and this value is compared to the initial attempt and adequately updated. This process is reiterated until the convergence of this parameter is achieved with the desired accuracy. Then,

another of the initially guessed parameters is evaluated in the same manner. The new converged value is used to evaluate again the first guessed parameter. This process is repeated until all parameters converge with the desired accuracy.

A.1.3 Bisection Method

The Bisection method applies when two values with opposite sign of a continuous function $f(x)$ are known. The method consists of repeatedly bisecting the interval defined by these values (see Figure A.2) until a subinterval in which the function changes sign is obtained as it contains the root. It is simple and robust however it converges relatively slowly. For this reason, often it is used as a first step to obtain a rough approximation to feed to other, faster methods.

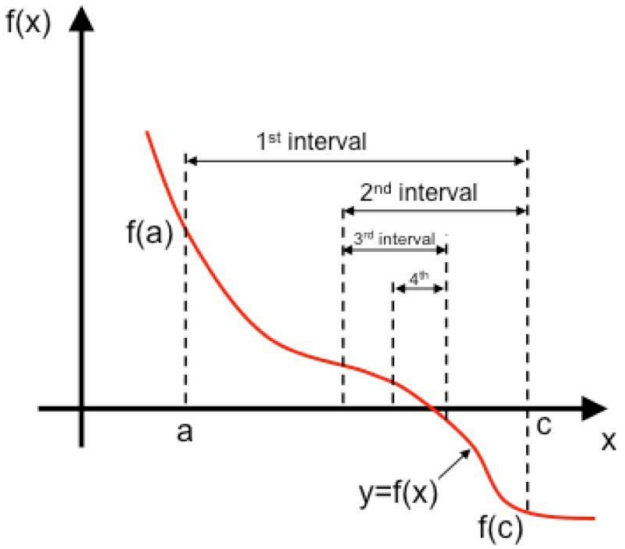

Figure A.2 Iteration for the Bisection method

A.2 Equations for Parameter Extraction

The four constraints (2.9)-(2.12)/(2.13) are applied to the governing equation of each model. The so-obtained equations are written in the normal form $f_i(\boldsymbol{X}) = 0$.

A.2.1 ISDM

The three constraints (2.9)-(2.11) are applied directly to the governing equation:

$$I(V) = I_{ph} - I_s\left[e^{\left(\frac{V}{aV_{th}}\right)} - 1\right] \tag{A.2}$$

Equations

1) matching of the Short-Circuit point $(0, I_{SC})$:

$$I_{ph} - I_{SC} = 0 \tag{A.3}$$

2) matching of the Open-Circuit point $(V_{OC}, 0)$:

$$I_{ph} - I_s\left[e^{\left(\frac{V_{OC}}{aV_{th}}\right)} - 1\right] = 0 \tag{A.4}$$

3) matching of the Maximum Power Point (V_{MPP}, I_{MPP}):

$$I_{ph} - I_s\left[e^{\left(\frac{V_{MPP}}{aV_{th}}\right)} - 1\right] - I_{MPP} = 0 \tag{A.5}$$

A.2.2 SSDM-p

The four constraints (2.9)-(2.12) are applied directly to the governing equation:

$$I(V) = I_{ph} - I_s\left[e^{\left(\frac{V}{aV_{th}}\right)} - 1\right] - \frac{V}{R_p} \tag{A.6}$$

Equations

1) matching of the Short-Circuit point $(0, I_{SC})$:

$$I_{ph} - I_{SC} = 0 \tag{A.7}$$

2) matching of the Open-Circuit point $(V_{OC}, 0)$:

$$I_{ph} - I_s\left[e^{\left(\frac{V_{OC}}{aV_{th}}\right)} - 1\right] - \frac{V_{OC}}{R_p} = 0 \tag{A.8}$$

3) matching of the Maximum Power Point (V_{MPP}, I_{MPP}):

$$I_{ph} - I_s\left[e^{\left(\frac{V_{MPP}}{aV_{th}}\right)} - 1\right] - \frac{V_{MPP}}{R_p} - I_{MPP} = 0 \tag{A.9}$$

4) first derivative of $P(V)$ calculated in the MPP equal to zero:

$$I_{SC} - I_s\left[\left(1 + \frac{V_{MPP}}{aV_{th}}\right)e^{\left(\frac{V_{MPP}}{aV_{th}}\right)} - 1\right] - \frac{2V_{MPP}}{R_p} = 0 \tag{A.10}$$

A.2.3 SSDM-s

The first three constraints (2.9)-(2.11) are applied directly to the governing equation:

$$I(V) = I_{ph} - I_s\left[e^{\left(\frac{V+IR_s}{aV_{th}}\right)} - 1\right] \tag{A.11}$$

whereas the fourth constraint (2.12) is applied to the inverse of (3.13):

$$V(I) = aV_{th}ln\left(\frac{I_{ph} + I_s - I}{I_s}\right) - IR_s \tag{A.12}$$

Equations

1) matching of the Short-Circuit point $(0, I_{SC})$:

$$I_{ph} - I_s\left[e^{\left(\frac{R_s I_{SC}}{aV_{th}}\right)} - 1\right] - I_{SC} = 0 \tag{A.13}$$

2) matching of the Open-Circuit point $(V_{OC}, 0)$:

$$I_{ph} - I_s\left[e^{\left(\frac{V_{OC}}{aV_{th}}\right)} - 1\right] = 0 \tag{A.14}$$

3) matching of the Maximum Power Point (V_{MPP}, I_{MPP}):

$$I_{ph} - I_s\left[e^{\left(\frac{V_{MPP}+R_s I_{MPP}}{aV_{th}}\right)} - 1\right] - I_{MPP} = 0 \tag{A.15}$$

4) first derivative of $P(V)$ calculated in the MPP equal to zero:

$$aV_{th}ln\left(\frac{I_{ph} + I_s - I_{MPP}}{I_s}\right) - aV_{th}I_{MPP}ln\left(\frac{1}{I_{ph} + I_s - I_{MPP}}\right) - 2I_{MPP}R_s = 0 \tag{A.16}$$

A.2.4 CSDM

The four constraints (2.9)-(2.12) are applied directly to the governing equation:

$$I(V) = I_{ph} - I_s\left[e^{\left(\frac{V+IR_s}{aV_{th}}\right)} - 1\right] - \frac{V + IR_s}{R_p} \tag{A.17}$$

Equations

1) matching of the Short-Circuit point $(0, I_{SC})$:

$$I_{ph} - I_s\left[e^{\left(\frac{I_{SC}R_s}{aV_{th}}\right)} - 1\right] - \frac{I_{SC}R_s}{R_p} - I_{SC} = 0 \tag{A.18}$$

2) matching of the Open-Circuit point $(V_{OC}, 0)$:

$$I_{ph} - I_s\left[e^{\left(\frac{V_{OC}}{aV_{th}}\right)} - 1\right] - \frac{V_{OC}}{R_p} = 0 \tag{A.19}$$

3) matching of the Maximum Power Point (V_{MPP}, I_{MPP}):

$$I_{ph} - I_s\left[e^{\left(\frac{V_{MPP}+I_{MPP}R_s}{aV_{th}}\right)} - 1\right] - \frac{V_{MPP} + I_{MPP}R_s}{R_p} - I_{MPP} = 0 \tag{A.20}$$

4) first derivative of $P(V)$ calculated in the MPP equal to zero:

$$\left(1-\frac{I_{MPP}}{V_{MPP}}R_s\right)\left[-\frac{I_s}{aV_{th}}e^{\left(\frac{V_{MPP}+I_{MPP}R_s}{aV_{th}}\right)}-\frac{1}{R_p}\right]+\frac{I_{MPP}}{V_{MPP}}=0 \tag{A.21}$$

Explicit (approximated) expressions for the parameters

If the ideality factor a is evaluated independently, the four constraints (A.18)-(A.21) are sufficient to write explicit expressions for the remaining four parameters I_{ph}, I_s, R_s and R_p [16]:

$$R_s = A\left[W_{-1}\left(B\ exp(C)\right)-(D+C)\right] \tag{A.22}$$

$$R_p = \frac{(V_{MPP}-I_{MPP}R_s)[V_{MPP}-R_s(I_{SC}-I_{MPP})-aV_{th}]}{(V_{MPP}-I_{MPP}R_s)(I_{SC}-I_{MPP})-aV_{th}I_{MPP}} \tag{A.23}$$

$$I_s = \frac{(R_p+R_s)I_{SC}-V_{OC}}{R_p\exp\left(\frac{V_{OC}}{aV_{th}}\right)} \tag{A.24}$$

$$I_{ph} = \frac{R_p+R_s}{R_p}I_{SC} \tag{A.25}$$

It is to be noted that these expressions have been obtained with some minor and justified simplifications based on the orders of magnitude of some terms. Also, Equation (A.22) is obtained applying the Lambert W-function to:

$$\begin{gathered}\frac{aV_{th}V_{MPP}(2I_{MPP}-I_{SC})}{[V_{MPP}I_{SC}+V_{OC}(I_{MPP}-I_{SC})](V_{MPP}-I_{MPP}R_s)-aV_{th}(V_{MPP}I_{SC}-V_{OC}I_{MPP})} \\ =\exp\left(\frac{V_{MPP}+I_{MPP}R_s-V_{OC}}{aV_{th}}\right)\end{gathered} \tag{A.26}$$

that is derived from the four constraints. Coefficients in (A.22) are defined as follows:

$$A = \frac{aV_{th}}{I_{MPP}} \tag{A.27}$$

$$B = \frac{V_{MPP}(2I_{MPP}-I_{SC})}{V_{MPP}I_{SC}+V_{OC}(I_{MPP}-I_{SC})} \tag{A.28}$$

$$C = -\frac{2V_{MPP}-V_{OC}}{aV_{th}}+\frac{V_{MPP}I_{SC}-V_{OC}I_{MPP}}{V_{MPP}I_{SC}+V_{OC}(I_{MPP}-I_{SC})} \tag{A.29}$$

$$D = \frac{V_{MPP}-V_{OC}}{aV_{th}} \tag{A.30}$$

A.3 Angle of Incidence and Effective Irradiance

A.3.1 Computation of the Angle of Incidence

The relation between the *angle of incidence* θ_s on a tilted surface and the surface-characterizing angles is given by [1]:

$$\begin{aligned} cos\theta_s = {} & sin\delta\ sin\varphi\ cos\beta - [sign(\varphi)]sin\delta\ cos\varphi\ sin\beta\ cos\alpha \\ & + cos\delta\ cos\varphi\ cos\beta\ cos\omega \\ & + [sign(\varphi)]cos\delta\ sin\varphi\ sin\beta\ cos\alpha\ cos\omega \\ & + cos\delta\ sin\alpha\ sin\omega\ sin\beta \end{aligned} \tag{A.31}$$

where:

- α is the *azimuth angle* (0° facing South),
- β is the *slope* (or *tilt*) *angle*,
- φ is the *latitude* (positive northwards from equator),
- δ is the *solar declination*, given by (daily variations can be neglected):

$$\delta = 23.45° \cdot \sin\left[\frac{360(d_n + 284)}{365}\right] \tag{A.32}$$

  where d_n is the day number counted from the beginning of the year,

- ω is the *solar hour,* given by:

$$\omega = 15° \cdot (LT - DST - 12) - (\lambda_{ref} - \lambda) \tag{A.33}$$

  where:

  - LT is the local time expressed in decimal 24-hour format,
  - DST is the Daylight Summer Time, being 1 if active and 0 otherwise,
  - λ is the longitude and λ_{ref} the longitude of the reference meridian for the timezone (positive eastwards from Greenwich).

A.3.2 Computation of the Effective Irradiance

The pyranometer-measured POA irradiance G_T (the subscript "T" stands for "tilted") is not the irradiance fed to the models as this value does not represent the radiant power *actually* reaching the semiconductor surface, i.e. the *effective irradiance* $G_{T,eff}$. In fact, only a fraction of this power effectively reaches the semiconductor below the glass covering for energy conversion. This is caused mainly by two phenomenons [10, 1]:

1) the glass cover has its own transmittance and reflectance that depends on the angle of incidence of the sun rays;
2) the glass cover is affected by a certain level of dirtiness;

with the first factor being significant for incidence angles over 65° [10] (see Figure A.3). Therefore, an *effective irradiance* $G_{Tb,eff}$ must computed from the reading of the pyranometer.

In general, the irradiance falling on a surface can be separated in two components, the *direct* (or *beam*) irradiance and the *diffuse* component [1]:

$$G_T = G_{Tb} + G_{Td} \tag{A.34}$$

The diffuse fraction is then made of the *isotropic* component and the *circumsolar* component:

$$G_{Td} = G_{Td,iso} + G_{Td,cir} \tag{A.35}$$

The model presented in [1] modifies each of these components as follows:

$$G_{Tb,eff} = G_{Tb} \cdot K_{trans} \tag{A.36}$$

$$G_{Td,iso,eff} = G_{Td,iso} \cdot 0{,}9 \tag{A.37}$$

$$G_{Td,cir,eff} = G_{Td,cir} \cdot K_{trans} \tag{A.38}$$

where:

$$K_{trans} = \frac{T_{dirt}(0)}{T_{clean}(0)} \cdot FT_b(\theta_s) \tag{A.39}$$

The factor $FT_B(\theta_s)$ is the "relative transmittance" for a given incidence angle θ_s:

$$FT_b(\theta_s) = 1 - \frac{\exp\left(-\frac{cos\theta_s}{a_r}\right) - \exp\left(-\frac{1}{a_r}\right)}{1 - \exp\left(-\frac{1}{a_r}\right)} \tag{A.40}$$

where a_r is an adjustable parameter associated with the degree of dirtiness. It must be noted that for normal incidence ($\theta_s = 0$), the relative transmittance $FT_B(\theta_s) = 1$, meaning that this parameter does not include the effect of dirt on the relative normal transmittance. For this reason in (A.36) the factor $T_{dirt}(0)/T_{clean}(0)$ appears, characterizing the degree of dirtiness for normal incidence ("relative normal transmittance"). Typical values of a_r and $T_{dirt}(0)/T_{clean}(0)$ are shown in Table A.1 while Figure A.3 plots $FT_b(\theta_s)$ for an average clean and dirty panel.

Table A.1 Recommended parameters for angular loss calculation

Dirtiness degree	$\boldsymbol{T_{dirt}(0)/T_{clean}(0)}$	$\boldsymbol{a_r}$
Clean	1	0.17
Low	0.98	0.20
Medium	0.97	0.21
High	0.92	0.27

According to (A.36), the effective irradiance depends only on the angle of incidence and must be computed for every moment for which the pyranometer collects the measurement as LT changes in (A.33) and so does the solar hour ω in (A.31).

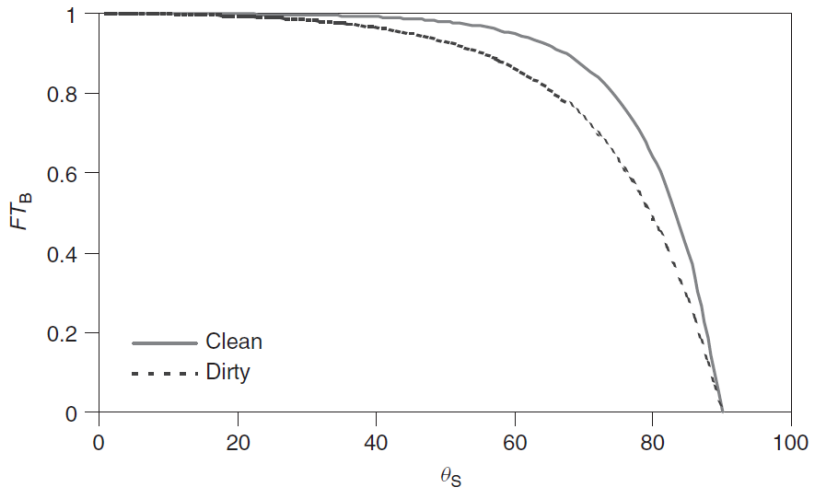

Figure A.3 The relative transmittance as a function of the angle of incidence [1]

The quantities defined in Equations (A.36)-(A.38) are computed from the measured DNI (Direct Normal Irradiance), DHI (Direct Horizontal Irradiance) and G_T as follows [1]:

$$G_{Tb} = DNI \cdot cos\theta_s \tag{A.41}$$

$$G_{Td,iso} = DHI \cdot \left(\frac{1 + cos\beta}{2}\right) \tag{A.42}$$

$$G_{Td,cir} = G_T - G_{Tb} - G_{Td,iso} \tag{A.43}$$

Finally, it is worth noting that in some of the studies reviewed, the authors had to calculate the POA irradiance from measurements on the horizontal plane, adding a source of possible errors for the validation (and parameter extraction, if collected data are used for it) of the models [10].